On-chip reconstitution of an FtsZ-based divisome for synthetic cells

Fanalista, Federico

DOI
10.4233/uuid:d8b89616-9cb6-4c0d-8f6b-a58c93614a25

Publication date
2020

Document Version
Final published version

Citation (APA)
Fanalista, F. (2020). *On-chip reconstitution of an FtsZ-based divisome for synthetic cells*. [Dissertation (TU Delft), Delft University of Technology]. https://doi.org/10.4233/uuid:d8b89616-9cb6-4c0d-8f6b-a58c93614a25

ON-CHIP RECONSTITUTION OF AN FTSZ-BASED DIVISOME FOR SYNTHETIC CELLS

ON-CHIP RECONSTITUTION OF AN FTSZ-BASED DIVISOME FOR SYNTHETIC CELLS

Dissertation

for the purpose of obtaining the degree of doctor
at Delft University of Technology,
by the authority of the Rector Magnificus prof.dr.ir. T.H.J.J. van der Hagen,
chair of the Board for Doctorates
to be defended publicly on
Friday 21-02-2020 at 10:00 o' clock

by

Federico FANALISTA

Master of Science in Physics,
Università degli Studi di Milano, Italy,
born in Milan, Italy

This dissertation has been approved by the promotor:

Prof. dr. C. Dekker

Composition of the doctoral committee:

Rector Magnificus,	chairperson
Prof. dr. C. Dekker,	Delft University of Technology, promotor
Independent members:	
Prof. dr. M. Dogterom	Delft University of Technology
Prof. dr. G. H. Koenderink	Delft University of Technology
Prof. dr. G. Rivas,	Centro de Investigationes Biológicas
Dr. C. Danelon,	Delft University of Technology
Dr. S. Holden,	Newcastle University
Dr. T. van der Blaauwen,	University of Amsterdam

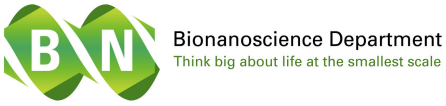

Keywords: FtsZ, synthetic cell, microfluidics, bottom-up biology

Printed by: Gildeprint

Front & Back: Jacob W. J. Kerssemakers

Casimir PhD Series, Delft-Leiden 2020-06

ISBN 978-90-8593-433-2

An electronic version of this dissertation is available at
`http://repository.tudelft.nl/`.

To my sisters, Carol and Meggie,
as a proof that success
is not strictly necessary
to have fun in life.

CONTENTS

1

INTRODUCTION

"Considerate la vostra semenza:
fatti non foste a viver come bruti,
ma per seguir virtute e canoscenza."

Dante Alighieri

1

1.1. INTRODUCTION

Since humans started to wonder about the marvels that compose the world around us, it appeared clear that certain entities, such as animals and plants, had specific traits that clearly were distinguishable from simple unanimated objects. This particular capacity of interacting with the environment, originally believed by Greek philosophers to be associated with the presence of a soul, is commonly defined as life. Although human science and technology developed exponentially since then, the question "what is life?" still lacks a good answer. If we face the question from a purely scientific point of view, scientists can agree on describing life through a sum of attributes, among which the following three probably stand as the most important ones: first, living entities are capable to reproduce themselves, giving birth to progenies; second, they are capable to interact with their own environment to autonomously uptake the nutrients required for self-maintenance; and third, each individual possesses specific traits that are encoded in its genetic information. These three aspects are strictly interconnected with each other, and they are fundamental in light of the Darwinian theory, where species evolve and adapt through the generations for better fit the surrounding environment in the effort to survival.

With this list at hand, we can look at the most simple form of life possessing these traits, namely, cells. These constitute the minimal building blocks of all life. Cells can be viewed as an ensemble of chemical reactions that are confined in space by a membrane. Through its metabolism, the cell is capable to obtain energy from its environment to fight entropic diffusion and maintain the necessary gradients for its reactions to occur. It possesses functional polymers, such as DNA, which encode the genetic information that is transmitted from parent cells, and that is used for the internal processes, *e.g.*, to produce proteins that perform all the cell fundamental functions.

1.2. SYNTHETIC CELLS

Despite the advancements in cell and molecular biology, cells as we know them embed a great amount of reactions and components, and we are still far from grasping the understanding of their great complexity. Thanks to the advancement of scientific techniques, it is however possible to isolate specific cellular components and to reconstitute and study their specific cellular functionalities in a controlled environment. This approach, that one might call "bottom-up biology", sees as its ultimate goal the recreation from scratch of a minimal cell that is capable to autonomously grow, divide, and transmit its genetic information. In view of this long-term plan, scientific groups working in this emerging field are specializing on specific aspects of the cells, working towards the reconstitution of one particular cellular function.

In this thesis, we worked towards the reconstitution of synthetic cell division, which in nature leads to the formation of two daughter cells out of a mother one. In most cellular organisms, depending on the specific domain of life, this function is achieved by different protein machineries. Cell division is often regulated through a contractile ring at the cell division plane which induces an invagination that leads to fission. Common examples are actomyosin rings found in eukaryotic cells, the largely unexplored cell-division system (cdv) found in archaea cells, and the Z-ring in most of bacterial cells. In

order to reconstitute a minimal cell that is able to replicate itself, few components are strictly necessary: a three-dimensional scaffold, or container, that defines the cell as an entity, a minimal protein machinery that performs the scission of such container, and possibly a positioning system to localize the protein machinery at the proper division plane.

In this thesis, we worked towards developing an artificial divisome by reconstituting a minimal bacterial protein machinery inside artificial confinements produced by microfluidic techniques. In the next paragraphs, we will give a brief overview of the most commonly employed artificial scaffolds in the field of bottom-up biology, focusing on their properties, production methods and employments. Afterwards, we will give a description of the Z-ring, including its assembly and localization in bacteria, followed by a summary of the main achievements so far in the understanding of the role of the key protein FtsZ in bacterial cytokinesis. Finally, we will give an overview of the work presented in this thesis.

1.3. SYNTHETIC CELL CONTAINERS

When thinking of a cell, we picture a three-dimensional object defined in space that is enclosed by a physical boundary that separates it from the surrounding environment. As *in vitro* bottom-up reconstitutions became more accurate and elaborated over recent years, we witnessed a technological development towards a better production of minimal containers that control the encapsulation of biological material. As a basic requirement, the confinement has to be biologically compatible: both the scaffold constituents and its enclosed environment must preserve the functionality of the biological material under study. The confinement should also allow the exchange of material with the surrounding environment, in order to acquire the energy necessary for the chemical reactions to occur. Last, if our aim is to induce the replication of the confinement through its division, the vesicle should be capable to undergo shape transformations, ideally induced by active protein machineries or, alternatively, by the external change of physicochemical parameters. Among the large variety of confinements employed for *in vitro* studies,[1] here we will focus on describing the ones employed in the experiments performed in this thesis.

LIPOSOMES

Liposomes are closed bilayers spontaneously formed by the self-assembly of amphiphilic molecules in water (Fig. 1.1a). Like cell membranes, liposomes are generally composed of phospholipids, molecules formed by a pair of hydrocarbon chains of various lengths and a polar head containing a phosphate group. Because they mimic the cell membrane in a minimalistic way, liposomes are the confinements that best fit to the above-mentioned requirements, and they are largely employed in *in vitro* reconstitutions of cellular components. For example, given their soft nature, liposomes offer an ideal platform to probe the capabilities of cytoskeletal proteins to remodel the membrane. The reconstitution of eukaryotic protein bundles, such as actin and tubulin inside liposomes has been observed to induce prominent reshaping of liposomes.[2, 3] Also, as we will discuss more in details in the next paragraph, the results obtained from FtsZ filaments reconstituted inside liposomes have been the major source of speculations con-

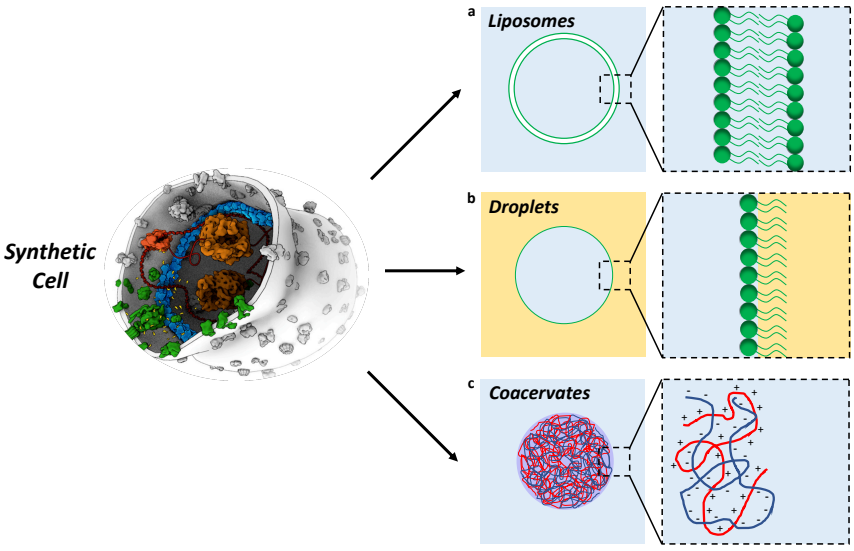

Figure 1.1: **Schematic representation of minimal containers for synthetic cells.** (a) Liposomes are closed containers formed by phospholipid molecules (green) dissolved in water (light-blue). Amphiphilic molecules as lipids possessing a hydrophobic hydrocarbon tail and a hydrophilic head arrange in polar solvents so to expose the heads and to hide the tails to the surrounding environment. Because of this, above a critical concentration, lipids in water spontaneously self-assemble into a variety of organized structures, such as micelles and liposomes. (b) Water droplets in oil solutions (yellow) can be stabilized by addition of surfactant molecules, such as lipids (green), which assemble a monolayer at the interface. (c) When dissolved in water, above a certain critical concentration polyelectrolytes possessing opposite charges (blue and red) spontaneously partition in a highly concentrated phase, forming membraneless liquid droplets named coacervates.

cerning the role of FtsZ as a septum-inducer in bacteria.[4]

To minimize the surface energy required to build the interface, liposomes tend to adopt a spherical shape, but variation of parameters such as temperature, osmotic pressure and lipid compositions have been shown to lead to a large variety of shape transformations.[5, 6] Also, the specific lipid composition can influence the liposome appearance, leading to fancy phenomena as membrane phase separation.[7]

In the scientific literature it is possible to find several methods to produce liposomes, which can be mainly grouped in two categories: the traditional bulk methods, and the newer microfluidics methods. The first category includes swelling, where liposomes assemble from the hydration of a lipid bilayer deposited on a surface, either spontaneously or with the help of an electric field;[8, 9] and emulsion transfer and cDICE, where water droplets are rapidly injected through an oil-water interface provided with lipids.[10, 11] In order to improve some of the weak points associated to these techniques, such as the encapsulation efficiency and size polydispersity, more complex and sophisticated methods have been developed. Such methods generally involve a microfluidic platform, such as PDMS channels or glass capillaries, where liposomes are obtained by solvent separation from double emulsions templates,[12, 13] or by a multi-step assembly of lipid layers at the interface of single emulsions.[14, 15]

DROPLETS

A water-in-oil emulsion (simply named "droplet") is a less sophisticated form of container that, as the name suggests, consists of a water-phase droplet that is suspended in an oil-phase environment. Amphipathic molecules, such as surfactants, lipids, or microbeads, are often employed to assemble a monolayer at the water-oil interface (Fig. 1.1b), which stabilizes the surface, preventing droplet merging, and allowing the functionalization of the surface with, for example, protein binding lipids. Droplets can be easily obtained in bulk by simply mixing water in an oil solution provided with surfactant molecules, or they can be produced on-chip, where a fast production rate and a fine control over the droplet size and internal composition are easily achieved by now commonly used microfluidics platforms.[16] Because of this, droplets offer a robust and relatively simple means to compartmentalize and study purified cellular components, such as, to name a few, cell-free protein expression,[17] pattern forming systems[18] and cytoskeletal components.[19]

In the specific context of cell division though, droplets are less favorable since, given their high surface tension, droplets are not easily deformable, and thus cannot undergo shape changes under the contractile action of protein machineries. Also, the surrounding oil phase presents a strong limitation for the exchange of material with the external environment, so nutrients molecules necessary for the reactions to occur are generally limited to those available at the moment of the encapsulation and difficult to replenish afterwards. These limitations can be partially overcome by microfluidic designs, through which it is possible to split and merge droplets[20] or, as recently proved by the work shown in Chapter 2 of this thesis, finely control their shape and their size.[21] Also, an electro-microfluidic platform to pico-inject droplets in a post-production phase has recently been developed, to facilitate the sequential encapsulation of several components into the aqueous phase.[22]

COACERVATES

Coacervates are membraneless condensates generated by the liquid-liquid phase separation of molecules.[23] In simple words, molecules with opposite charges spontaneously condensate to form liquid droplets when dissolved in water above a certain concentration.(Fig. 1.1c) Since the recent discovery that certain type of bodies, such as P granules, nucleoli, stress granules, etc[24–26] indeed possess liquid-like properties in eukaryotic cells, coacervates are receiving a constantly increasing attention from the scientific community.[27] The fact that they are also easy to reconstitute *in vitro*, in addition to their intricate physio-chemical properties, make them an interesting topic of research not only for cell biology, but also for bottom-up essays. Several biological molecules have been shown to undergo coacervation, including peptides and nucleotides, peptides and RNA, and intrinsically disordered proteins.[28–31] Recently, microfluidics-based methods have been developed to control the formation of coacervates inside liposomes, leading to a more complex level of organization in artificial compartments.[32, 33]

As electrostatic interactions favor condensation against the entropy driven tendency towards a homogeneous system, coacervates stability can be controlled by salt concentration, pH conditions, or by active modification of the molecules constituting the condensates.[34] Given the absence of a physical membrane, the coacervate surface allows on the one hand the continuous exchange of molecules, and on the other allows

to increase the local concentration of chemical components, promoting and enhancing the reaction rate of biological rections, such as RNA transcription and protein filament interactions.[35, 36] Thanks to these properties, coacervates can be viewed not only as a new membraneless form of intracellular compartmentalization, but also as potential alternative scaffolds for bottom-up biology. Indeed, cytoskeletal active protein bundles have been shown to partition in coacervates, inducing various forms of shape deformation.[37–39] Also, recent theoretical work suggested that coacervates that are kept away from thermodynamic equilibrium can spontaneously divide.[40] Altogether, these results emphasize the importance of coacervates as possible minimal cells, supporting Oparin's century old hypothesis that primordial life form may have been started from molecular condensates more so than from membrane-bound liposomes.[41]

1.4. BACTERIAL REPLICATION: THE Z-RING

The "filamentous temperature sensitive" fts genes that are fundamental for prokaryotic cell division were already identified 40 years ago,[42] and a major milestone was the discovery that FtsZ protein forms a ring-like structure at the nascent division site.[43] This indicated that, similar to eukaryotic cells, bacterial cell division was orchestrated by cytoskeletal proteins, a quite profound result back in the days. Today, we know that the division machinery, named the Z-ring, is composed of more than 20 known proteins, which functions is still only partly understood. Here, we present a brief overview of the major results achieved by different groups aimed to understand the processes of ring assembly and localization, with particular attention on the role of FtsZ in cytokinesis.

Z-RING ASSEMBLY

Soon after its discovery, it was observed that, in analogy to the eukaryotic tubulin, FtsZ employs guanosine triphosphate (GTP) to assemble in a cooperative manner into 100-200 nm long filaments, which dynamic behavior is associated with nucleotide hydrolysis.[44–46] FtsZ filaments have been observed to further condense into higher-ordered multi-strand structures, such as tubules and sheets, generally referred to as bundles.[47] When reconstituted *in vitro*, both the single filament dynamics and the bundle conformation strongly depend on the ionic content and the crowding conditions of the buffer employed for the study.[48–51]

FtsZ is composed of a N-terminus globular domain, responsible for the GTPase activity and the linear polymerization of the protein into filaments,[52] connected to a flexible intrinsically disordered tail with a length that varies depending on the bacterial species, which connects to a short highly conserved peptide, and a C-terminal variable region at the very end.[53] The length of the flexible linker has been shown to be important for the proper assembly of the ring, as it gives FtsZ the mobility necessary to interact with the other ring-associated proteins and organize in filaments.[54, 55] The conserved C-terminal peptide is also responsible for the interaction with the other ring-associated proteins, while the variable C-terminal region plays an important role in establishing the lateral associations between FtsZ filaments responsible for their condensation into bundles.[56]

At early stages of the cell cycle, FtsZ filaments starts assembling into a ring structure at the cell mid-plane, by docking to the lipids via interaction with two membrane

anchor proteins, ZipA and FtsA. Both proteins are recruited together at the division site via interaction with FtsZ C-terminal peptide, and their concentration appears constant throughout the cell cycle.[57–61] While FtsA is highly conserved, ZipA is present only in gammaproteobacteria.[62] In the absence of one of the two anchors the ring is still able to assemble in *E. coli*, but division does not occur, while the ring does not assemble when both proteins are lacking.[60] The point-mutation protein FtsA* has been shown *in vivo* to be able to overcome the lack of ZipA, suggesting a role of ZipA as accessory protein to stabilize the Z-ring.[63] *In vitro* work aimed to explore the capability of ZipA to stabilize or enhancing FtsZ filament lateral interactions so far led to contradictory results: some results found enhanced FtsZ bundling activity in presence of ZipA,[64, 65] while others reported a low binding affinity between the two proteins, and a role to ZipA of mere anchor protein.[66–68] Differently, recent TEM images have shown that FtsA forms dodecameric mini-rings, which would prevent the lateral association of FtsZ filaments, while the FtsA* mutant forms open rings structures, which allows the formation of bundles.[69] More importantly, the behavior of FtsZ filaments on a supported lipid bilayer is strongly dependent on the membrane anchor protein employed, with FtsA-bound FtsZ filaments undergoing treadmilling dynamics, while ZipA-bound filaments were stable over time.[70] As we will discuss more in detail below, treadmilling filaments were also observed *in vivo*, redefining the role of FtsZ in cytokinesis.[71] Together with FtsZ, ZipA and FtsA, a few other accessory proteins are recruited at the early stage, such as ZapA and EzrA (in gram-positive bacteria), which interact directly with FtsZ and act as, respectively, positive and negative regulators for the integrity and stability of the Z-ring.[72–74]

Z-RING POSITIONING

To ensure a symmetric division into two daughters, the cell possess different mechanisms to ensure the proper localization of the Z-ring at the mid-plane, which vary among bacterial species. In *E. coli*, there are three main known regulator factors: negative regulators, such as the Min-proteins and the nucleoid-occlusion systems, which prevent ring assembly at aberrant positions, and positive marker proteins associated to the DNA *ter* region, which mark the proper positioning at the replication site.[75]

The Min proteins constitute a fascinating pattern-formation system composed by three elements: MinC, MinD, and MinE.[76] MinD employs ATP to bind to the cell membrane in a dimeric structure, with which MinE can interact, inducing nucleotide hydrolysis and MinD release from the membrane.[77, 78] The repetition of this process establishes a reaction-diffusion mechanism, which has been reconstituted *in vitro* in the form of protein patterns travelling along the lipid membrane.[79] Both in cells and in artificial chambers, this travelling waves have been observed to be highly sensitive to the confinement geometry.[80–82] In *E. coli* cells, Min proteins oscillate between the cell poles, establishing a protein gradient with a lower concentration towards the cell mid-plane.[83, 84] MinC, which also binds to MinD and thus follows the oscillatory pattern, interacts with the C-terminus domain of FtsZ, obstructing filament polymerization and in this way preventing Z-ring formation at the cell poles.[85, 86]

SlmA is a nucleoid-associated protein that also obstructs FtsZ polymerization, preventing Z-ring to form over unsegregated DNA and cell division to occur at the wrong division plane.[87, 88] Such a mechanism has also been identified also in *B. subtilis*, where

the nucleoid-associated Noc protein plays a role analog to SlmA in *E. coli*.[89] Nucleoid occlusion has been shown to be more of a redundant safety mechanism, as cells lacking SlmA did not show any strong difference in ring positioning.[90] Also, in the absence of Min proteins, bacteria still showed a preferential localization of the division ring at the cell mid-plane, suggesting the existence of yet an additional localization mechanism for the Z-ring.[91, 92] Recent evidences indeed suggested a connection between MatP, a protein associated to the *ter* chromosome macrodomain, and ZapB, a protein associated to the division machinery through link with ZapA.[93] In cells lacking Min proteins and SlmA, ter domain is observed to migrate towards the mid-plane at early stage of the cell cycle, followed by the assembly of the Z-ring at the same position.[91] Altogether these results indicate an additional positive localization mechanism, involving a mutual spatial organization of the segregated chromosome and the division ring.

THE ROLE OF FTSZ IN CYTOKINESIS

Since the discovery that the Z ring constitutes the main scaffold of the divisome machinery, the role of FtsZ in the process of cell division has been at the center of many studies and speculations. Most importantly, the long-standing hypothesis that FtsZ filaments may generate the force necessary to invaginate the membrane and promote cell septation has been debated.[94, 95] The main evidences supporting this idea came from *in vitro* reconstitutions of FtsZ filaments inside liposomes, which induced shape deformation of the lipid membrane. Specifically, Osawa *et al.*[4] showed how FtsZ, when provided with a membrane targeting sequence (mts), assembled into rings that were able to perform constrictions in multilamellar tubular liposomes.(Fig. 1.2a). Also, they showed that FtsZ induce a convex or concave deformation depending on which side of the protein the mts was attached to, proving that FtsZ has a fixed direction of curvature.[96] In a different paper, FtsZ bundles, attached to the membrane of giant unilamellar liposomes via a soluble version of the membrane anchor protein ZipA, were shown to induce liposome shrinkage (Fig. 1.2b), with a rate that depended on the GTP hydrolysis rate.[97] Also, cryo-EM images of small liposomes encapsulating FtsZ and FtsA showed continuous protein rings encircling the membrane of a liposome which presented several invaginations (Fig. 1.2c).[98] Despite these promising results, until today no one has been able to report clear evidence of an FtsZ-ring capable of inducing membrane invagination down to liposome division.

The evidence of the early experiments inspired different models concerning the mechanism underlying FtsZ force generation. One hypothesis speculates that attractive lateral interactions between FtsZ filaments, responsible for the condensation into multistrand bundles, would induce the ring to contract via either filaments sliding in parallel or filaments condensing into bundles.[98, 99] Super-resolution imaging of the Z-ring however revealed a structure of the Z ring that is rather patchy and not-uniform, and the role of lateral interactions is still quite unclear.[100, 101] A second major hypothesis speculates that FtsZ filaments would increase their curvature under GTP hydrolysis, inducing membrane bending. This second model is the one that received most attention, in consideration of some results in support of it.[94, 102, 103] It is not surprising, however, that protein polymers with a certain bending rigidity are capable to mechanically deform a soft membrane.[2, 3] Also membrane-binding proteins possessing a transmembrane domain or an amphipathic helix can induce local curvature changes

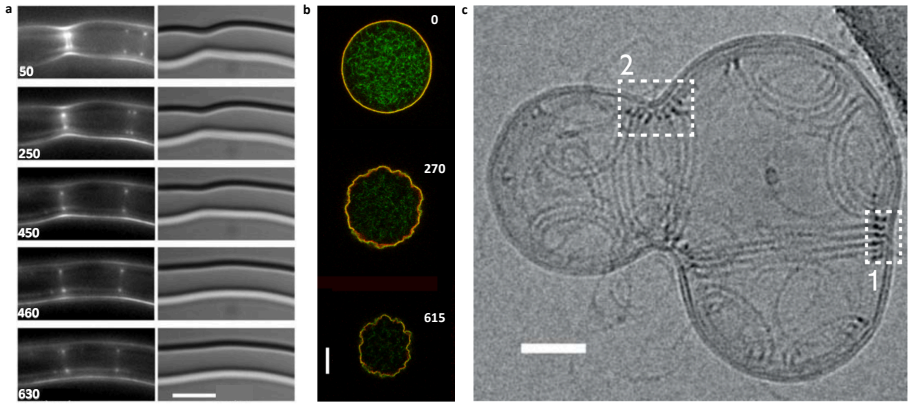

Figure 1.2: **Examples of FtsZ-driven liposome deformation.** (a) Osawa *et al.*[4] first reconstituted contractile FtsZ rings in multilamellar tubular liposomes, using a modified FtsZ with a mts lipid-binding sequence. Left: visualization of YFP-fluorescently labelled FtsZ in liposomes. Right: bright field images of liposome constrictions. Scale bar is 5 μm, time label is in seconds. (b) Cabré *et al.*[97] observed that FtsZ (green), attached to the liposome membrane via its anchor ZipA (red), induce liposome shrinkage upon hydrolysis of GTP. Scale bar is 10 μm, time label is in seconds. (c) Cryo-EM images of membrane invaginations in small liposomes encircled by FtsZ-FtsA filaments.[98]. Scale bar is 50 nm.

when adhered to lipid membranes, as it has been observed for example in the case of FtsA alone.[104]

The results discussed so far indicate that FtsZ filaments can deform a liposome, but the real cell membrane constitutes a far more complicated system than a simple lipid bilayer. Even if we ignored the presence of a rigid wall, the cell has a strong turgor pressure acting against its boundaries, ranging between 0.3 MPa and 3 MPa, depending on the species. This means that the protein should exert a force in the order of nN, a thousand times higher than forces generally associated with protein conformational changes.[95]

More importantly, the majority of the recent *in vivo* studies performed in the field of bacterial cell division seem to play in disfavor of the role of FtsZ as the main force generator. Two milestone recent works proved that FtsZ filaments treadmill around the cell circumference at the division plane, driving the peptidoglycan machinery around the septum.[71, 105] These results redefined the role of FtsZ, suggesting that the cell wall synthesis, carried by FtsZ filaments, is responsible for invagination and septation. In support of this model, it has been shown that FtsZ leaves the division site before septation is concluded, again indicating that other factor external to the FtsZ protein are responsible for dividing the cell.[106] Also, very recent evidences showed that, while FtsZ treadmilling is essential to initiate invagination, in *S. aureus* cytokinesis is independent from FtsZ treadmilling once the cell wall synthesis already progressed.[107] It could be argued that FtsZ, if does not finish septation, could induce membrane invagination and start the constriction, positioning the cell-wall-generating machinery to the septum site. Even if the protoring is assembled at early stage of the cell cycle, constriction is not initiated until FtsN is recruited at the ring at a later stage.[108, 109] The exact mechanism

by which this occurs is still under study, and involves the interaction between several different proteins composing the ring (FtsA, FtsQ, FtsL, FtsB, FtsW, FtsI), which will not be discussed here in further detail.[110]

In summary, the precise mechanism of bacterial cytokinesis is still not fully understood. With the current knowledge available, the model that FtsZ serves as both a scaffold and as force generator seems at this point in time outdated. Instead, a more complex scenario, where peptidoglycan synthesis plays a major role in shape remodeling and cell division, seems more likely.

1.5. THIS THESIS

In this thesis, we aimed to reconstitute and understand the Z-ring protein machinery involved in bacterial cell division. We explored both the mechanical and assembling properties of FtsZ filaments, as well possible scaffolds for building the minimal machinery.

First, we realized that the selection of methods in bottom-up biology to tune the size and the shape of artificial confinements is quite limited, despite the important role that such parameters play over a large variety of cellular processes. For this reason, in Chapter 2 we developed an innovative microfluidic platform, where droplets, double emulsions and liposomes can be inserted in traps, to consequently deform into specifically designed shapes that resemble real cells. As a proof of concept, we showed how filamentous protein bundles, that randomly arranged in spherical droplets, spatially realigned along the axis of symmetry in tubular droplets.

In Chapter 3 we explored the proper conditions for FtsZ bundles to form in a membrane-enclosed confinement. By encapsulating FtsZ and ZipA into droplets with a lipid monolayer at the surface, we verified how the presence of macromolecular crowders is a necessary requirement towards the condensation of FtsZ filaments into bundles, while the process is more robust against variations of the protein concentration. We furthermore found that ZipA appeared to promote the bundling of FtsZ filaments. Interestingly, also the confinement size seemed to play a role over the organization properties of FtsZ, as bundling appeared more robust in smaller droplets.

In Chapter 4, we investigated whether FtsZ filaments are capable, under appropriate conditions, of inducing membrane deformation, and what possible mechanism may relate to that. We used microfluidics to encapsulate FtsZ and its membrane anchor protein ZipA into liposomes, and observed membrane deformation followed by the condensation of filaments into bundles. In liposomes smaller than a certain dimension (diameter < 5 μm), FtsZ filaments assembled into a ring, which however did not perform constriction. From AFM measurements on single FtsZ filaments, we observed that the filament curvature did not depend on the nucleotide state, indicating that the membrane deformation observed was most likely induced by the condensation of filaments into bundles, more than by a change of curvature consequent to GTP hydrolysis.

Finally, in Chapter 5 we explored the possibility of employing coacervates as a scaffold to build an artificial minimal cell. By means of a microfluidic device, membraneless liquid droplets were obtained by mixing positively charged polylysine with negatively charged GTP. FtsZ was shown to strongly partition on the coacervate surface and, likely due to its GTPase activity, to destabilize their structure. Also, the interaction between

FtsZ filaments adhered to the coacervate appeared enhanced, as long filamentous bundles protrude out of the surface, deforming the coacervates into aster-like objects. Altogether, coacervates proved to be capable of providing energy to FtsZ, enhancing its functionality and undergoing shape deformation, three key requirements for a potential scaffold of a minimal cell.

1

REFERENCES

[1] W. K. Spoelstra, S. Deshpande, and C. Dekker, *Tailoring the appearance: what will synthetic cells look like?* Current Opinion in Biotechnology **51**, 47 (2018).

[2] F. C. Tsai and G. H. Koenderink, *Shape control of lipid bilayer membranes by confined actin bundles,* Soft Matter **11**, 8834 (2015).

[3] T. Kaneko, T. J. Itoh, and H. Hotani, *Morphological transformation of liposomes caused by assembly of encapsulated tubulin and determination of shape by microtubule-associated proteins (MAPs),* Journal of Molecular Biology **284**, 1671 (1998).

[4] M. Osawa, D. E. Anderson, and H. P. Erickson, *Reconstitution of Contractile FtsZ Rings in Liposomes,* Science **320**, 792 LP (2008).

[5] U. Seifert, K. Berndl, and R. Lipowsky, *Shape transformations of vesicles: Phase diagram for spontaneous curvature and bilayer-coupling models,* Physical Review A **44**, 1182 (1991).

[6] J. Käs and E. Sackmann, *Shape transitions and shape stability of giant phospholipid vesicles in pure water induced by area-to-volume changes,* Biophysical Journal **60**, 825 (1991).

[7] T. Baumgart, S. T. Hess, and W. W. Webb, *Imaging coexisting fluid domains in biomembrane models coupling curvature and line tension,* Nature **425**, 821 (2003).

[8] D. S. Dimitrov and M. I. Angelova, *Lipid swelling and liposome formation mediated by electric fields,* Journal of Electroanalytical Chemistry **253**, 323 (1988).

[9] M. I. Angelova and D. S. Dimitrov, *Liposome Electro formation,* Faraday Discuss. Chem. Soc. **81**, 303 (1986).

[10] S. Pautot, B. J. Frisken, and D. A. Weitz, *Production of unilamellar vesicles using an inverted emulsion,* Langmuir **19**, 2870 (2003).

[11] M. Abkarian, E. Loiseau, and G. Massiera, *Continuous droplet interface crossing encapsulation (cDICE) for high throughput monodisperse vesicle design,* Soft Matter **7**, 4610 (2011).

[12] S. Deshpande, Y. Caspi, A. E. Meijering, and C. Dekker, *Octanol-assisted liposome assembly on chip,* Nature Communications **7**, 1 (2016).

[13] N. N. Deng, M. Yelleswarapu, and W. T. Huck, *Monodisperse Uni- and Multicompartment Liposomes,* Journal of the American Chemical Society **138**, 7584 (2016).

[14] M. Weiss, J. P. Frohnmayer, L. T. Benk, B. Haller, J. W. Janiesch, T. Heitkamp, M. Börsch, R. B. Lira, R. Dimova, R. Lipowsky, E. Bodenschatz, J. C. Baret, T. Vidakovic-Koch, K. Sundmacher, I. Platzman, and J. P. Spatz, *Sequential bottom-up assembly of mechanically stabilized synthetic cells by microfluidics,* Nature Materials **17**, 89 (2018).

[15] S. Matosevic and B. M. Paegel, *Layer-by-layer cell membrane assembly,* Nature Chemistry **5**, 958 (2013), NIHMS150003 .

[16] S. Y. Teh, R. Lin, L. H. Hung, and A. P. Lee, *Droplet microfluidics,* Lab on a Chip **8**, 198 (2008).

[17] P. Torre, C. D. Keating, and S. S. Mansy, *Multiphase water-in-oil emulsion droplets for cell-free transcription-translation,* Langmuir **30**, 5695 (2014).

[18] K. Zieske, G. Chwastek, and P. Schwille, *Protein Patterns and Oscillations on Lipid Monolayers and in Microdroplets,* Angewandte Chemie - International Edition **55**, 13455 (2016).

[19] M. Miyazaki, M. Chiba, H. Eguchi, T. Ohki, and S. Ishiwata, *Cell-sized spherical confinement induces the spontaneous formation of contractile actomyosin rings in vitro,* Nature Cell Biology **17**, 480 (2015).

[20] G. F. Christopher, J. Bergstein, N. B. End, M. Poon, C. Nguyen, and S. L. Anna, *Coalescence and splitting of confined droplets at microfluidic junctions,* Lab on a Chip **9**, 1102 (2009).

[21] F. Fanalista, A. Birnie, R. Maan, F. Burla, K. Charles, G. Pawlik, S. Deshpande, G. H. Koenderink, M. Dogterom, and C. Dekker, *Shape and Size Control of Artificial Cells for Bottom-Up Biology,* ACS Nano **13**, 5439 (2019).

[22] A. R. Abate, T. Hung, P. Marya, J. J. Agresti, and D. A. Weitz, *High-throughput injection with microfluidics using picoinjectors using picoinjectors,* Proceedings of the National Academy of Sciences of the United States of America **107**, 19163 (2010).

[23] C. P. Brangwynne, P. Tompa, and R. V. Pappu, *Polymer physics of intracellular phase transitions,* Nature Physics **11**, 899 (2015).

[24] C. Hoege, J. Gharakhani, F. Jülicher, and A. A. Hyman, *Germline P Granules Are Liquid Droplets That Localize by Controlled Dissolution/Condensation,* Science **5** (2009).

[25] C. P. Brangwynne, T. J. Mitchison, and A. A. Hyman, *Active liquid-like behavior of nucleoli determines their size and shape in Xenopus laevis oocytes,* Proceedings of the National Academy of Sciences of the United States of America **108**, 4334 (2011).

[26] A. Patel, H. O. Lee, L. Jawerth, S. Maharana, M. Jahnel, M. Y. Hein, S. Stoynov, J. Mahamid, S. Saha, T. M. Franzmann, A. Pozniakovski, I. Poser, N. Maghelli, L. A. Royer, M. Weigert, E. W. Myers, S. Grill, D. Drechsel, A. A. Hyman, and S. Alberti, *A Liquid-to-Solid Phase Transition of the ALS Protein FUS Accelerated by Disease Mutation,* Cell **162**, 1066 (2015).

[27] A. A. Hyman, C. A. Weber, and F. Jülicher, *Liquid-Liquid Phase Separation in Biology,* Annual Review of Cell and Developmental Biology **30**, 39 (2014).

[28] W. M. Aumiller and C. D. Keating, *Phosphorylation-mediated RNA/peptide complex coacervation as a model for intracellular liquid organelles,* Nature Chemistry **8**, 129 (2015).

[29] S. Koga, D. S. Williams, A. W. Perriman, and S. Mann, *Peptide-nucleotide microdroplets as a step towards a membrane-free protocell model,* Nature Chemistry **3**, 720 (2011).

[30] J. R. Simon, N. J. Carroll, M. Rubinstein, A. Chilkoti, and G. P. López, *Programming molecular self-assembly of intrinsically disordered proteins containing sequences of low complexity,* Nature Chemistry **9**, 509 (2017).

[31] C. W. Pak, M. Kosno, A. S. Holehouse, S. B. Padrick, A. Mittal, R. Ali, A. A. Yunus, D. R. Liu, R. V. Pappu, and M. K. Rosen, *Sequence Determinants of Intracellular Phase Separation by Complex Coacervation of a Disordered Protein,* Molecular Cell **63**, 72 (2016).

[32] S. Deshpande, F. Brandenburg, A. Lau, M. G. F. Last, W. K. Spoelstra, L. Reese, S. Wunnava, M. Dogterom, and C. Dekker, *Spatiotemporal control of coacervate formation within liposomes,* Nature Communications **10**, 1800 (2019).

[33] N. N. Deng and W. T. Huck, *Microfluidic Formation of Monodisperse Coacervate Organelles in Liposomes,* Angewandte Chemie - International Edition **56**, 9736 (2017).

[34] D. Priftis and M. Tirrell, *Phase behaviour and complex coacervation of aqueous polypeptide solutions,* Soft Matter **8**, 9396 (2012).

[35] E. Sokolova, E. Spruijt, M. M. K. Hansen, E. Dubuc, J. Groen, V. Chokkalingam, A. Piruska, H. A. Heus, and W. T. S. Huck, *Enhanced transcription rates in membrane-free protocells formed by coacervation of cell lysate,* Proceedings of the National Academy of Sciences **110**, 11692 (2013).

[36] P. M. McCall, S. Srivastava, S. L. Perry, D. R. Kovar, M. L. Gardel, and M. V. Tirrell, *Partitioning and Enhanced Self-Assembly of Actin in Polypeptide Coacervates,* Biophysical Journal **114**, 1636 (2018).

[37] A. Hernández-Vega, M. Braun, L. Scharrel, M. Jahnel, S. Wegmann, B. T. Hyman, S. Alberti, S. Diez, and A. A. Hyman, *Local Nucleation of Microtubule Bundles through Tubulin Concentration into a Condensed Tau Phase,* Cell Reports **20**, 2304 (2017).

[38] F. Fanalista, S. Deshpande, A. Lau, G. Pawlik, and C. Dekker, *FtsZ-Induced Shape Transformation of Coacervates,* Advanced Biosystems **1800136**, 1 (2018).

[39] E. te Brinke, J. Groen, A. Herrmann, H. A. Heus, G. Rivas, E. Spruijt, and W. T. S. Huck, *Dissipative adaptation in driven self-assembly leading to self-dividing fibrils,* Nature Nanotechnology **13**, 849 (2018).

[40] D. Zwicker, R. Seyboldt, C. A. Weber, A. A. Hyman, and F. Jülicher, *Growth and division of active droplets provides a model for protocells,* Nature Physics **13**, 408 (2017).

[41] S. L. Miller, J. William Schopf, and A. Lazcano, *Oparin's "origin of life": Sixty years later,* Journal of Molecular Evolution **44**, 351 (1997).

[42] J. F. Lutkenhaus, H. Wolf-Watz, and W. D. Donachie, *Organization of genes in the ftsA-envA region of the Escherichia coli genetic map and identification of a new fts locus (ftsZ),* Journal of Bacteriology **142**, 615 (1980).

[43] E. Bi and J. Lutkenhaus, *FtsZ ring structure associated with division in Escherichia coli,* Nature **354**, 161 (1991).

[44] A. Mukherjee and J. Lutkenhaus, *Guanine nucleotide-dependent assembly of FtsZ into filaments,* Journal of Bacteriology **176**, 2754 (1994).

[45] A. Mukherjee and J. Lutkenhaus, *Dynamic assembly of FtsZ regulated by GTP hydrolysis,* EMBO Journal **17**, 462 (1998).

[46] H. P. Erickson, *FtsZ, a prokaryotic homolog of tubulin?* Cell **80**, 367 (1995).

[47] K. H. Huang, J. Durand-Heredia, and A. Janakiraman, *FtsZ ring stability: Of bundles, tubules, crosslinks, and curves,* Journal of Bacteriology **195**, 1859 (2013).

[48] A. Mukherjee and J. Lutkenhaus, *Analysis of FtsZ Assembly by Light Scattering and Determination of the Role of Divalent Metal Cations Analysis of FtsZ Assembly by Light Scattering and Determination of the Role of Divalent Metal Cations,* Journal of Bacteriology **181**, 823 (1999).

[49] J. M. González, M. Jiménez, M. Vélez, J. Mingorance, J. M. Andreu, M. Vicente, and G. Rivas, *Essential cell division protein FtsZ assembles into one monomer-thick ribbons under conditions resembling the crowded intracellular environment,* Journal of Biological Chemistry **278**, 37664 (2003).

[50] J. Löwe and L. A. Amos, *Tubulin-like protofilaments in Ca2+-induced FtsZ sheets,* EMBO Journal **18**, 2364 (1999).

[51] J. Groen, D. Foschepoth, E. Te Brinke, A. J. Boersma, H. Imamura, G. Rivas, H. A. Heus, and W. T. Huck, *Associative interactions in crowded solutions of biopolymers counteract depletion effects,* Journal of the American Chemical Society **137**, 13041 (2015).

[52] S. D. Redick, J. Stricker, G. Briscoe, P. Erickson, and H. P. Erickson, *Mutants of FtsZ Targeting the Protofilament Interface : Effects on Cell Division and GTPase Activity Mutants of FtsZ Targeting the Protofilament Interface : Effects on Cell Division and GTPase Activity,* Society **187**, 2727 (2005).

[53] J. Löwe and L. A. Amos, *Crystal structure of the bacterial cell division protein FtsZ.* Nature **391**, 203 (1998).

[54] P. J. Buske and P. A. Levin, *A flexible C-terminal linker is required for proper FtsZ assembly in vitro and cytokinetic ring formation in vivo,* Molecular Microbiology **89**, 249 (2013).

[55] K. A. Gardner, D. A. Moore, and H. P. Erickson, *The C-terminal linker of Escherichia coliFtsZ functions as an intrinsically disordered peptide,* Molecular Microbiology **89**, 264 (2013).

[56] P. J. Buske and P. A. Levin, *Extreme C terminus of bacterial cytoskeletal protein FtsZ plays fundamental role in assembly independent of modulatory proteins,* Journal of Biological Chemistry **287**, 10945 (2012).

[57] S. Rueda, M. Vicente, and J. Mingorance, *Concentration and assembly of the division ring proteins FtsZ, FtsA, and ZipA during the Escherichia coli cell cycle,* Journal of Bacteriology **185**, 3344 (2003).

[58] L. Mosyak, Y. Zhang, E. Glasfeld, S. Haney, M. Stahl, J. Seehra, and S. W. Somers, *The bacterial cell-division protein ZipA and its interaction with an FtsZ fragment revealed by X-ray crystallography,* The EMBO Journal **19**, 3179 (2000).

[59] Z. Liu, A. Mukherjee, and J. Lutkenhaus, *Recruitment of ZipA to the division site by interaction with FtsZ,* Molecular Microbiology **31**, 1853 (2003).

[60] S. Pichoff and J. Lutkenhaus, *Unique and overlapping roles for ZipA and FtsA in septal ring assembly in Escherichia coli,* EMBO Journal **21**, 685 (2002).

[61] C. A. Hale and P. A. J. De Boer, *Recruitment of ZipA to the septal ring of Escherichia coli is dependent on FtsZ and independent of FtsA,* Journal of Bacteriology **181**, 167 (1999).

[62] W. Margolin, *Themes and variations in prokaryotic cell division,* FEMS microbiology reviews **24**, 531 (2000).

[63] B. Geissler, D. Elraheb, and W. Margolin, *A gain-of-function mutation in ftsA bypasses the requirement for the essential cell division gene zipA in Escherichia coli,* Proceedings of the National Academy of Sciences of the United States of America **100**, 4197 (2003).

[64] C. A. Hale, A. C. Rhee, P. A. J. D. Boer, and A. M. Y. C. Rhee, *ZipA-Induced Bundling of FtsZ Polymers Mediated by an Interaction between C-Terminal Domains ZipA-Induced Bundling of FtsZ Polymers Mediated by an Interaction between C-Terminal Domains,* Society **182**, 5153 (2000).

[65] A. Kuchibhatla, A. Bhattacharya, and D. Panda, *ZipA binds to FtsZ with high affinity and enhances the stability of FtsZ protofilaments,* PLoS ONE **6**, 4 (2011).

[66] V. M. Hernández-Rocamora, B. Reija, C. García, P. Natale, C. Alfonso, A. P. Minton, S. Zorrilla, G. Rivas, and M. Vicente, *Dynamic interaction of the Escherichia coli cell division ZipA and FtsZ proteins evidenced in nanodiscs,* Journal of Biological Chemistry **287**, 30097 (2012).

[67] V. M. Hernández-Rocamora, C. García-Montañés, G. Rivas, and O. Llorca, *Reconstitution of the Escherichia coli cell division ZipA-FtsZ complexes in nanodiscs as revealed by electron microscopy,* Journal of Structural Biology **180**, 531 (2012).

[68] M. Krupka, M. Sobrinos-Sanguino, M. Jiménez, G. Rivas, and W. Margolin, *Escherichia coli ZipA Organizes FtsZ Polymers into Dynamic Ring-Like Protofilament Structures,* mBio **9**, 1 (2018).

[69] M. Krupka, V. W. Rowlett, D. Morado, H. Vitrac, K. Schoenemann, J. Liu, and W. Margolin, *Escherichia coli FtsA forms lipid-bound minirings that antagonize lateral interactions between FtsZ protofilaments,* Nature Communications **8**, 1 (2017).

[70] M. Loose and T. J. Mitchison, *The bacterial cell division proteins ftsA and ftsZ self-organize into dynamic cytoskeletal patterns,* Nature Cell Biology **16**, 38 (2014).

[71] A. W. Bisson-Filho, Y. P. Hsu, G. R. Squyres, E. Kuru, F. Wu, C. Jukes, Y. Sun, C. Dekker, S. Holden, M. S. VanNieuwenhze, Y. V. Brun, and E. C. Garner, *Treadmilling by FtsZ filaments drives peptidoglycan synthesis and bacterial cell division,* Science **355**, 739 (2017).

[72] F. J. Gueiros-Filho and R. Losick, *A widely conserved bacterial cell division protein that promotes assembly of the tubulin-like protein FtsZ,* Genes and Development **16**, 2544 (2002).

[73] D. W. Adams and J. Errington, *Bacterial cell division: Assembly, maintenance and disassembly of the Z ring,* Nature Reviews Microbiology **7**, 642 (2009).

[74] P. A. Levin, I. G. Kurtser, and A. D. Grossman, *Identification and characterization of a negative regulator of FtsZ ring formation in Bacillus subtilis,* Proceedings of the National Academy of Sciences of the United States of America **96**, 9642 (1999).

[75] J. Männik and M. W. Bailey, *Spatial coordination between chromosomes and cell division proteins in Escherichia coli,* Frontiers in Microbiology **6**, 1 (2015).

[76] P. A. de Boer, R. E. Crossley, and L. I. Rothfield, *A division inhibitor and a topological specificity factor coded for by the minicell locus determine proper placement of the division septum in E. coli,* Cell **56**, 641 (1989).

[77] Z. Hu, E. P. Gogol, and J. Lutkenhaus, *Dynamic assembly of MinD on phospholipid vesicles regulated by ATP and MinE,* Proceedings of the National Academy of Sciences of the United States of America **99**, 6761 (2002).

[78] M. Loose, E. Fischer-Friedrich, C. Herold, K. Kruse, and P. Schwille, *Min protein patterns emerge from rapid rebinding and membrane interaction of MinE,* Nature Structural and Molecular Biology **18**, 577 (2011).

[79] M. Loose, E. Fischer-friedrich, J. Ries, K. Kruse, and P. Schwille, *Spatial Regulators for Bacterial Cell Division Self-Organize into Surface Waves in Vitro,* Science (New York, N.Y.) **320**, 789 (2008).

[80] F. Wu, B. G. Van Schie, J. E. Keymer, and C. Dekker, *Symmetry and scale orient Min protein patterns in shaped bacterial sculptures,* Nature Nanotechnology **10**, 1 (2015).

[81] Y. Caspi and C. Dekker, *Mapping out Min protein patterns in fully confined fluidic chambers,* eLife **5**, e19271 (2016).

[82] K. Zieske and P. Schwille, *Reconstitution of pole-to-pole oscillations of min proteins in microengineered polydimethylsiloxane compartments,* Angewandte Chemie - International Edition **52**, 459 (2013).

[83] P. A. de Boer and D. M. Raskin, *Rapid pole-to-pole oscillation of a protein required for directing division to the middle of Escherichia coli.* Proceedings of the National Academy of Sciences of the United States of America **96**, 4971 (1999).

[84] Z. Hu and J. Lutkenhaus, *Topological regulation of cell division in Escherichia coli involves rapid pole to pole oscillation of the division inhibitor MinC under the control of MinD and MinE,* Molecular Microbiology **34**, 82 (1999).

[85] Z. Hu, A. Mukherjee, S. Pichoff, and J. Lutkenhaus, *The MinC component of the division site selection system in Escherichia coli interacts with FtsZ to prevent polymerization,* Proceedings of the National Academy of Sciences of the United States of America **96**, 14819 (1999).

[86] S. C. Cordell, R. E. Anderson, and J. Löwe, *Crystal structure of the bacterial cell division inhibitor MinC,* EMBO Journal **20**, 2454 (2001).

[87] H. Cho, H. R. McManus, S. L. Dove, and T. G. Bernhardt, *Nucleoid occlusion factor SlmA is a DNA-activated FtsZ polymerization antagonist,* Proceedings of the National Academy of Sciences **108**, 3773 (2011).

[88] S. Du and J. Lutkenhaus, *SlmA Antagonism of FtsZ Assembly Employs a Two-pronged Mechanism like MinCD,* PLoS Genetics **10** (2014).

[89] L. J. Wu and J. Errington, *Coordination of cell division and chromosome segregation by a nucleoid occlusion protein in Bacillus subtilis,* Cell **117**, 915 (2004).

[90] J. Männik, F. Wu, F. J. Hol, P. Bisicchia, D. J. Sherratt, J. E. Keymer, and C. Dekker, *Robustness and accuracy of cell division in Escherichia coli in diverse cell shapes,* Proceedings of the National Academy of Sciences of the United States of America **109**, 6957 (2012).

[91] M. W. Bailey, P. Bisicchia, B. T. Warren, D. J. Sherratt, and J. Männik, *Evidence for Divisome Localization Mechanisms Independent of the Min System and SlmA in Escherichia coli,* PLoS Genetics **10** (2014).

[92] C. D. Rodrigues and E. J. Harry, *The min system and nucleoid occlusion are not required for identifying the division site in bacillus subtilis but ensure its efficient utilization,* PLoS Genetics **8** (2012).

[93] O. Espéli, R. Borne, P. Dupaigne, A. Thiel, E. Gigant, R. Mercier, and F. Boccard, *A MatP-divisome interaction coordinates chromosome segregation with cell division in E. coli,* EMBO Journal **31**, 3198 (2012).

[94] H. P. Erickson, D. E. Anderson, and M. Osawa, *FtsZ in Bacterial Cytokinesis: Cytoskeleton and Force Generator All in One,* Microbiology and Molecular Biology Reviews **74**, 504 (2010).

[95] J. Xiao and E. D. Goley, *Redefining the roles of the FtsZ-ring in bacterial cytokinesis,* Current Opinion in Microbiology **34**, 90 (2016).

[96] M. Osawa, D. E. Anderson, and H. P. Erickson, *Curved FtsZ protofilaments generate bending forces on liposome membranes,* EMBO Journal **28**, 3476 (2009).

[97] E. J. Cabré, A. Sánchez-Gorostiaga, P. Carrara, N. Ropero, M. Casanova, P. Palacios, P. Stano, M. Jiménez, G. Rivas, and M. Vicente, *Bacterial division proteins FtsZ and ZipA induce vesicle shrinkage and cell membrane invagination,* Journal of Biological Chemistry **288**, 26625 (2013).

[98] P. Szwedziak, Q. Wang, T. A. M. Bharat, M. Tsim, and J. Löwe, *Architecture of the ring formed by the tubulin homologue FtsZ in bacterial cell division,* eLife **3**, e04601 (2014).

[99] G. Lan, B. R. Daniels, T. M. Dobrowsky, D. Wirtz, and S. X. Sun, *Condensation of FtsZ filaments can drive bacterial cell division,* Proceedings of the National Academy of Sciences **106**, 121 (2008).

[100] G. Fu, T. Huang, J. Buss, C. Coltharp, Z. Hensel, and J. Xiao, *In Vivo structure of the E. coli FtsZ-ring revealed by photoactivated localization microscopy (PALM),* PLoS ONE **5**, 1 (2010).

[101] S. J. Holden, T. Pengo, K. L. Meibom, C. F. Fernandez, J. Collier, and S. Manley, *High throughput 3D super-resolution microscopy reveals Caulobacter crescentus in vivo Z-ring organization,* Proceedings of the National Academy of Sciences of the United States of America **111**, 4566 (2014).

[102] C. Lu, M. Reedy, and H. P. Erickson, *Straight and curved conformations of FtsZ are regulated by GTP hydrolysis,* Journal of Bacteriology **182**, 164 (2000).

[103] Y. Li, J. Hsin, L. Zhao, Y. Cheng, W. Shang, K. C. Huang, H.-W. Wang, and S. Ye, *FtsZ Protofilaments Use a Hinge-Opening Mechanism for Constrictive Force Generation,* Science **341**, 392 LP (2013).

[104] J. Conti, M. G. Viola, and J. L. Camberg, *FtsA reshapes membrane architecture and remodels the Z-ring in Escherichia coli,* Molecular Microbiology **107**, 558 (2018).

[105] X. Yang, Z. Lyu, A. Miguel, R. Mcquillen, and K. C. Huang, *GTPase activity – coupled treadmilling of the bacterial tubulin FtsZ organizes septal cell wall synthesis,* Science **747**, 744 (2017).

[106] B. Söderström, K. Skoog, H. Blom, D. S. Weiss, G. von Heijne, and D. O. Daley, *Disassembly of the divisome in Escherichia coli: Evidence that FtsZ dissociates before compartmentalization,* Molecular Microbiology **92**, 1 (2014).

[107] J. M. Monteiro, A. R. Pereira, N. T. Reichmann, B. M. Saraiva, P. B. Fernandes, H. Veiga, A. C. Tavares, M. Santos, M. T. Ferreira, V. Macário, M. S. VanNieuwenhze, S. R. Filipe, and M. G. Pinho, *Peptidoglycan synthesis drives an FtsZ-treadmilling-independent step of cytokinesis,* Nature **554**, 528 (2018).

[108] D. O. Daley, U. Skoglund, and B. Söderström, *FtsZ does not initiate membrane constriction at the onset of division,* Scientific Reports **6**, 33138 (2016).

[109] J. Lutkenhaus, *FtsN—trigger for septation,* Journal of bacteriology **191**, 7381 (2009).

[110] D. S. Weiss, *Last but not least: New insights into how FtsN triggers constriction during Escherichiacoli cell division,* Molecular Microbiology **95**, 903 (2015).

2

SHAPE AND SIZE CONTROL OF ARTIFICIAL CELLS FOR BOTTOM-UP BIOLOGY

Bottom-up biology is an expanding research field that aims to understand the mechanisms underlying biological processes via in vitro assembly of their essential components in synthetic cells. As encapsulation and controlled manipulation of these elements is a crucial step in the recreation of such cell-like objects, microfluidics is increasingly used for the production of minimal artificial containers such as single-emulsion droplets, double-emulsion droplets, and liposomes. Despite the importance of cell morphology on cellular dynamics, current synthetic-cell studies mainly use spherical containers, and methods to actively shape manipulate these have been lacking. In this paper, we describe a microfluidic platform to deform the shape of artificial cells into a variety of shapes (rods and discs) with adjustable cell-like dimensions below 5 μm, thereby mimicking realistic cell morphologies. To illustrate the potential of our method, we reconstitute three biologically relevant protein systems (FtsZ, microtubules, collagen) inside rod-shaped containers and study the arrangement of the protein networks inside these synthetic containers with physiologically relevant morphologies resembling those found in living cells.

This chapter has been published: F. Fanalista, A. Birnie, R. Maan, F. Burla, K. Charles, G. Pawlik, S. Deshpande, G. H. Koenderink, M. Dogterom, and C. Dekker, *Shape and Size Control of Artificial Cells for Bottom-Up Biology*, ACS Nano 13, 5439 (2019).

2.1. INTRODUCTION

Throughout evolution, cells have radiated into a dazzling variety of morphologies, where prokaryotes are found in the shape of, for example, rods, spheres, and spirals,[1] archaea can exhibit even triangular or flattened square shapes,[2] and eukaryotic cells range from orderly shaped plant cells[3] to the extensively branched dendritic cells of the immune system.[4] This wide morphological diversity raises questions on the underlying reasons and the interplay between morphology and the myriad of internal cellular processes. The shape and size of a cell are the product of internal molecular processes that drive cellular growth and division and are also guided by external environmental factors such as the surrounding cells or simply the amount of available space. The cellular container shell itself is maintained by cytoskeleton and membrane machineries[5–9] that are present in all kingdoms of life. Unicellular organisms may benefit from specific shapes for a selective advantage,[7, 10] while for multicellular organisms, the cellular morphology is closely linked to cell–cell interactions and the extracellular matrix (ECM).[11, 12] Similarly, cells in colonies of unicellular organisms such as biofilms display a morphological variation depending on their function at a particular position and time within the colony lifecycle.[13, 14] To accommodate such variations in morphology, the processes inside a cell should be robust against variations of the cellular shape. For example, to ensure faithful division, pattern-formation processes should successfully guide the cellular division machinery to the right location, irrespective of the precise shape and size of the cellular boundary.[15, 16] The mechanisms through which such processes remain robust in varying environments and boundary conditions are a topic of active research.[17] Confinement and shape not only influence cellular processes but also have an effect on extracellular structures such as the ECM, the fibrous network located in the space between eukaryotic cells in tissues and prokaryotic cells in biofilms.[18, 19] The large morphological variety of cells also poses interesting questions from the perspective of polymer physics. Cells contain many polymers, such as cytoskeletal components and the genomic material. The spatial distribution and dynamics of polymers are in general sensitive to the spatial confinement,[20–25] and as a result, biopolymers such as actin networks[26] and the genome[27–29] will re-organize upon morphological perturbation of the cellular container. Confronted with the imposing complexity and connectivity of cellular processes, researchers are aiming to reconstitute essential cellular systems with a minimal set of components inside controlled confinements.[30, 31]The nature of the artificial containers used in these endeavors is quite diverse, ranging from liposomes, single-emulsion droplets (water-in-oil droplets, from now on called droplets), to double-emulsion droplets (water-in-oil-in-water droplets, henceforth called double emulsions) and even solid-state microchambers.[32, 33] With such bottom-up approaches, cytoskeletal components (*e.g.*, actin,[34] tubulin,[35] MreB,[36], FtsZ[37]), cytokinesis and segregation machinery (*e.g.*, actin-myosin rings,[38] mitotic spindles[39]), cell-free expression systems (*e.g.*, cell extracts,[40] PURE system[41]), pattern formation systems (*e.g.*, the Min system[42]), and genomes[43] can be encapsulated inside such artificial containers (Fig. 2.1, top).

The shape of the artificial containers is an often-overlooked parameter in mimicking cells. Indeed, thus far, the majority of synthetic cell studies used simple spherical containers with a diameter of 10-50 μm.[32] However, most living cells are nonspher-

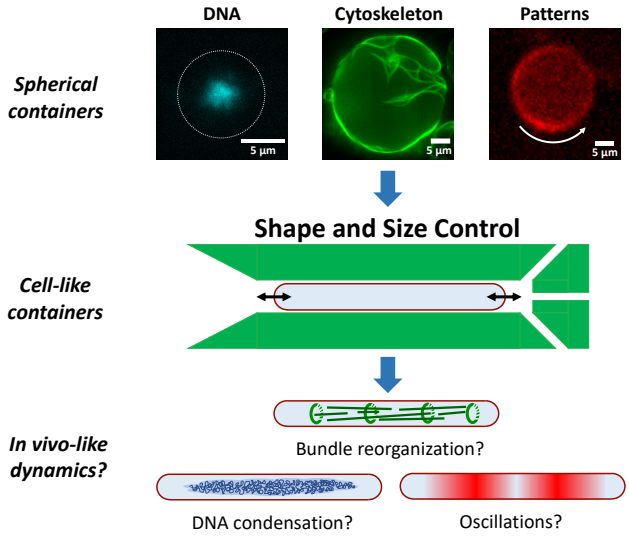

Figure 2.1: **Shape and size control of synthetic cells to explore the influence of confinement and geometry on cellular processes.** Most current approaches to bottom-up biology encapsulate purified cellular components inside large, spherical containers. For example, on the top row, three prokaryotic key systems, which in some form are present in all kingdoms of life, are reconstituted in spherical droplets: DNA (*E. coli* nucleoid, blue), cytoskeletal components (FtsZ, green), and pattern formation systems (Min proteins, red). However, these key systems are, like most processes and structures inside a cell, sensitive to the confinement size and the geometry. Using a microfluidic approach (middle), we manipulate the shape and size of the initially spherical synthetic cells. In this manner, we are able to experimentally access a set of parameters which were hitherto unexplored in the field of bottom-up biology. The method offers the possibility of observing more *in vivo*-like dynamics for various cellular systems encapsulated inside synthetic cells (bottom).

ical, and while this size range is fitting for eukaryotic cells, it applies much less so for the more abundant bacterial and archaeal cells. In the past two decades, research in bottom-up biology has also been performed in microfabricated chambers that allow for a range of shapes,[44–46] but those are obviously nondeformable, preventing the observation of dynamics as a function of changing confinement size. Furthermore, the open-top geometry ("a chamber without a roof") that was used in some cases[44] decreases the ratio between the bulk volume of the protein reservoir and the surface with which these proteins interact, introducing ambiguities in the local protein concentrations that are important for pattern-formation processes.[17] There have been some reports on the manipulation of spherical vesicles, but these efforts mainly concentrated on the immobilization of droplets through mechanical trapping[47–50] and some elaborated manipulation with dielectrophoresis.[51] While Boukellal *et al.* introduced a method to trap droplets in tubular-shaped confinements,[52] these containers were so large (upward of 100 µm) that they were not well applicable for synthetic cell research. Furthermore, methods to split containers on-chip by running them against T- or Y-shaped junctions have been developed both for droplets[53] and liposomes,[54] offering a tool to obtain containers with half the original volumes. Some osmosis-based size control of spherical droplets and double emulsions was demonstrated recently as well,[40, 43] but again, the

involved size ranges were not well suited for reconstituting bacterial systems in artificial cells. Here, we introduce a general microfluidic platform to control the shape and size of various deformable containers, from droplets to liposomes, at cell-like scales in the sub-5 μm range (Fig. 2.1, middle). Using this system, we are able to access the same shape and size parameter space as is present in the cells from which the reconstituted components are isolated. Specifically, we are able to shape various artificial cell containers into confinements with dimensions down to almost 1 μm. Furthermore, we demonstrate the ability to precisely and reversibly control the size of these containers. The method offers experimental avenues to unravel the interconnection between cellular processes and the confinement geometry. We provide examples for three biologically relevant protein systems (FtsZ, microtubules, collagen) inside rod-shaped containers. We anticipate that this platform will contribute to closing the gap between the dynamics in artificial cells and the *in vivo* dynamics of real cells (Fig. 2.1, bottom).

2.2. RESULTS

To obtain an efficient system for shaping artificial cells on-chip and impose user-defined dimensions to a variety of initially spherical containers, we designed and fabricated a simple but effective microfluidic chip with an array of local micropatterned structures ("traps"). We first tested the functionality of the design using water-in-oil droplets. Technical details of the experimental procedure, from the droplet production to the device design and operation, are described in Figure 2.8. Figure 2.2a shows an example of the shape manipulation process of a droplet that is transformed into a tubular geometry: a spherical droplet gets caught at the trap entrance and subsequently is reshaped into a cylindrical shape. Because of the presence of fluorescent lipids into the oil phase, the trap profile and the droplet are clearly distinguishable as dark regions. Fluid flow through the trap, necessary to catch the droplets, was ensured by including three exit holes that are visible at the end of the structure. The entrance of the traps has a conical funnel shape that narrows down to the predefined trap width, so that a minimal fluid pressure has to be applied to squeeze the droplets inside. Upon entering the trap, the droplet gets deformed and remains fixed in the desired shape. With an array of these traps, it is possible to stably observe tens of such rod-shaped droplets in a single field-of-view (Figure 2.9a). Aided by the precision provided by cleanroom-based fabrication techniques, we tested the versatility of our trap design over a wide range of confinements and aspect ratios. To mimic small organisms such as Escherichia coli, we mainly focused our efforts on obtaining small containers with diameters below 5 μm, thereby recreating the rod-shaped morphology that many bacteria possess.[1] By varying both the width of the traps and the overall height of the device, we obtained rod-shaped droplets of arbitrary lengths and widths ranging from 4.8 μm down to 1.4 μm (Fig. 2.2b and Fig. 2.9b). We determined the trapping efficiency of these designs as the ratio of the number of traps that stably contained a tubular droplet over the total number of traps present in the device: For the design with the largest trap width (4.8 μm, Fig. 2.2b), we found that 98% of the traps (N = 103/105) contained a rod-shaped droplet. Designs with narrower traps have a higher hydrodynamic resistance[55] and hence require higher fluid pressures and, as a result, are less straightforward to operate. For the design with the narrowest traps achieved in this work (1.4 μm, Fig. 2.2b), we found that 33% (N = 19/57) of the traps con-

tained a rod-shaped droplet. We also explored the potential of our microfluidics-based approach to deform spherical droplets into flat circular discs ("pancakes"). To do so, we employed multiheight microfluidic devices. Figure 2.2c shows an example where spherical droplets first travel undeformed within a large channel of 15 μm height. When they encounter narrower channels of 2 μm height, they are forced into the confining channels by the fluid pressure and consequently are deformed into pancake-like containers that mimic the morphology of, for example, certain disc-shaped archaea.[2] In addition, the disc-shaped droplets can be immobilized and stored for analysis in an array of microfluidic traps, as shown in Figure 2.8c.

Another fascinating aspect of living systems is the capacity of cellular processes to adapt and re-arrange over time as the cell changes during its growth and life cycle. To enable the investigation of such phenomena in vitro, isolated cellular components should be reconstituted into artificial containers with a size that can be controllably changed over time. Using a system inspired by the work of Shim *et al.*,[56] we managed to vary the size of the droplets captured in the traps. Specifically, we assembled a multilayer polydimethylsiloxane (PDMS) device consisting of three parts, see Figure 2.3a: a thick rectangular piece of PDMS containing a hole ("water chamber") sitting on top of a thin layer imprinted with microfluidic traps, which in its turn is sealed off at the bottom by a PDMS-covered glass coverslip. By taking advantage of the fact that PDMS is permeable to water, it is possible to induce osmosis between the droplets and the water chamber through the thin PDMS membrane that separates them. Consequently, when the aqueous solution of the droplets has a salt concentration lower or higher compared to the one in the water chamber, water is able to flow across the PDMS membrane to restore isotonicity, leading to, respectively, shrinking or expanding droplets. When forced into a tubular shape, the droplets consequently re-adjusted their volume by shortening or elongating along their main axis inside the traps (Fig. 2.3b, left and right). Immediately after the trapping, for the first 20 min, the length of the droplets changed quickly to reduce the osmolarity difference with the water chamber. As the osmotic balance between the droplets and the water chamber is approached, the size of the droplets tended to stabilize. By contrast, in isotonic conditions, the volume of the droplets remained approximately constant (Fig. 2.3b, middle).

Beyond droplets, we explored size and shape manipulation of containers that are physiologically closer to living cells, namely, double emulsions and liposomes. We used our microfluidic octanol-assisted liposome assembly (OLA) platform to produce double emulsions on-chip (Fig. 2.4a). By dissolving the lipids in oleic acid, the double emulsions undergo a process of partial dewetting,[57, 58] by which the excess solvent and lipids accumulate in a side pocket. The volume of double emulsions can be varied using an applied osmotic pressure difference due to new buffer fluid that is administered through side channels (Fig. 2.4a). Upon inducing such volume changes, excess material in the side-pocket may act as a reservoir to concurrently re-adjust the surface area (Fig. 2.4b). In other words, as the water flows through the membrane to restore osmotic balance, the surface automatically re-adjusts its area to fit the new volume, using the side pocket as a source or sink for membrane lipids. To check this hypothesis, we produced and immobilized oleic acid double emulsions in an array of traps (Fig. 2.4c). Next, an aqueous solution was flushed *via* a feeding channel to create an osmotic imbalance be-

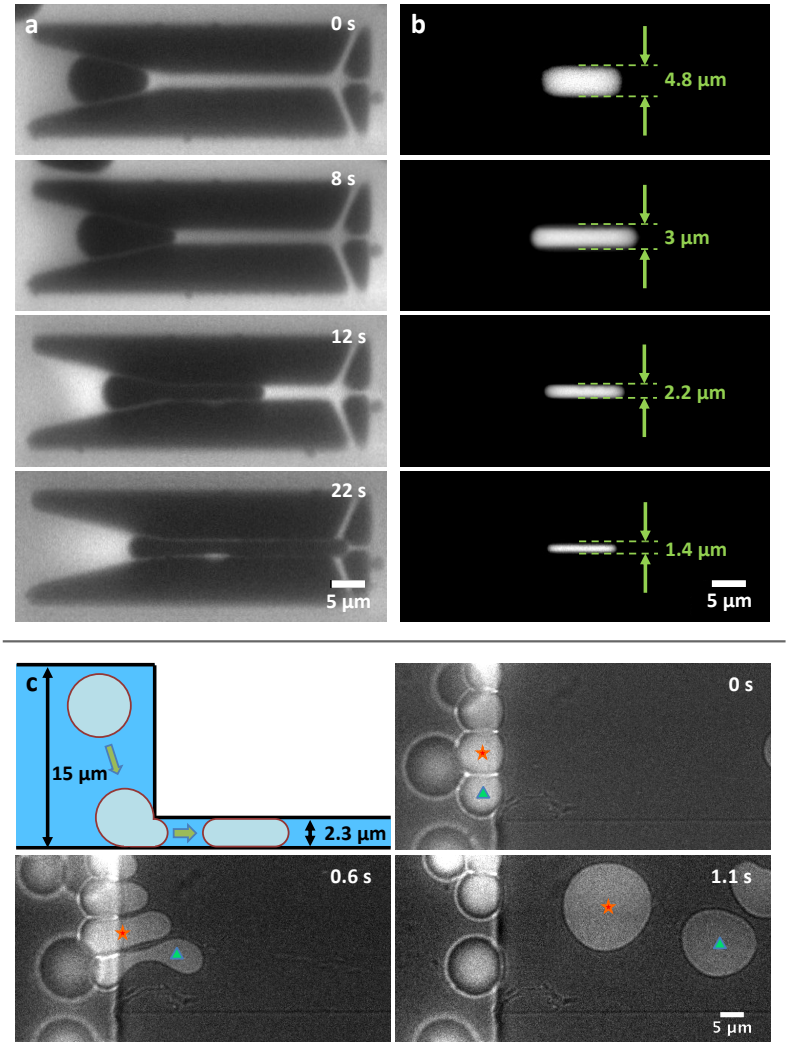

Figure 2.2: **Shape control of water-in-oil droplets *via* microfluidic structures.** (a) Droplet loading into a tubular trap: the droplet is captured at the entrance of the trap and progressively squeezed into the confinement, assuming the imposed geometry. RhodPE lipids are dissolved in the oil phase to enhance the contrast between the oil phase, the aqueous phase, and the profile of the trap. (b) The tubular trap design offers the possibility to deform droplets into rod-shaped geometries of different dimensions. To visualize the droplets, Alexa647 fluorescent dye is encapsulated in the aqueous phase. (c) A multiheight microfluidic device is used for the deformation of spherical droplets into thin disc-shaped containers or "pancakes". As they pass from a 15 µm to a 2 µm high channel, the spherical droplets get consequently squeezed into a disc shape. The figure shows the deformation process of two droplets, marked with a red star and green triangle. The images combine both bright-field and fluorescent signals from the Alexa647 fluorescent dye encapsulated inside the droplets.

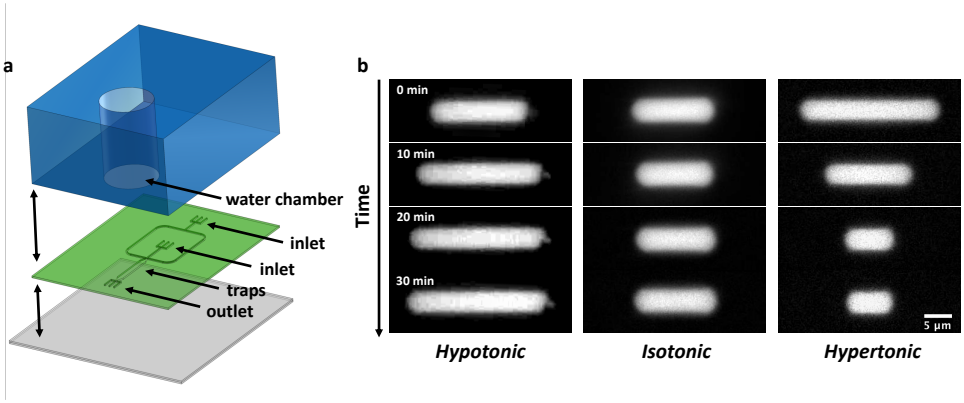

Figure 2.3: **Size control of water-in-oil droplets *via* a multilayer microfluidic device.** (a) Schematic of the three different layers composing the device. The bottom layer (gray) consists of a PMDS-covered glass coverslip, followed by a second layer (green) of a thin PDMS membrane imprinted with the microfluidic channels and traps design. The design includes two inlet channels, the first one for the droplets and a second one for oil, which cross each other in a large T-junction. After this junction, a single large channel leads to the array of traps to capture and manipulate the droplets. The third layer (blue) is a thicker piece of PDMS containing a water chamber, placed above the array of traps. (b) Water-in-oil droplets contain Alexa647 for visualization and 200 mM KCl. Depending on the relative salt concentration between the water chamber and the droplets, different behaviors are observed over time: in hypotonic conditions (100 mM KCl in water chamber), the droplets expand (left); in isotonic conditions (200 mM KCl in the water chamber), the droplet size remains qualitatively stable (center); and in hypertonic conditions (300 mM KCl in the water chamber), the droplets shrink consistently relative to their original volume (right).

tween the inner and outer aqueous environment of the double emulsions. In hypertonic conditions, the osmosis process led to a fast reduction of the double emulsion volume (Fig. 2.4d, top), which shrank from an average diameter value $d = 12.3 \pm 0.1$ µm down to $d = 7.5 \pm 0.1$ µm (N = 45). Simultaneously, the membrane surface area re-adjusted to the new volume, with a consequent visible growth of the side pockets. When the original osmotic conditions were restored, the same double emulsions underwent the inverse process (Fig. 2.4d, bottom): the volume expanded back close to the original size ($d = 11.1 \pm 0.2$ µm), with an associated membrane area increase at the cost of the side pocket, showing that the process is largely reversible. Looking at the variation of the double emulsion diameters over time compared to their original size (Fig. 2.4e), the shrinkage and the expansion processes appeared symmetric. The size variation was initially slow and then was followed by a phase of faster size change. As the osmolarity difference between the outer and the inner aqueous phases was re-equilibrated, the size variation slowed down again. The degree by which the double emulsions shrank or expanded under, respectively, hypertonic or hypotonic conditions was quantified by measuring the diameter of each double emulsion after and before each size manipulation. The ratio between these

diameters was obtained, and two distinct peaks are observed (Fig. 2.4f). This indicates that specific osmolarity differences lead to specific volume re-adjustments and that the size manipulation is a well-controlled process. These data show that the size of the double emulsions can be tuned through the surrounding osmotic conditions in a reversible manner, providing artificial scaffolds for reconstituting cellular systems into containers of adaptable size.

Encouraged by the ease of the size manipulation of double emulsions, we verified that it is possible to deform them into rod shapes resembling bacterial cells. To do so, we punched a hole at the end of the microfluidic circuit ("collection well", Fig. 2.5a) and collected double emulsions from the well to transfer them into the device containing the tubular traps. The insertion of double emulsions into the traps is found to be significantly aided by the presence of the side-pocket, since the membrane can dynamically adapt to the new geometry by using material from the side-pocket reservoir to accommodate the changing surface-to-volume ratio. Figure 2.4c–d shows two examples where we deformed double emulsions into tubular geometries with widths of 4 and 1.3 μm. For the former design, we found that a trapping yield of nearly 100% (Fig. 2.5b) is easily achievable, meaning that essentially all the traps (N = 105 per device) contained a double emulsion after a few minutes. As with droplets, filling smaller traps appeared more difficult as double emulsions occasionally broke as a result of the higher pressure required for the entrapping due to the higher hydrodynamic resistance.[55] Given that the deformation of double emulsions worked for the traps with dimensions as small as 1.3 μm, we assumed that it would also be successful for the larger sizes explored with droplets (Fig. 2.2b). Next to double emulsions, we also explored the deformation of liposomes from spherical into other shapes. Since liposomes only tolerate a small areal strain (5%) before rupture,[59] we induced an external osmotic pressure to create a reduced volume and thus excess surface area,[60] which made the liposomes "floppy" and predisposed to accommodate the increase in surface-to-volume ratio upon shape change. When transferred inside the trap device, we observed a fraction of liposomes that successfully deformed into the traps, alongside with liposomes showing various defects (Fig. 2.10a). Possibly, the induced floppiness made the liposomes prone to damage during the transfer process into the trap device, resulting in the observed heterogeneous population. Still, we managed to obtain liposomes comparable in size and shape to *E. coli* cells (Fig. 2.10b), which is a helpful step toward the proper recreation of artificial minimal cells.

To illustrate how our platform can be useful for applications in the synthetic cell field, we encapsulated a variety of fiber-network forming proteins inside nonspherical containers. For these experiments, we chose droplets, due to the ease of their production process. Specifically, we studied three important proteins from diverse biological systems and environments: FtsZ, a key protein necessary for division in almost all bacteria;[61] its eukaryotic homologue tubulin, which is a key element of the cytoskeleton in eukaryotic cells; and collagen,[62] the most abundant protein in extracellular matrix structures. First, to reconstitute FtsZ bundles on a membrane, we assembled a lipid monolayer at the water-oil interface of droplets by adding a mixture of DOPC and DGS-NTA lipids to the oil phase. ZipA, a protein responsible to anchor FtsZ to the membrane in Gammaproteobacteria (like *E. coli*),[63] is added to the inner aqueous phase (Fig. 2.6a, bottom), providing to FtsZ-filaments a way to properly dock to the mem-

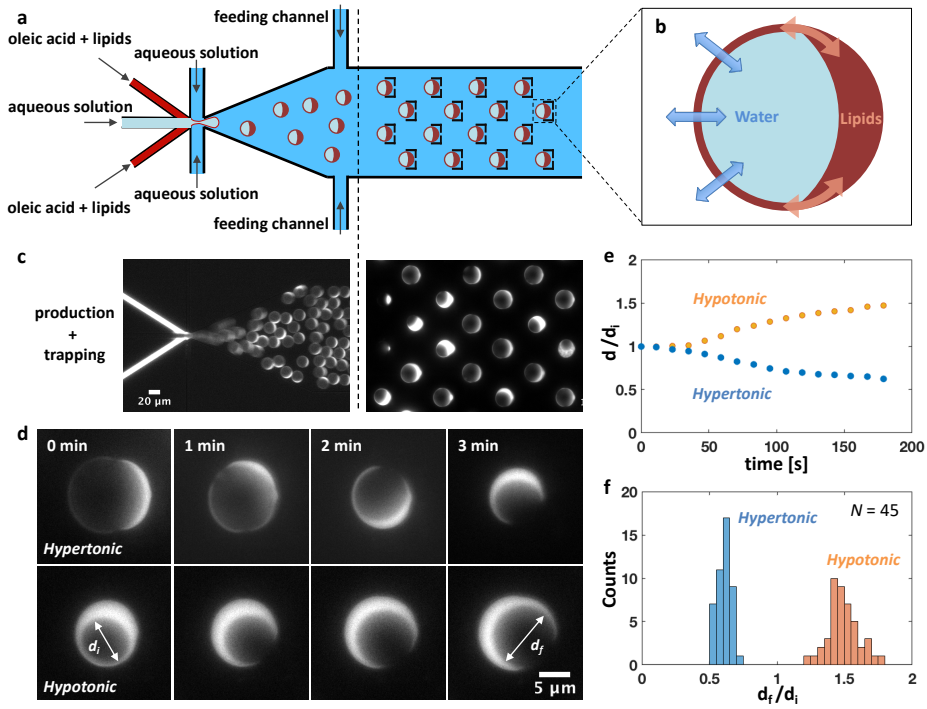

Figure 2.4: **Size control of oleic acid double emulsions on-chip.** (a) Design of the microfluidic device: six channels containing an inner aqueous phase, a lipid phase, and an outer aqueous phase cross in a junction where double emulsions are produced. The inner aqueous solution blows a bubble into two streams of DOPC lipids dissolved in oleic acid. The resulting lipid film is pinched-off by the outer aqueous stream, and a double emulsion is formed. An array of traps downstream from the production junction immobilizes the double emulsions, and two additional feeding channels allow further adjustment of the outer aqueous solution forming the environment of the trapped double emulsions. (b) Schematic representation of an oleic acid double emulsion: by inducing an osmotic pressure difference, water is able to flow through the membrane to re-establish osmotic equilibrium. At the same time, the side pocket formed by the excess of lipids and solvent can serve as a reservoir for the surface to expand or shrink as required by the volume change. (c) Fluorescent image showing the production process and the trapping of oleic acid double emulsions on-chip. RhodPE fluorescent lipids allow the visualization of the lipid phase. (d) By inducing an osmotic pressure difference, it is possible to vary the size of double emulsions. Both inner aqueous and outer aqueous solutions initially contain 25 mM sucrose. After a solution containing 200 mM sucrose is flushed through the feeding channel, to re-establish osmotic equilibrium, the double emulsions consequently shrink (top). Afterward, the same batch of double emulsions is re-exposed to the original outer aqueous solution (bottom), so their volume re-expanded. (e) Size variation of double emulsions (N = 10) over time: in hypotonic or hypertonic conditions, the diameter of the double emulsions, respectively, increased or decreased over time. (f) Histogram showing the ratio of the double emulsion (N = 45) diameters measured at the end (d_f) and at the beginning (d_i) of both processes. In a hypertonic condition, the double emulsions shrink by an average factor of $d_f/d_i = 0.61 \pm 0.01$. When back in hypotonic conditions, we measured a factor $d_f/d_i = 1.49 \pm 0.02$.

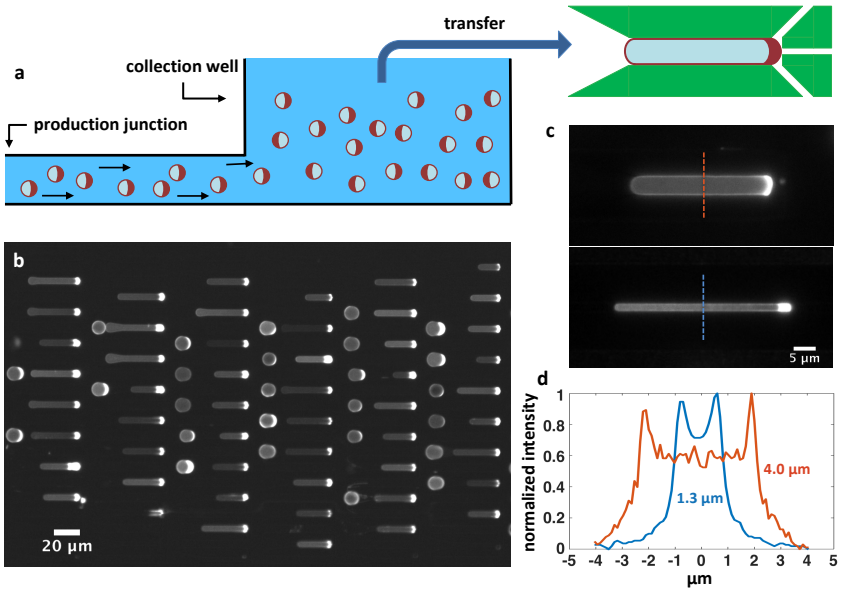

Figure 2.5: **Shape manipulation of oleic acid double emulsions on-chip.** (a) Schematic cross section of the collection well: at the end of the microfluidic circuit, after the production junction, a 4 mm diameter hole is punched. The double emulsions contain 5 mM dextran to make them denser than the environment and consequently sink to the bottom of the well. After sufficient production, double emulsions are pipetted from the well and introduced into a device containing the microfluidic traps. (b) Fluorescent image showing an array of double emulsions captured in tubular traps. Thanks to their side pocket, which serves as a membrane reservoir, double emulsions are easily reshaped, so that almost all traps in the device (N = 105) contained a double emulsion. Fluorescent signal comes from RhodPE lipids in the lipid phase. (c) Zoom-in of single double emulsions in tubular traps of different dimensions: 5 µm diameter (top) and 2 µm diameter (bottom). (d) Fluorescent profiles measured at the midcell cross section of tubular double emulsions. The peaks indicate the location of the membrane and provide a measure of the width of the double emulsion.

brane. To simplify the experiment, ZipA's N-terminus hydrophobic domain, responsible for membrane docking in cells, was replaced by a His-tag to increase protein solubility in water. Through fluorescent labeling of FtsZ it is possible to visualize how its filamentous bundles are localized on the surface of tubular droplets confined in the traps (Fig. 2.6a, middle), as is also observed in spherical droplets (Fig. 2.6a, top). The clear presence of bundles on the surface, compared to the lumen, indicate the successful attachment of FtsZ to the lipid monolayer at the interface. Next, we tested whether it is possible to grow microtubules inside the rod-shaped droplets. Tubulin seeds bound to nonhydrolyzable guanosine triphosphate (GMPCPP) were co-encapsulated in the inner aqueous solution, together with tubulin dimers and guanosine triphosphate (GTP) (Fig. 2.6b, middle). As GTP hydrolysis is required for the disassembly of microtubules, the tubulin seeds act as

a stable template from which the microtubules can grow. Since the seeds and the tubulin dimers were labeled with different dyes, it was possible to observe long microtubules (green) that were grown from the seeds (red) and spanned the length of the rod-shaped droplet following the prevalent axis of symmetry (Fig. 2.6b, right), contrasting to the situation in spherical droplets (Fig. 2.6a, left), where the microtubules grew without an obvious preferential orientation. This observation is confirmed by a quantitative analysis of the microtubule orientations: in the spherical droplets, microtubules did not show any strong preferential orientation, while in rod-shaped droplets, the measured angles distinctly peaked around zero degrees, that is, the microtubules were aligned along the droplet main axis (Fig. 2.6b, right). Finally, we applied our method to an in vitro assay for collagen type 1, which is an important component of the extracellular matrix. Fig. 2.6c shows that it is possible to successfully reconstitute collagen type 1 fibers inside rod-shaped droplets. Similar to the microtubules, a quantitative analysis of the fiber orientations (Fig. 2.6c, right) showed that the collagen fibers oriented themselves along the symmetry axis of the cylindrical container, which again is markedly different to what is observed in spherical droplets.

2.3. DISCUSSION

In this paper, we presented a method that enables the control of the shape and the size of a range of cell-like containers, a useful research tool within the synthetic cell field. In fact, as is schematically illustrated in Fig. 2.7, our system provides access to a much broader range of morphologies than is currently possible in the synthetic cell field. By pushing the boundaries of both volume and aspect ratio by 1-2 orders of magnitude as compared to previous methods, we bridged the gap between the dimensions of natural cells and artificial containers inside which the isolated cellular components are reconstituted.

We showed that droplets, double emulsions, and liposomes can be deformed into a variety of shapes, from tubes of different diameters and lengths, to pancake-shape discs with a high aspect ratio between their height and diameter. Second, through the principle of osmosis, we were able to regulate the volume of such artificial cells. And finally, as a proof-of-concept of the range of possibilities that our approach offers, we encapsulated three different filamentous protein networks inside droplets with a tubular shape. The resulting organization of the protein networks in the tubular containers was markedly different from the situation in spherical droplets, underlining the importance of the container shape and size. Reconstitution of protein bundles such as microtubules and extracellular matrix collagen inside shaped droplets enables us to study how fibrous networks adapt their conformation depending on the geometry of the confinement. Microtubule orientation is an important feature in eukaryotic cells to establish cell polarity: by elongating from the nucleus toward cell extremities, microtubules drive several polarizing factors toward opposite cell poles. Differently from what is observed in spherical droplets, microtubules encapsulated into rod-shaped droplets appeared aligned along the main symmetry axis of the confinement. The shape and dimensions of the confinement, together with the microtubule alignment, are features that well resemble the conditions found in model eukaryotic cells, such as fission yeast.[64] The possibility to control the orientation of cytoskeletal components inside artificial containers thus offers the possibility to reconstitute microtubule-driven polarization in minimal artificial

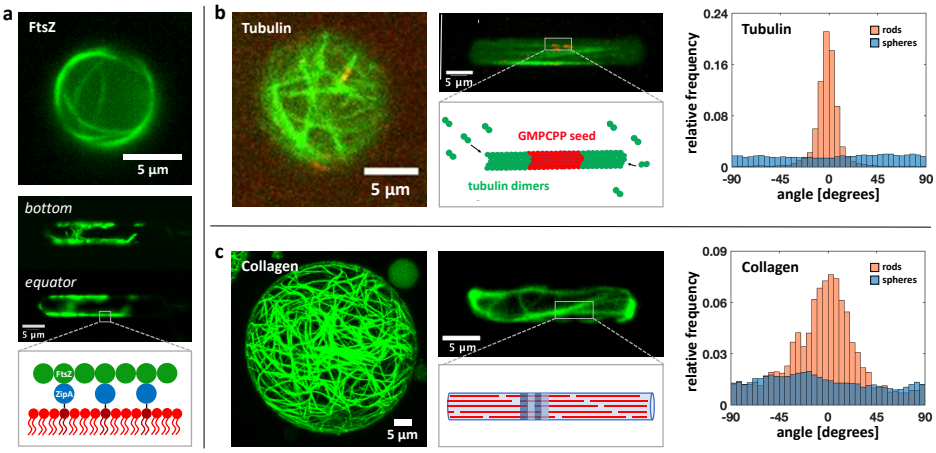

Figure 2.6: **Impact of container geometry on the organization of various protein bundle networks encapsulated inside rod-shaped droplets.** (a) FtsZ filamentous bundles in spherical (top) and rod-shaped (middle) water-in-oil droplets. The FtsZ superstructures visible on the bottom plane of the rod-shaped droplet (middle) adhere to the surface of the droplet, as is also seen on the equatorial plane. A lipid monolayer containing DGS-NTA lipids (dark red) and DOPC (red) is assembled at the water–oil interface. By replacing its transmembrane tail with a His-tag, which can bind to the Ni-tag on the headgroup of DGS-NTA lipids, ZipA functions as a membrane anchor for the FtsZ filaments (bottom). FtsZ is labeled with Alexa488. (b) Microtubules grown in spherical (left) and rod-shaped droplets (middle). As shown both qualitatively in the images and quantitatively by the analysis of the fiber orientations (right), the microtubules inside spherical droplets (N = 10) grow without any strong preferential orientation, whereas in the rod-shaped droplets (N = 10), the network appears to follow the symmetry axis of the droplet. For the reconstitution of microtubules, GMPCPP stabilized seeds (labeled with rhodamine tubulin) serve as templates for the growth of microtubules through the addition of tubulin dimers in solution (bottom). Fluorescent HiLyte 488 tubulin was used to label the microtubules. (c) Collagen fibril reconstituted inside spherical- (left) and rod-shaped droplets (middle). Similar to what is observed for microtubules, the analysis of the fiber orientation (right) shows that the collagen network in spherical droplets (N = 4) remains weakly organized, but inside the rod-shaped droplets (N = 4), it re-arranges to align with the symmetry axis of the droplet. As sketched (middle-bottom), a collagen fibril is formed by the staggering of collagen triple-helix monomers (red) driven by noncovalent interactions, which give rise to a characteristic periodic pattern (blue and light-blue).

cells. Similar phenomena are observed for the extracellular matrix. *In vivo*, the ECM is secreted and assembled in the narrow spaces between cells, and collagen matrix fibers therefore adapt their arrangement depending on the imposed geometrical constraints. Our microfluidic platform provides microscopic confinements with dimensions spanning a broad range of aspect ratios, resembling those found in some tissues.[65] As *in vivo*, our results indicate that the geometry of the confinement directly influences the collagen matrix configuration. Similar to what is observed in many tissues, *e.g.*, the cornea or the tendon,[66, 67] we can induce the collagen fibers to align along a prevalent symmetry axis. Being able to recreate the orientation of the collagen fibers in the extracellular matrix is of fundamental importance, since the network architecture determines the tissue response to mechanical deformations. Thus, we anticipate that the possibility

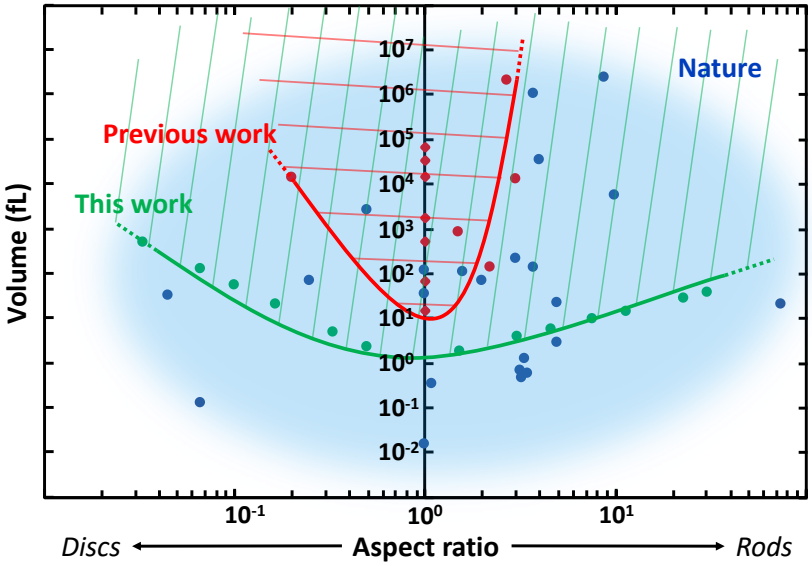

Figure 2.7: **Phase diagram comparing the shape and size of various cells found in nature with the deformable artificial containers used in previous research work and those presented in this paper.** Assuming roughly spheroid-like containers and cells, the morphological space is defined by the aspect ratio of the smallest and the largest axis of the containers (x-axis), and the volume (y-axis). The space is divided between rods (right), spheres (y-axis), and discs (left). In blue, an approximate cloud encircles the morphologies adopted by a selected number of living organisms (blue dots, see Table 2.2). The red dots represent container geometries reported previously in the field (see Table 2.2), with the red line showing the lower morphological boundaries achieved so far. Similarly, the green line delineates the new lower boundaries achieved within this work. Compared to previous research, we expanded the boundaries of volume and aspect ratio by one to two orders of magnitude. This advance enables us to cover a broader range of shapes and sizes and it bridges the gap between artificial and natural cells.

provided by our method to control the collagen network arrangement *via* the morphology of the container will allow to more closely mimic the architecture and mechanical response of living tissues. Moreover, since our platform uses deformable containers, it provides the opportunity to observe how protein networks and other biopolymers rearrange dynamically in response to evolving boundaries and gradual changes in crowding and salt concentrations. The reversibility of the volume change of double emulsions (Fig. 2.4) makes it possible to study whether changes in the protein network configuration are reversible or display some form of hysteresis. Given the range of sizes that can be enforced upon vesicles, our approach also allows to study the influence of the confinement surface curvature on the alignment and positioning of membrane-bound proteins, which is key for many proteins involved in membrane remodeling. We believe that our approach to shape and size control can be broadly applied. The ability to

tune the container volume will, for example, aid the study of how the crowding environment impacts the dynamics of various cellular processes. The approach also allows to explore the relation between membrane curvature and the spatial arrangement of lipids domains and membrane proteins.[68] Finally, similar to recent *in vivo* studies of shape-sculpted bacteria,[15, 16, 28, 29, 69] the platform offers the chance to investigate pattern formation and chromosome dynamics as a function of confinement geometry.

2.4. METHODS

MICROFABRICATION

Microfluidic devices were fabricated in a cleanroom with the following protocol. A layer of hexamethyldisilazane (HMDS, BASF SE) was deposited on a 4-in. silicon wafer by spin-coating at 1000 rpm for 1 min. The wafer was baked at 200 °C for 2 min. Subsequently, a layer of NEB22a negative e-beam resist (Sumitomo Chemical) was spin-coated at 1000 rpm for 1 min and baked at 110 °C for 3 min. Correct adhesion of the NEB22a onto the silicon surface is ensured by the first HMDS layer. The designs were written on the coated wafer using electron beam lithography (EBPG-5000+, Raith GmbH, dose: 16 $\mu C\ cm^{-2}$, acceleration voltage: 100 kV, aperture: 400 μm). Post-exposure baking of wafer was performed at 105 °C for 3 min. The patterns were then developed by submerging the wafer in MF322 (Dow Chemical Company) for 1 min, then in diluted MF322 (distilled water:MF322 = 1:10) for 30 s, and finally rinsing in distilled water for 30 s. Bosch process deep reactive-ion etching was used to dry etch the structures into the silicon wafer, with an inductive coupled plasma reactive-ion etcher (Adixen AMS 100 I-speeder). During the process, the pressure was kept at about 0.04 mbar, the temperature of the wafer was kept at 10 °C, while the plasma temperature was 200 °C. The sample holder was held at 200 mm from the plasma source. The etching step involved 200 sccm SF6 for 7 s with the ICP power set to 2000 W without a bias on the wafer itself. The passivation step was done with 80 sccm C4F8 for 3 s with the ICP power set to 2000 W and the bias power on the wafer alternate with a low frequency: 80 W, for 10 ms, and 0 W for 90 ms. Total etching time depended on the desired final height of the device (etching depths for the wafers containing tubular traps used in each figure are listed in Table 2.1). Finally, the excess of resist was removed from the wafer by exposure to oxygen plasma for 10 min. In the case of multiheight devices (Fig. 2.2b), the parts of the device with bigger height were patterned on the wafer after the small channels through optical lithography, being careful to properly align the two structures. To do so, silicon wafer was spin-coated with a SU-8 2000 negative resist (Microchem), then soft baked for 3 min at 95 °C, exposed with 140 mJ cm^{-2} dose, and then baked at 4 min 95 °C. Development of the structured followed as described. Silanization of the wafer was done with (tridecafluoro-1,1,2,2-tetrahydrooctyl) trichlorosilane (ABCR GmbH & Co.) overnight in a vacuum desiccator to enhance hydrophobicity of the surface and facilitate subsequent peeling-off of the PDMS.

SOFT LITHOGRAPHY

Single-layer PDMS devices were cured and assembled following the procedure previously described.[70] Multilayer devices for control of water-in-oil droplets size were produced by the assembly of three different layers obtained from three different wafers. A

thin layer of PDMS was spin-coated on the device-wafer using a spin-coater (POLOS) at 200 rpm for 5 s and 300 rpm for 20 s (acceleration 100 rpm/s). The second wafer (silanized and without any patterned structures) was used to prepare glass coverslips with a thin PDMS coating. This was achieved by firmly pressing down the coverslips on the wafer through the uncured PDMS, so that a thin PDMS layer was formed beneath them. The third wafer (silanized and without any patterned structures) was used to produce a ~5 mm-thick PDMS slab. All of the wafers were baked for 4 h at 80 °C. The coverslips and the PDMS slab were removed from the plain wafers. The slab was cut into separate pieces (approximately 1 cm × 2 cm), and a 4 mm hole was punched in each of them to create a water chamber using a rapid core punch (World Precision Instruments, 4 mm diameter). Both the PDMS-covered device-wafer and the water chambers were cleaned with isopropanol, blow-dried with nitrogen, and then activated by exposing them to oxygen plasma (Plasmatic System, Inc.) for about 10 s. Each water chamber was then bonded to the device-wafer, taking care that the water chamber was aligned with the part of the device containing the microfluidic traps. The device-wafer with bonded water chambers was then baked for 20 min at 80 °C. Subsequently, the thin PDMS layer with bonded water chambers on top was peeled off from the device-wafer. The devices were cut to size with scissors, and inlet and exit holes were punched into the devices using a rapid core punch (World Precision Instruments, 0.75 mm diameter). Both PDMS coverslips and devices were cleaned with isopropanol and bonded by the oxygen plasma procedure described above. After bonding, devices were left overnight at 80 °C to enhance the device hydrophobicity. For the experiment shown in Fig. 2.6a, the channels walls were treated by flushing RainX for 2 min immediately after bonding, in order to further enhance surface hydrophobicity. The solutions were introduced into the devices *via* tubing (Tygon Microbore Tubing, 0.2 mm inner diameter) fitted with home-built metal connectors using pressure-driven microfluidic pumps (Fluigent, controlled by Fluigent MAESFLO software).

IMAGE ACQUISITION AND PROCESSING

Wide-field microscopy measurements were performed using an Olympus IX-81 inverted microscope combined with epifluorescence illumination and appropriate filter sets. Images were acquired and recorded using an Olympus 60× PlanApo (NA 1.45, oil) objective and a Zyla 4.2 PLUS CMOS camera (Andor Technology). The microscope was operated through Micromanager software (version 1.4.14). Confocal microscopy of fluorescent collagen fibers was performed using an inverted Olympus IX81 combined with an Andor Revolution illumination system and a Yokogawa CSU X1 detection system. Images were acquired with a 60× UPlanFLN (NA 1.25, oil) objective and recorded with an EM-CCD Andor iXon X3 DU897 camera. Confocal microscopy of tubulin was performed at 30 °C using Nikon Ti-E microscope (Nikon, Japan) equipped with a Nikon plan Apo 100× 1.45 NA oil immersion objective and an Evolve 512 EMCCD camera (Roper Scientific, Germany). Images of collagen in spherical droplets were captured with an inverted Eclipse Ti Nikon microscope in combination with a Nikon 100× objective (NA 1.49, oil). The resulting images (Figures 1 and 6c) were obtained by a z-stack projection over a depth of 20 μm (0.2 μm step size). Images were analyzed and background appropriately subtracted using Fiji (ImageJ).

LIPID SOLUTIONS

All lipids were purchased from Avanti Polar lipids, Inc. in chloroform solutions. For water-in-oil droplets, lipids were mixed according to the required ratios and dried in a glass tube by desiccating for at least 1 h. The resulting dried film was then resuspended in mineral oil (light oil bioXtra, Sigma-Aldrich) at the desired concentration and sonicated for 30 min at room temperature. For production of double emulsion and liposomes, lipids were mixed in the desired ratios, dried for at least 1 h, and then resuspended in chloroform or ethanol at a concentration of 100 mg mL^{-1}.

DOUBLE EMULSIONS

Three solutions were used to produce double emulsions on-chip: a lipid-containing solution, an inner aqueous solution, and an outer aqueous solution. The lipid-containing solution was composed of 2 mg mL^{-1} lipids (99.9 mol % DOPC + 0.1 mol % Liss Rhod PE) dissolved in oleic acid. In all of the experiments involving double emulsions, both inner and outer aqueous and the feeding channel solutions contained 5% v/v pluronic surfactant (poloxamer 188, Sigma-Aldrich) and 15% v/v glycerol. For the experiments shown in Fig. 2.4, the inner aqueous and outer aqueous contained an additional 25 mM sucrose and 5 mM $MgCl^2$. The solution flushed through the feeding channel to induce an osmotic pressure difference contained an additional 200 mM sucrose. To make the double emulsion denser than the surrounding solution and thereby facilitate their extraction from the device (Fig. 2.5), an additional 5 mM dextran was added to the inner aqueous solution and osmotically balanced by 5 mM of glucose in the outer aqueous solution.

LIPOSOMES

Liposomes were produced using OLA, an on-chip microfluidic method that results in unilamellar liposomes.[70] All liposomes in Figure 2.10 were made with the lipid-carrying organic phase containing 2 mg mL^{-1} lipids (99.9 mol % DOPC + 0.1 mol % Liss Rhod PE) dissolved in 1-octanol. The inner aqueous phase consisted of 15% v/v glycerol (Fig. 2.10a–b), 5 μM Alexa-647 (Fig. 2.10a), 5 mM PEG-8000 (Fig. 2.10a), 100 mM sucrose (Fig. 2.10b), and 5 μM 72-bases long ssDNA (Fig. 2.10b); the outer aqueous phase was a solution of 5% v/v pluronic surfactant poloxamer 188 (Fig. 2.10a–b), 15% v/v glycerol (Fig. 2.10a–b), 5 mM PEG-8000 (Fig. 2.10a), 100 mM sucrose (Fig. 2.10b); the collection well contained 20 μL (added upon the liposomes reaching the collection well) of 15% v/v glycerol (Fig. 2.10a–b), 5 mM PEG-8000 (Fig. 2.10a), and 100 mM glucose (Fig. 2.10b). After sufficient production (thousands of liposomes in the collection well), liposomes were carefully harvested from the collection well by pipetting out 15 μL of the solution. The liposomes were then pumped into the microfluidic device containing the trap design. For Figure 2.9a, before being pumped into the device containing the traps, the liposomes were mixed with another solution in order to bring the outside environment to a concentration of 8 mM PEG-8000 and 15% v/v glycerol and to induce an osmotic pressure difference.

WATER-IN-OIL DROPLETS

Water-in-oil droplets were produced with two different protocols: droplets in Fig. 2.1a containing nucleoids, and droplets in Figures 2a and 6b were produced on-chip *via* a

standard cross-junction method, where the aqueous stream gets pinched into droplets by the continuous oil stream. The droplets produced were then trapped downstream from the junction on the same device. All of the droplets showed in the other figures were produced by pipetting up and down a few microliters (2-5 μL) of aqueous solutions into 100 μL of oil solution. The shear forces provided by the pipetting broke the droplets into smaller ones. In Fig. 2.2a, to enhance the contrast with the microfluidic traps, fluorescent lipids were added to the oil solution (0.1 mol % Liss Rhod PE) together with 1% v/v SPAN 80 surfactant. For the experiments shown in Figures 2 and 3, the oil solution contained 5% v/v SPAN 80 surfactant. The inner aqueous solution of the droplets shown in Figures 2 and 3 contained 5 μM Alexa 647 fluorescent dye. Additionally, droplets shown in Fig. 2.3 contained 200 mM KCl, while the water chamber contained 100, 200, and 300 mM KCl water solution to, respectively, create hypotonic, isotonic, and hypertonic environments for the droplets.

MIN PROTEINS IN DROPLETS

Min protein oscillations in spherical droplets (Fig. 2.1a) were observed in water-in-oil droplets containing the following inner aqueous: 0.8 μM MinD, 0.2 μM MinD-Cy3, 0.8 μM MinE, 0.2 μM MinE-Cy5, 5 mM ATP, 4 mM phosphoenolpyruvate, 0.01 mg mL^{-1} of pyruvate kinase, 25 mM Tris-HCl (pH 7.5), 150 mM KCL, and 5 mM $MgCl^2$. Min proteins were isolated and labeled as described previously. For these experiments, 2 mg mL^{-1} of lipids (66.6 mol % DOPC + 33.3 mol % DOPG + 0.1 mol % Liss Rhod PE) were dissolved in mineral oil as described above

FTSZ IN DROPLETS

The inner aqueous solution for experiments involving FtsZ in water-in-oil droplets contained 12 μM FtsZ, 6 μM ZipA, 2 mM guanosine triphosphate (GTP), 180 mM KCl, 25 mM Tris-HCl (pH 7.4), 5 mM $MgCl^2$, and 15% v/v glycerol. The oil phase contained 25 mg mL^{-1} of lipids (89.9 mol % DOPC+10 mol % DGS-NTA(Ni) + 0.1 mol % Liss Rhod-PE) for spherical droplets (Fig. 2.1), while the same composition at a lower concentration (1 mg mL^{-1}) was used for tubular droplets (Fig. 2.6a). Proteins were isolated and labeled as described previously.[71]

NUCLEOIDS IN DROPLETS

The nucleoid isolation protocol is based on Cunha *et al.*[72] The BN2179 strain containing Ori1/Ter3 labels and HUmYpet (AB1157, *Ori1::lacOx240-hygR, Ter3::tetOx240-accC1* Δ*galK::tetR-mCerulean frt,* Δ*leuB::lacI-mCherry frt*) was used for the experiments.(30) Cells were grown in LB medium for 65 h. One mL of culture was spun down at 10000g for 2.5 min and resuspended in 475 μL of ice cold sucrose buffer, containing 0.58 M sucrose, 10 mM NaPi buffer (pH 7.0-7.4, Na2HPO4/NaH2PO4), 10 mM EDTA, and 100 mM NaCl. Immediately after this cold shock, 25 μL of lysozyme solution (1 mg mL^{-1} in ultrapure water) was added, and the cell suspension was briefly vortexed and incubated at room temperature for 15 min, resulting in spheroplasts. To lyse the spheroplasts and obtain isolated nucleoids, 20 μL of the spheroplast suspension was slowly added, using a cut pipet tip, to 1 mL of a solution containing 10 mM NaPi (pH 7.4) and 100 ng mL^{-1} DAPI, after which the Eppendorf was inverted once. This nucleoid suspension was used as the aqueous phase for microfluidically produced water-in-oil droplets of 10 μm diameter.

The oil phase was HFE-7500 (Novec Engineering Fluids) with 0.1% v/v Picosurf-1 surfactant (Dolomite Microfluidics). The droplets were immobilized for observation using an array of traps that was placed downstream of the production junction.

TUBULIN IN DROPLETS

The aqueous solution contained MRB80 buffer (80 mM PIPES, 4 mM $MgCl^2$, 1 mM EGTA, pH 6.8) with 39 μM unlabeled tubulin, 1 μM labeled tubulin (HiLyte 488), 3 mM GTP, 50 mM KCl, 4 mM DTT, 2 mg mL^{-1} of bovine serum albumin, 1 mg mL^{-1} of glucose oxidase, 0.5 mg mL^{-1} of catalase, and 50 mM glucose. The oil phase contained 1 mg mL^{-1} of lipids (90% DOPS + 10% PEG2000-PE) in mineral oil with 2% v/v SPAN 80. To nucleate microtubules in droplets, short microtubules (labeled with 12% Hilyte 561 tubulin) of an approximate length of 1 μM were added, stabilized with guanylyl-(α,β)-methylene-diphosphonate (GMPCPP), into the aqueous solution.

COLLAGEN IN DROPLETS

To obtain collagen networks in spherical confinement, telopeptide collagen (TeloCol, CellSystems, supplied at 3.1 mg mL^{-1} in 0.01 M HCl) was brought to a neutral pH with the addition of NaOH (Sigma Aldrich) in phosphate buffered saline (PBS, Sigma Aldrich), to obtain a final collagen concentration of 1 mg mL^{-1} for the spherical droplets and 2 mg mL^{-1} for the droplets in the tubular confinement. The collagen-binding protein CNA35 fluorescently labelled with EGFP (a kind gift from Maarten Merkx, AddGene) was added to collagen in a molar ratio 20 : 1 to allow for collagen network visualization. The oil phase contained 2% v/v SPAN 80 surfactant in mineral oil (Sigma Aldrich). The collagen was allowed to polymerize for at least 90 minutes at room temperature before visualization. For imaging the spherical droplets, the water-in-oil solution was placed between two coverslips (Menzel™Microscope Coverslips 24 mm x 60 mm, #1, Thermo Scientific) separated by a silicone chamber (Grace Bio-Labs CultureWell™chambered coverglass, Sigma Aldrich).

DATA ANALYSIS

The width of the droplets in Figure 2.2 were obtained from the fluorescent profiles measured at the middle of the tubular droplet across its width (see Fig. 2.9b) of ten individual droplets per type of trap. For each droplet, the width was obtained from the FWHM (full width at half maximum) of its profile and these values were then averaged to obtain, for each type of trap, a measure of the width. Errors were omitted since the standard error-of-the-mean value (<100 nm) was smaller than the optical resolution of our microscope. The size change of the double emulsions in Figure 2.4 was measured every 12 frames (12 seconds) in the 3-minute time lapse, for both the shrinking process (hypertonic condition) and the expansion process (hypotonic condition). Using Fiji (ImageJ), a circle was manually fitted to the outer contour of the double emulsion, excluding the side-pocket. The errors quoted in Figure 2.4 are the standard error-of-the-mean.

In Figure 2.6, the values of tubulin and collagen bundle orientations were obtained using Fiji (OrientationJ plugin) after background was appropriately subtracted. In Figure 2.7 we calculated the aspect ratio and volumes of the artificial cell containers and natural cells, of which the smallest and largest dimensions are listed in Table 2.2 as obtained from literature (for dots denoted as 'Previous Work' and 'Nature') or as measured

in our experiments (for dots labeled as 'This Work'). We approximated the cell shapes as spheroids characterized by longest and shortest semi-axes a and c. Discs correspond to oblate spheroids with $c < a$, while rods are equivalent to prolate spheroids with $c > a$. The aspect ratio in Figure 2.7 is defined as c/a. The volume of a spheroid is calculated as $V = (4\pi/3)\, a^2 c$.

2.5. SUPPLEMENTARY INFORMATION

Figure	Etch depth (μm)
2.2b, i (top); 2.3b; 2.6b; 2.8a	5.2
2.2b, iii	3.0
2.2b, iv (bottom); 2.9b	2.5
2.5c ii (bottom)	1.9
2.6a; 2.6c; 2.5b; 2.5c, i (top); 2.9a	5.3

Table 2.1: **The etch depths of the wafers containing tubular traps used in the various figures.** The measurements were done at three different points on the wafer using a profilometer. The quoted value is the mean of these measurements.

Category	Type	Largest dimension (μm)	Smallest dimension (μm)	Reference
Previous work	Spheres	3	3	[37, 73]
		5	5	[37, 73]
		10	10	[37, 73]
		15	15	[37, 73]
		30	30	[37, 73]
		40	40	[37, 73]
		50	50	[37, 73]
	Discs	50	10	[37]
	Rods	11	5	[74]
		15	10	[74]
		60	20	[37]
		300	110	[52]
This work	Discs	2	1	
		3	1	
		6	1	
		10	1	
		15	1	
		30	1	
	Rods	3	1.4	
		4	1.4	
		5	1.4	
		10	1.4	
		15	1.3	
		30	1.3	

Continued on next page

Table 2.2 – *Continued from previous page*

Category	**Type**	**Largest dimension (μm)**	**Smallest dimension (μm)**	**Reference**
		40	1.3	
		50	1.3	
Nature	*Escherichia coli*	2.05	0.63	[75]
		2.35	0.67	[75]
		2.34	0.73	[75]
		2.94	0.87	[75]
	Saccharomyces cerevisiae	3	3	[76]
		6	6	[76]
	Schizosaccharomyces pombe	7	3	[74]
		14	3	[74]
	Bacillus subtilis	5	1	[77]
		10	2	[77]
	S. aureus	0.9	0.82	[78]
	HeLa cells	20	10	[79]
	Red blood cell	8	2	[80]
	Cardiomyocyte	100	10	[81]
		100	25	[81]
	Haloquadratum walsbyi	1.5	0.1	[82]
		11	0.5	[82]
	Onion epidermis	300	80	[83]
	Filamentous *E.coli*	60	0.80	[84]
	Filamentous *Epulopiscium*	600	80	[85]
	Mycoplasma (average size)	0.3	0.3	[86]

Table 2.2: **Dimensions of deformable artificial cell containers and natural cells displayed in Fig. 2.7.** The dimensions of the artificial cell containers are taken from 'Previous Work' (spheres, discs and rods) and 'This Work' (discs and rods), whereas the 'Nature' section includes a representative selection of sizes and aspect ratios covered by natural cells used to sketch the blue area in Fig. 2.7. For 'Previous Work', we selected spherical containers employed so far in the synthetic cell field. In addition, we included examples of previous attempts at deforming spherical containers into discs and rods. For 'This Work', we selected the largest aspect ratios that we experimentally achieved for this paper. These points then form the lower boundary of the green area in Fig. 2.7.

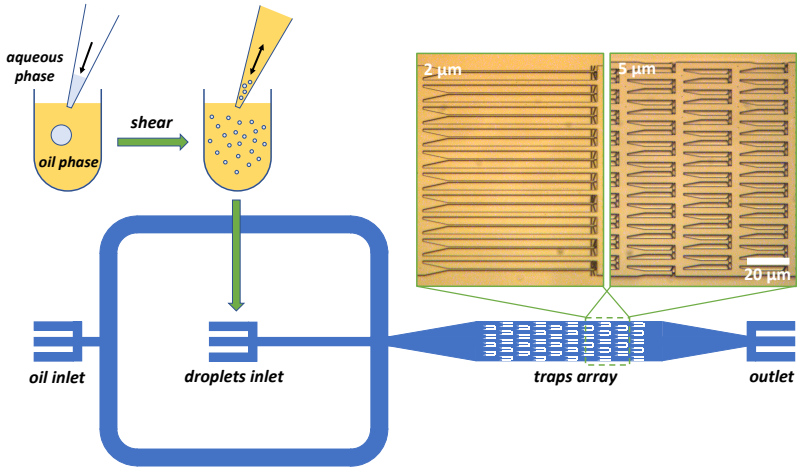

Figure 2.8: **Schematic of the experimental procedure and device operation to obtain rod-shape droplets.** A few microliters (2-5 µL) of an aqueous solution are pipetted into 100 µL of oil solution. Shear forces induced by repeatedly pipetting the solution up and down break the large droplets into smaller ones.[73] Droplet coalescence is prevented by surfactant molecules dissolved in the oil, which stabilize the water-oil interface of the droplets. The oil solution containing the droplets and a second oil solution without droplets are inserted *via* a pressure-driven pump into the device through two different inlets, as indicated. Past a junction where these two fluid streams meet, the droplets enter into a chamber containing an array of microfluidic traps. Once a satisfying number of droplets is caught at the entrance of the traps, the pressure of the outer oil stream is increased. In this way, the droplets get pushed inside the traps and thus deformed into the desired shape. The droplets that do not get caught by a trap are pushed towards the outlet and removed from the chamber. The pressure required to insert the droplets into the device is lower than the one required to insert the droplets inside the traps, and both pressures strongly depend on the dimensions of the device. As representative examples, two trap designs with dimensions on the opposite sides of the size range explored in this work are visible in the bright-field microscopy images in the top right part of the figure. In the case of traps with a 5 µm x 5 µm square cross-section (right), we experience that a minimum overpressure of ~0.1 bar is required to insert droplets into the device, which has to be increased to roughly ~0.2 bar to squeeze the droplets into the traps. For traps with a 2 µm x 2 µm cross-section, the minimal overpressures required to insert droplets into the device and then into the traps are respectively around ~0.5 bar and ~0.8 bar. The droplets remained stably trapped as long as the pressure is kept constant. Otherwise, it is possible to release the droplets by lowering the pressure, as they slide back towards the entrance of the trap to minimize deformation. Alternatively, by increasing the pressure up to >1 bar, the droplets would eventually escape through the small exit holes of the traps. The detailed design of the traps varies depending on the final desired shape to be imposed on the artificial containers. Given that smaller structures require higher pressures, the walls of narrower traps are wider, in order to ensure that the trap walls remain bonded to the top PDMS membrane during the experiments. At the end of each trap, exit holes provide fluid flow through the structure. Generally speaking, the width of the exit hole equals half of the trap width. Also, to further facilitate the flow through the smaller traps, the number of lateral exit holes is increased. Finally, as the artificial containers preserve their original volume during deformation, the traps with smaller cross-sections are designed with an increased length. As the fluidic chamber containing the traps has the same dimension for all designs, the chamber contains a different number of traps depending on the trap dimensions: 57 for the 2 µm design and 105 for the 5 µm design. In principle the chamber can be designed as large as preferred, for example to accommodate a higher number of traps, as these devices are scalable, due the lithography-based method of fabrication.

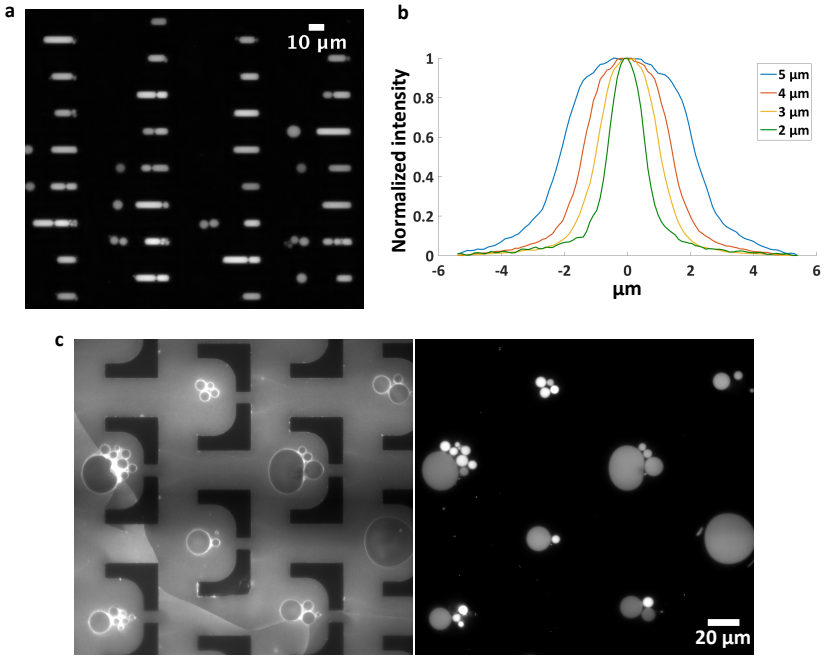

Figure 2.9: **Fluorescent images of droplets deformed into different shapes by means of a microfluidic device.** (a) Array of 5 µm-wide microfluidic traps containing water-in-oil droplets. Fluorescent signal comes from Alexa 647 fluorescent dye in the aqueous phase. (b) Normalized fluorescent profile of droplets in Fig. 2.2b, measured at the mid-length equatorial cross section of tubular droplets over traps of different width. The plot shows the clear difference between the droplet widths. (c) 2 µm high disc-shaped droplets immobilized in an array of microfluidic traps. On the left image, the fluorescence signal comes from fluorescent lipids dissolved in the oil phase and partitioned at the droplet interface, while on the right image fluorescent signal comes from Alexa 647 fluorescent dye in the aqueous phase.

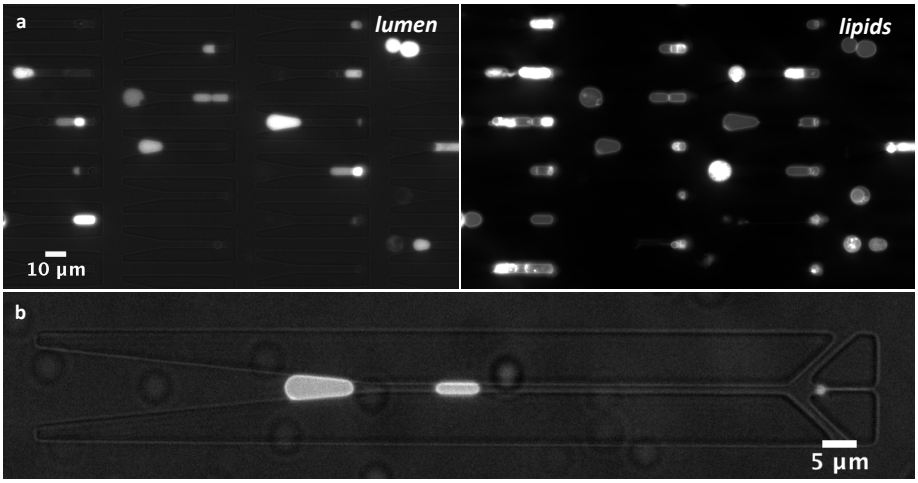

Figure 2.10: **Fluorescent images of liposomes into tubular traps.** (a) Array of tubular traps containing liposomes. Left: fluorescent signal coming from Alexa 647 inside the liposomes. Right: fluorescent signal coming from inclusion of Rhod PE embedded within the lipid membrane. Once trapped the resulting population shows some tense liposomes that did not enter into the traps, as well as liposomes that lost the fluorescent dye that was originally encapsulated at the moment of the production. We conjecture that the membrane floppiness induced by the osmotic pressure difference make the liposomes prone to split or simply to suffer temporary membrane defects during the insertion into the microfluidic chip, which would explain both the lack of membrane floppiness and loss of fluorescent dye from the lumen. (b) Liposome deformed into a bacteria shape and size like *E. coli* (width ~1 µm).

REFERENCES

[1] A. M. Randich and Y. V. Brun, *Molecular mechanisms for the evolution of bacterial morphologies and growth modes,* Frontiers in Microbiology **6**, 580 (2015).

[2] A. W. Bisson-Filho, J. Zheng, and E. Garner, *Archaeal imaging: leading the hunt for new discoveries,* Molecular Biology of the Cell **29**, 1675 (2018).

[3] A. Ivakov and S. Persson, *Plant cell shape: modulators and measurements,* Frontiers in Plant Science **4**, 439 (2013).

[4] R. M. Steinman and Z. A. Cohn, *Identification of a novel cell type in peripheral lymphoid organs of mice. I. Morphology, quantitation, tissue distribution.* The Journal of experimental medicine **137**, 1142 (1973).

[5] W. Margolin, *Sculpting the Bacterial Cell,* (2009).

[6] K. D. Young, *Bacterial shape,* Molecular Microbiology **49**, 571 (2003).

[7] K. D. Young, *Bacterial morphology: why have different shapes?* (2007).

[8] Y. Mulla, A. Aufderhorst-Roberts, and G. H. Koenderink, *Shaping up synthetic cells,* Physical Biology **15**, 041001 (2018).

[9] D. A. Fletcher and R. D. Mullins, *Cell mechanics and the cytoskeleton,* Nature **463**, 485 (2010).

[10] S. S. Justice, D. A. Hunstad, L. Cegelski, and S. J. Hultgren, *Morphological plasticity as a bacterial survival strategy,* Nature Reviews Microbiology **6**, 162 (2008).

[11] C. S. Chen, M. Mrksich, S. Huang, G. M. Whitesides, and D. E. Ingber, *Geometric control of cell life and death.* Science (New York, N.Y.) **276**, 1425 (1997).

[12] A. Mogilner and K. Keren, *The Shape of Motile Cells,* (2009).

[13] W. P. J. Smith, Y. Davit, J. M. Osborne, W. Kim, K. R. Foster, and J. M. Pitt-Francis, *Cell morphology drives spatial patterning in microbial communities.* Proceedings of the National Academy of Sciences of the United States of America **114**, E280 (2017).

[14] D. C. Yang, K. M. Blair, and N. R. Salama, *Staying in Shape: the Impact of Cell Shape on Bacterial Survival in Diverse Environments.* Microbiology and molecular biology reviews : MMBR **80**, 187 (2016).

[15] F. Wu, B. G. Van Schie, J. E. Keymer, and C. Dekker, *Symmetry and scale orient Min protein patterns in shaped bacterial sculptures,* Nature Nanotechnology **10**, 1 (2015).

[16] J. Männik, F. Wu, F. J. Hol, P. Bisicchia, D. J. Sherratt, J. E. Keymer, and C. Dekker, *Robustness and accuracy of cell division in Escherichia coli in diverse cell shapes,* Proceedings of the National Academy of Sciences of the United States of America **109**, 6957 (2012).

[17] E. Frey, J. Halatek, S. Kretschmer, and P. Schwille, *Protein pattern formation,* in *Physics of Biological Membranes*, edited by P. Bassereau and P. Sens (Springer International Publishing, Cham, 2018) pp. 229–260.

[18] B. E. Vos, L. C. Liebrand, M. Vahabi, A. Biebricher, G. J. Wuite, E. J. Peterman, N. A. Kurniawan, F. C. MacKintosh, and G. H. Koenderink, *Programming the mechanics of cohesive fiber networks by compression,* Soft Matter **13**, 8886 (2017).

[19] A. Dragoš and Á. T. Kovács, *The Peculiar Functions of the Bacterial Extracellular Matrix,* Trends in Microbiology **25**, 257 (2017).

[20] B. S. Govindan and W. B. Spillman, *Steady states of a microtubule assembly in a confined geometry,* Physical Review E - Statistical Physics, Plasmas, Fluids, and Related Interdisciplinary Topics **70**, 4 (2004).

[21] B. Zelinski, N. Müller, and J. Kierfeld, *Dynamics and length distribution of microtubules under force and confinement,* Physical Review E - Statistical, Nonlinear, and Soft Matter Physics **86** (2012).

[22] M. C. Lagomarsino, C. Tanase, J. W. Vos, A. M. C. Emons, B. M. Mulder, and M. Dogterom, *Microtubule organization in three-dimensional confined geometries: Evaluating the role of elasticity through a combined in vitro and modeling approach,* Biophysical Journal **92**, 1046 (2007).

[23] I. Junier, F. Boccard, and O. Espéli, *Polymer modeling of the E. coli genome reveals the involvement of locus positioning and macrodomain structuring for the control of chromosome conformation and segregation,* Nucleic Acids Research **42**, 1461 (2014).

[24] D. Marenduzzo, C. Micheletti, and E. Orlandini, *Biopolymer organization upon confinement,* Journal of Physics Condensed Matter **22**, 283102 (2010).

[25] S. Jun and B. Mulder, *Entropy-driven spatial organization of highly confined polymers: Lessons for the bacterial chromosome,* Proceedings of the National Academy of Sciences **103**, 12388 (2006).

[26] M. F. Olson and E. Sahai, *The actin cytoskeleton in cancer cell motility,* Clinical & Experimental Metastasis **26**, 273 (2009).

[27] A. L. McGregor, C.-R. Hsia, and J. Lammerding, *Squish and squeeze-the nucleus as a physical barrier during migration in confined environments.* Current opinion in cell biology **40**, 32 (2016).

[28] F. Wu, A. Japaridze, X. Zheng, J. Wiktor, J. W. Kerssemakers, and C. Dekker, *Direct imaging of the circular chromosome in a live bacterium,* Nature Communications **10**, 1 (2019).

[29] F. Wu, P. Swain, L. Kuijpers, X. Zheng, K. Felter, M. Guurink, J. Solari, S. Jun, T. S. Shimizu, D. Chaudhuri, B. Mulder, and C. Dekker, *Cell Boundary Confinement Sets the Size and Position of the E. coli Chromosome,* Current Biology **29**, 2131 (2019).

[30] P. Schwille, *Jump-starting life? Fundamental aspects of synthetic biology,* The Journal of Cell Biology **210**, 687 (2015).

[31] J. W. Szostak, D. P. Bartel, and P. L. Luisi, *Synthesizing life,* Nature **409**, 387 (2001).

[32] W. K. Spoelstra, S. Deshpande, and C. Dekker, *Tailoring the appearance: what will synthetic cells look like?* Current Opinion in Biotechnology **51**, 47 (2018).

[33] B. C. Buddingh' and J. C. M. van Hest, *Artificial Cells: Synthetic Compartments with Life-like Functionality and Adaptivity,* Accounts of Chemical Research **50**, 769 (2017).

[34] J. Alvarado, B. M. Mulder, and G. H. Koenderink, *Alignment of nematic and bundled semiflexible polymers in cell-sized confinement,* Soft Matter **10**, 2354 (2014).

[35] T. Sanchez, D. T. N. Chen, S. J. DeCamp, M. Heymann, and Z. Dogic, *Spontaneous motion in hierarchically assembled active matter,* Nature **491**, 431 (2012).

[36] M. Chanasakulniyom, C. Martino, D. Paterson, L. Horsfall, S. Rosser, and J. M. Cooper, *Expression of membrane-associated proteins within single emulsion cell facsimiles,* The Analyst **137**, 2939 (2012).

[37] S. Mellouli, B. Monterroso, H. R. Vutukuri, E. te Brinke, V. Chokkalingam, G. Rivas, and W. T. S. Huck, *Self-organization of the bacterial cell-division protein FtsZ in confined environments,* Soft Matter **9**, 10493 (2013).

[38] M. Miyazaki, M. Chiba, H. Eguchi, T. Ohki, and S. Ishiwata, *Cell-sized spherical confinement induces the spontaneous formation of contractile actomyosin rings in vitro,* Nature Cell Biology **17**, 480 (2015).

[39] M. C. Good, M. D. Vahey, A. Skandarajah, D. A. Fletcher, and R. Heald, *Cytoplasmic Volume Modulates Spindle Size During Embryogenesis,* Science **342**, 856 (2013).

[40] E. Sokolova, E. Spruijt, M. M. K. Hansen, E. Dubuc, J. Groen, V. Chokkalingam, A. Piruska, H. A. Heus, and W. T. S. Huck, *Enhanced transcription rates in membrane-free protocells formed by coacervation of cell lysate,* Proceedings of the National Academy of Sciences **110**, 11692 (2013).

[41] P. Van Nies, I. Westerlaken, D. Blanken, M. Salas, M. Mencía, and C. Danelon, *Self-replication of DNA by its encoded proteins in liposome-based synthetic cells,* Nature Communications **9**, 1583 (2018).

[42] K. Zieske and P. Schwille, *Reconstitution of self-organizing protein gradients as spatial cues in cell-free systems,* eLife **3**, e03949 (2014).

[43] N. N. Deng, M. A. Vibhute, L. Zheng, H. Zhao, M. Yelleswarapu, and W. T. Huck, *Macromolecularly Crowded Protocells from Reversibly Shrinking Monodisperse Liposomes,* Journal of the American Chemical Society **140**, 7399 (2018).

[44] K. Zieske and P. Schwille, *Reconstitution of pole-to-pole oscillations of min proteins in microengineered polydimethylsiloxane compartments,* Angewandte Chemie - International Edition **52**, 459 (2013).

[45] T. E. Holy, M. Dogterom, B. Yurke, and S. Leibler, *Assembly and positioning of microtubule asters in microfabricated chambers,* Proceedings of the National Academy of Sciences **94**, 6228 (1997).

[46] S. Deshpande and T. Pfohl, *Real-Time Dynamics of Emerging Actin Networks in Cell-Mimicking Compartments,* PLOS ONE **10**, e0116521 (2015).

[47] A. Huebner, D. Bratton, G. Whyte, M. Yang, A. J. Demello, C. Abell, and F. Hollfelder, *Static microdroplet arrays: A microfluidic device for droplet trapping, incubation and release for enzymatic and cell-based assays,* Lab on a Chip **9**, 692 (2009).

[48] W. Wang, C. Yang, and C. M. Li, *On-demand microfluidic droplet trapping and fusion for on-chip static droplet assays,* Lab on a Chip **9**, 1504 (2009).

[49] W. Shi, J. Qin, N. Ye, and B. Lin, *Droplet-based microfluidic system for individual Caenorhabditis elegans assay,* Lab on a Chip **8**, 1432 (2008).

[50] L. Yu, M. C. Chen, and K. C. Cheung, *Droplet-based microfluidic system for multicellular tumor spheroid formation and anticancer drug testing,* Lab on a Chip **10**, 2424 (2010).

[51] T. P. Hunt, D. Issadore, and R. M. Westervelt, *Integrated circuit/microfluidic chip to programmably trap and move cells and droplets with dielectrophoresis,* Lab on a Chip **8**, 81 (2007).

[52] H. Boukellal, Š. Selimović, Y. Jia, G. Cristobal, and S. Fraden, *Simple, robust storage of drops and fluids in a microfluidic device,* Lab on a Chip **9**, 331 (2009).

[53] G. F. Christopher, J. Bergstein, N. B. End, M. Poon, C. Nguyen, and S. L. Anna, *Coalescence and splitting of confined droplets at microfluidic junctions,* Lab on a Chip **9**, 1102 (2009).

[54] S. Deshpande, W. K. Spoelstra, M. Van Doorn, J. Kerssemakers, and C. Dekker, *Mechanical Division of Cell-Sized Liposomes,* ACS Nano **12**, 2560 (2018).

[55] J. McGrath, M. Jimenez, and H. Bridle, *Deterministic lateral displacement for particle separation: A review,* Lab on a Chip **14**, 4139 (2014).

[56] J. U. Shim, G. Cristobal, D. R. Link, T. Thorsen, Y. Jia, K. Piattelli, and S. Fraden, *Control and measurement of the phase behavior of aqueous solutions using microfluidics,* Journal of the American Chemical Society **129**, 8825 (2007).

[57] H. C. Shum, D. Lee, I. Yoon, T. Kodger, and D. A. Weitz, *Double Emulsion Templated Monodisperse Phospholipid Vesicles,* Langmuir , 7651 (2008).

[58] H. C. Shum, E. Santanach-carreras, J.-w. Kim, A. Ehrlicher, J. Bibette, and D. A. Weitz, *Dewetting-Induced Membrane Formation by Adhesion of Amphiphile-Laden Interfaces,* Journal of the American Chemical Society , 4420 (2011).

[59] F. R. Hallett, J. Marsh, B. G. Nickel, and J. M. Wood, *Mechanical properties of vesicles. II. A model for osmotic swelling and lysis,* Biophysical Journal **64**, 435 (1993).

[60] U. Seifert, K. Berndl, and R. Lipowsky, *Shape transformations of vesicles: Phase diagram for spontaneous curvature and bilayer-coupling models,* Physical Review A **44**, 1182 (1991).

[61] E. Bi and J. Lutkenhaus, *FtsZ ring structure associated with division in Escherichia coli,* Nature **354**, 161 (1991).

[62] G. N. Ramachandran and G. Kartha, *Structure of Collagen,* Nature **174**, 269 (1954).

[63] T. den Blaauwen, L. W. Hamoen, and P. A. Levin, *The divisome at 25: the road ahead,* Current Opinion in Microbiology **36**, 85 (2017).

[64] F. Chang and S. G. Martin, *Shaping Fission Yeast with Microtubules,* Cold Spring Harbor perspectives in biology , 1 (2009).

[65] J. Tønnesen, V. K. Inavalli, and U. V. Nägerl, *Super-resolution imaging of the extracellular space in living brain tissue,* Cell **172**, 1108 (2018).

[66] P. P. Provenzano and R. V. Jr, *Collagen fibril morphology and organization : Implications for force transmission in ligament and tendon,* Matrix Biology **25**, 71 (2006).

[67] T. Gutsmann, G. E. Fantner, M. Venturoni, A. Ekani-nkodo, J. B. Thompson, J. H. Kindt, D. E. Morse, K. Fygenson, and P. K. Hansma, *Evidence that Collagen Fibrils in Tendons Are Inhomogeneously Structured in a Tubelike Manner,* Biophysical Journal **84**, 2593 (2003).

[68] H. T. McMahon and J. L. Gallop, *Membrane curvature and mechanisms of dynamic cell membrane remodelling,* Nature **438**, 590 (2005).

[69] B. Söderström, A. Badrutdinov, H. Chan, and U. Skoglund, *Cell shape-independent FtsZ dynamics in synthetically remodeled bacterial cells,* Nature Communications **9**, 4323 (2018).

[70] S. Deshpande, Y. Caspi, A. E. Meijering, and C. Dekker, *Octanol-assisted liposome assembly on chip,* Nature Communications **7**, 1 (2016).

[71] Y. Caspi and C. Dekker, *Mapping out Min protein patterns in fully confined fluidic chambers,* eLife **5**, e19271 (2016).

[72] S. Cunha, C. L. Woldringh, and T. Odijk, *Polymer-Mediated Compaction and Internal Dynamics of Isolated Escherichia coli Nucleoids,* Journal of Structural Biology **136**, 53 (2001).

[73] K. Zieske, G. Chwastek, and P. Schwille, *Protein Patterns and Oscillations on Lipid Monolayers and in Microdroplets,* Angewandte Chemie - International Edition **55**, 13455 (2016).

[74] N. Taberner, A. Lof, S. Roth, D. Lamers, H. Zeijlemaker, and M. Dogterom, *Chapter 1 - in vitro systems for the study of microtubule-based cell polarity in fission yeast,* in *Building a Cell from its Component Parts,* Methods in Cell Biology, Vol. 128, edited by J. Ross and W. F. Marshall (Academic Press, 2015) pp. 1 – 22.

[75] O. Pierucci, *Dimensions of escherichia coli at various growth rates: model for envelope growth.* Journal of Bacteriology **135**, 559 (1978).

[76] M. R. Ahmad, M. Nakajima, S. Kojima, M. Homma, and T. Fukuda, *The effects of cell sizes, environmental conditions, and growth phases on the strength of individual W303 yeast cells inside ESEM,* IEEE Transactions on Nanobioscience **7**, 185 (2008).

[77] W. F. Marshall, K. D. Young, M. Swaffer, E. Wood, P. Nurse, A. Kimura, J. Frankel, J. Wallingford, V. Walbot, X. Qu, and A. H. K. Roeder, *What determines cell size?* BMC Biology **10**, 101 (2012).

[78] S. Maass, S. Sievers, D. Zühlke, J. Kuzinski, P. K. Sappa, J. Muntel, B. Hessling, J. Bernhardt, R. Sietmann, U. Völker, M. Hecker, and D. Becher, *Efficient, Global-Scale Quantification of Absolute Protein Amounts by Integration of Targeted Mass Spectrometry and Two-Dimensional Gel-Based Proteomics,* Analytical Chemistry **83**, 2677 (2011).

[79] L. Zhao, C. D. Kroenke, J. Song, D. Piwnica-Worms, J. J. H. Ackerman, and J. J. Neil, *Intracellular water-specific MR of microbead-adherent cells: the HeLa cell intracellular water exchange lifetime,* NMR in Biomedicine **21**, 159 (2008).

[80] M. Diez-Silva, M. Dao, J. Han, C.-T. Lim, and S. Suresh, *Shape and Biomechanical Characteristics of Human Red Blood Cells in Health and Disease,* MRS Bulletin **35**, 382 (2010).

[81] S. Göktepe, O. J. Abilez, K. K. Parker, and E. Kuhl, *A multiscale model for eccentric and concentric cardiac growth through sarcomerogenesis,* Journal of Theoretical Biology **265**, 433 (2010).

[82] S. Albers, J. Eichler, and M. Aebi, *Archaea,* in *Essentials of Glycobiology. 3rd edition* (Cold Spring Harbor Laboratory Press, 2017).

[83] D. Suslov, J.-P. Verbelen, and K. Vissenberg, *Onion epidermis as a new model to study the control of growth anisotropy in higher plants,* Journal of Experimental Botany **60**, 4175 (2009).

[84] F. L. Lederer, T. J. Günther, U. Weinert, J. Raff, and K. Pollmann, *Development of functionalised polyelectrolyte capsules using filamentous Escherichia coli cells,* Microbial Cell Factories **11**, 163 (2012).

[85] K. D. Young, *The Selective Value of Bacterial Shape,* Microbiology and Molecular Biology Reviews **70**, 660 (2006).

[86] H. Zhao, U. Dreses-Werringloer, P. Davies, and P. Marambaud, *Amyloid-beta peptide degradation in cell cultures by mycoplasma contaminants,* BMC Research Notes **1**, 38 (2008).

3

FtsZ bundle formation in cell-mimicking droplets

Bacterial cell division is a fascinating process orchestrated by the Z-ring, a complex protein structure which assembles at the cell mid-plane to constrict the division site. The key element of its machinery is FtsZ, a protein that in E. coli polymerizes into filaments which dock to the membrane via two anchor proteins, ZipA and FtsA. FtsZ filaments are thought to laterally associate into thicker bundles that constitute the scaffold and coordinate all the other proteins composing the Z-ring machinery. It is yet unclear how factors such as crowding conditions, protein concentrations, and the membrane anchor proteins, do regulate this bundling. Here, we reconstitute a minimal version of this system, i.e., FtsZ and a soluble version of ZipA, on the inner lipid membrane of microns-size water-in-oil droplets. We find that the capability of FtsZ filaments to assemble into bundles is heavily influenced by the crowding conditions, while variation of FtsZ concentration is not crucial. ZipA densely partitions along the FtsZ filaments and promotes bundle formation. Furthermore, FtsZ bundle assembling appeared to be more robust in smaller droplets. Altogether, our results identify the proper conditions to promote FtsZ bundle formation, a much welcome step towards the bottom-up assembly of a functional divisome in synthetic cells.

This chapter has been submitted: F. Fanalista, J. W. J. Kerssemakers, and C. Dekker, *FtsZ bundle formation in cell-mimicking droplets.*

3.1. INTRODUCTION

Cell replication is a marvelously organized process that ensures the proliferation of cellular organisms via the division of a mother cell into daughter ones. In most bacteria, the binary fission of the cell is orchestrated by the so called Z-ring, a ring-like multi-protein structure which assembles at the cell mid-plane and which progressively constricts the division site.[1, 2] The key-element of this structure is FtsZ, a prokaryotic homologue of tubulin, which employs guanosine triphosphate (GTP) to assemble 100-200 nm long filaments constituting the main scaffold of the Z-ring.[3, 4] These filaments have been shown in cells to undergo treadmilling dynamics, driving the enzymes responsible for the cell wall synthesis along the cellular circumference at the division site.[5, 6] While it is clear that FtsZ plays a central role as an organizer of the divisome, it is still under debate whether FtsZ filaments does generate a force to induce an invagination of the cell.[7, 8] It is known that FtsZ is recruited at early stages of the cell-cycle at the cell mid-plane, concurrently with its membrane anchor proteins ZipA and FtsA and a few other additional accessory proteins.[9, 10] While FtsA is conserved across most bacteria, ZipA is present as a membrane anchor protein only in gammaproteobacteria.[11] In *E. coli* the ring is still able to assemble in absence of one of the two anchors, but constriction and consequent division is not observed. When the cell lacks both membrane anchors, the ring does not assemble at all.[12] By laterally associating into multi-strand structures, that from here on we will refer to as 'bundles', FtsZ filaments form a ring that super-resolution microscopy revealed to be rather nonuniform and patchy along its circumference.[13, 14]

Lateral interactions between FtsZ filaments have been shown to be fundamental for the proper proliferation of the cell.[15] While the polymerization of FtsZ monomers into a linear single-strand filament and GTP activity are regulated by the FtsZ globular domain close to the N-terminus,[16] the protein region near the C-terminus appears to be responsible for the lateral interaction between the filaments. Evidences supporting this hypothesis involve both the C-terminal flexible linker,[17, 18] as well as the C-terminus region.[19] Interestingly, the FtsZ C-terminus domain also interacts with the membrane anchor proteins ZipA and FtsA, ensuring the proper docking of the filaments to the lipid membrane.[20] Whether and how the two membrane anchor proteins may mediate the interaction between FtsZ filaments is still unclear.

Several *in vitro* experiments previously reported the formation of multi-strand FtsZ structures in bulk in different buffer conditions.[21–24] However, the cell is a membrane-enclosed and heavily crowded environment,[25] and a systematic study on the conditions for FtsZ bundles to form within a closed lipid membrane via interaction with one or more anchor proteins is yet missing. Earlier interesting *in vitro* efforts made in this direction led to varying conclusions. For example, when encapsulating FtsZ inside artificial microns-size confinements in the absence of anchor proteins, the bundling properties of FtsZ filaments were found to be strongly dependent on the addition of macromolecular crowders.[26, 27] Next to that, on supported lipid bilayers and in the absence of macromolecular crowders, FtsZ filaments were shown to organize into bundles which dynamics strongly depended on the specific membrane anchoring system employed.[28, 29] Regarding ZipA, experimental evidence that accumulated so far led to contrasting conclusions: while electron and fluorescence microscopy imaging revealed

how ZipA promotes the association of FtsZ filaments into bundles in bulk,[30, 31] work on lipid nanodiscs assigned a limiting role to ZipA as a mere passive membrane anchor protein.[32, 33]

Given the discrepancy between experimental outcomes and the large variety of experimental conditions employed in previous studies, we here aimed to shine some light on the above-mentioned questions by reconstituting a minimal version of the protoring inside cell-mimicking microns-size compartments and systematically varying conditions. Specifically, we encapsulated FtsZ and a soluble version of ZipA inside water-in-oil droplets (henceforth simply referred to as "droplets") that featured a lipid monolayer at the interface. By means of fluorescence microscopy, we show that the formation of FtsZ filamentous bundles on the surface of the droplets is heavily affected by the crowding conditions and the confinement size, while the protein concentration plays a less decisive role. Furthermore, we show that ZipA densely partitions along the FtsZ bundles and promotes their association into higher-ordered structures.

3.2. RESULTS

To reconstitute FtsZ bundles on the membrane of microns-size confinements, an aqueous solution containing 12 μM FtsZ and 6 μM of a soluble version of the membrane anchor protein ZipA was pipetted into an oil solution provided with lipids. By applying shear stress through vortexing (Fig. 3.1a), droplets broke down to microns-size (see methods section for details) and the lipids that were dissolved in the oil phase spontaneously assembled a monolayer at the water-oil interface, stabilizing the droplet surface and inhibiting re-merging of droplets. Note that the hydrophobic transmembrane domain of ZipA was replaced by a His-tag, which binds to the nickel tag on the headgroup of DGS-NTA lipids,[34] so that the protein served as a means for FtsZ filaments to attach to the membrane (Fig. 3.1b). To induce FtsZ polymerization into filaments, the proteins were mixed together with GTP. To promote lateral association between FtsZ filaments, we recreated a crowded environment by the addition of an inert macromolecular crowding agent (Ficoll 70) to the aqueous phase, to a final concentration of 62.5 mg ml^{-1}. Image acquisition started roughly five minutes after droplet production. In these conditions, some droplets already displayed protein clusters randomly arranged on the lipid membrane (Fig. 3.1c). Following, in a few minutes such clusters appeared to grow and extend to form long structures, until a filamentous network was formed. It is interesting to notice that the ZipA colocalized with FtsZ during this process. In different droplets, the formation of protein bundles occurred at different time, and after roughly one hour from the moment of production, essentially all droplets in the sample displayed long filamentous FtsZ bundles. By acquiring a z-stack over different focal planes scanning the whole volume of the droplets, it was possible to observe that a dense filamentous protein network was localized at the surface (Fig. 3.2), indicating proper attachment of the proteins to the lipid monolayer. ZipA did appear not to be homogeneously distributed along the membrane, but arranged into bundles that matched the spatial configuration of FtsZ (Fig. 3.2, right). Once formed, the bundles appeared to become thicker, while the background intensity decreased over time, suggesting that more FtsZ filaments from within the droplets were adhering to the already formed network, which did not show any major rearrangement and remained stable for several hours (Fig. 3.6). By contrast,

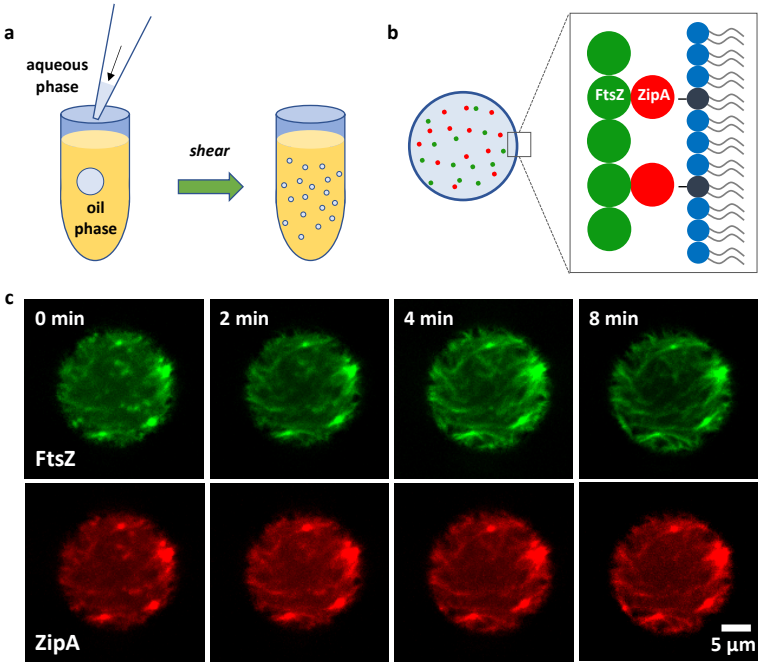

Figure 3.1: **Reconstitution of FtsZ bundles inside water-in-oil droplets.** (a) Schematic of the droplet production process: an aqueous phase containing the protein system is pipetted into a mineral oil solution where lipids are dissolved. The shear stress produced by briefly vortexing the solution induced the droplets to break into smaller ones, down to micron-size range. Thanks to their amphiphilic nature, the lipids dissolved into the oil phase spontaneously assembled a mono-layer at the droplet surface, stabilizing the water-oil interface and preventing droplets from re-merging. (b) Schematic of the reconstituted protein system: upon addition of GTP, FtsZ (green) polymerizes into filaments, which attached to the lipid membrane via a soluble version of ZipA (red). Such modified anchor protein lacks of the natural transmembrane hydrophobic helix, replaced by a His-tag that binds the Ni-group of the DGS-NTA lipids (dark-blue) present on the droplet surface. (c) Fluorescence confocal images showing the dynamics of FtsZ bundles forming on the droplet membrane. Images were obtained by 2D-projection of a Z-stack acquired at the bottom surface of the droplets. Protein clusters were visible in some droplets already at the start of image acquisition, roughly 5 minutes from droplet production. Such clusters appeared to be stably located on the membrane, and to elongate over time, leading to the formation of a complex bundle network within a few minutes. FtsZ (top row) and ZipA (bottom row) were fluorescently labelled with, respectively, Alexa488 and Alexa 647.

without ZipA or DGS-NTA lipids, FtsZ bundles were either not visible, or displaced within the bulk volume in a consistent fraction of droplets (Fig. 3.7a-b). The remaining droplets appeared to have only a few bundles at the surface (Fig. 3.7c), in stark contrast with the dense network formed on the membrane in the presence of the proper anchoring system.

To understand how FtsZ and ZipA interact and partition into filamentous structures, we measured the fluorescent signal emitted by the two proteins in two distinct cases: when bundles formed on the droplet surface (Fig. 3.3a, top), and when both DGS-NTA

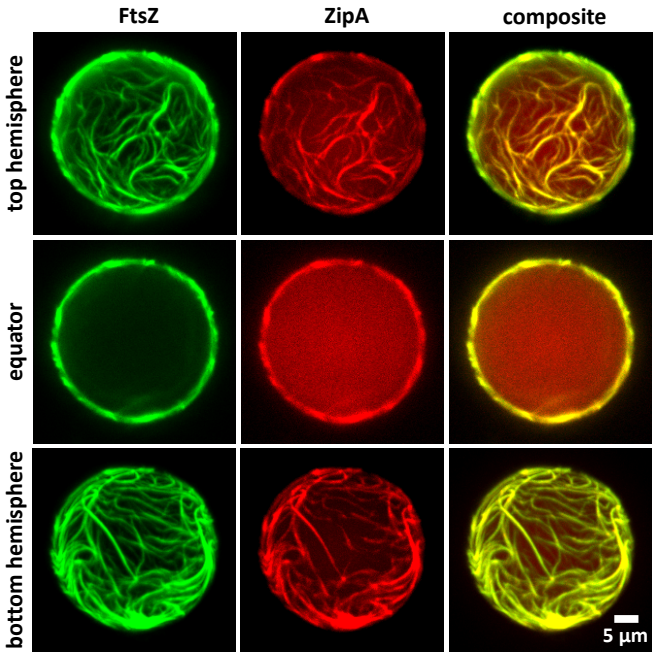

Figure 3.2: **Fluorescence confocal microscopy of FtsZ/ZipA protein structures inside droplets.** The top and bottom row depict, respectively, the top and the bottom droplet hemispheres. Long filamentous protein structures are seen to be present at the droplet surface. On the middle row, the equatorial cross section further indicates the adhesion of the proteins to the droplet membrane. Both FtsZ (left column) and ZipA (center column) appear distributed in filamentous bundles. By overlapping the two signals (right column), it is evident that the two proteins colocalized.

lipids and GTP were removed from the system to prevent, respectively, protein binding to the membrane and FtsZ polymerization (Fig. 3.3a, bottom). For each droplet, we averaged the fluorescent intensity profiles acquired at the equatorial cross section along radial lines going from the droplet center to the external oil phase. The average profile from multiple droplets (N = 32) showed that, when bundles are formed, both FtsZ (Fig. 3.3b, green, left) and ZipA (Fig. 3.3b, red, right) partitioned to the membrane (i.e., at 100% radial distance), while the signal did not show any preferential localization in the droplets when FtsZ polymerization and membrane binding were prevented (N = 27). To measure the partitioning of FtsZ and ZipA inside the droplets, we analyzed the ratio r between the two protein signals. The ratio measured in absence of bundles appeared to be approximately constant inside the droplet volume, as expected and further indicating that both proteins were homogeneously distributed within the droplets. Giving that the plateau ratio r = 1.10 ± 0.02 between the fluorophore intensities of FtsZ and ZipA represents the 2:1 molar ratio between the proteins that was administered in the experiments, we recalibrated the profiles in Figure 3c such that the bulk ratio measured r = 2, which

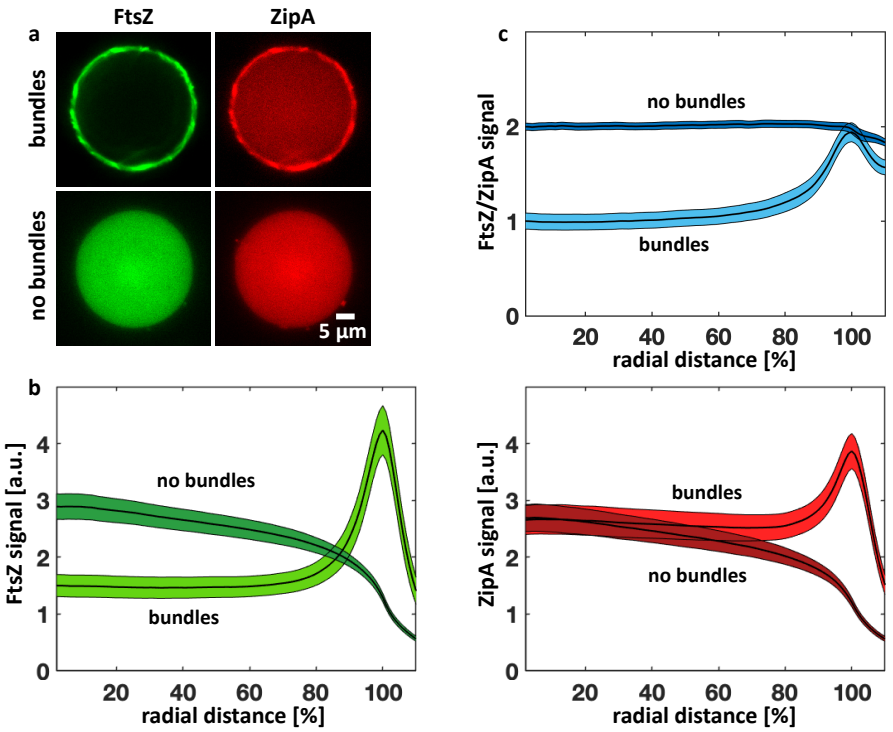

Figure 3.3: **Analysis of FtsZ and ZipA fluorescence signal in the presence or lack of protein bundles on the droplet surface.** a) Confocal fluorescence images of FtsZ (green) and ZipA (red) distribution at the droplet equatorial plane. FtsZ bundles formed at the membrane appeared as a bright fluorescent ring (top). In absence of GTP and DGS-NTA lipids, the two proteins appeared homogeneously distributed within the droplet volume (bottom). b) FtsZ (left panel) and ZipA (right panel) fluorescence profile measured along radial direction at the droplet equatorial plane. In absence of bundle formation, both protein signals decreased from the droplet center (0% radial distance) to the oil phase outside the droplets, indicating a homogenous protein distribution inside the spherical droplets. By contrast, when bundles were formed, the signals clearly indicated a strong protein recruitment to the lipid membrane at the droplet surface (100% radial distance). c) Ratio between FtsZ and ZipA fluorescent signals. In the absence of FtsZ bundles, the ratio between the two protein inside the droplet is constant, while the ratio peaked at the lipid membrane when bundles were formed. The colored area around the plot lines represent the error on the mean from different droplets (bundles N = 32, no bundles N = 27).

accounts for the different fluorophore-to-concentration couplings. In the presence of bundles, the protein ratio $r < 2$ within the droplet volume then indicated how the major part of FtsZ was recruited to bundles at the droplet surface. At the membrane surface, however, the ratio adopted a value of $r = 2$, revealing that in the protein bundles there are two molecules of FtsZ for every molecule of ZipA, which amounts to a high density of anchors along the filamentous structures.

In *E. coli*, FtsZ and ZipA concentrations have been shown to be quite constant throughout the cell cycle,[9] while a more recent work has found mild variations.[35] We decided to investigate to what extent the capability of FtsZ to form bundles would be affected by a variation of protein concentrations inside our cell-mimicking closed en-

vironments. We varied the amount of FtsZ and ZipA encapsulated inside the droplets, while maintaining a continuous high density of crowding agent (62.5 mg ml^{-1} Ficoll 70) to create a favorable condition for bundles to form. To resemble physiological conditions, we explored a range of FtsZ concentration around 5 μM,[7] and we kept the molar ratio between FtsZ and ZipA constant to a ratio of 2:1.[9] From our observations, we classified the droplets into three main categories, depending on the apparent status of FtsZ filament condensation on their membranes (Fig. 3.4a): the droplets which showed long filamentous bundles on their surface; droplets where a homogeneous fluorescent signal indicated the presence of unaggregated FtsZ filaments (too tiny to be individually resolved by our microscope setup);[36] and a third category, more frequent at lower FtsZ concentrations, where FtsZ filaments did not appear as homogeneously distributed, but associated into small and short clusters that were not extended into long bundles. In all experiments, we analyzed the droplets after 1 hour from the production, a time frame long enough for the protein bundle network to form in 98% of droplets (N = 133) for 12 μM FtsZ. Noticeably, the capacity of FtsZ filaments to aggregate into bundles did not seem to depend in a critically way on the protein concentration (Fig. 3.4b): at FtsZ concentrations of 8 μM, 4 μM and 2 μM, a large fraction of droplets (respectively 95%, 69%, and 41%) still showed long filamentous bundles on the membrane. For the same FtsZ concentrations, the fraction of droplets showing cluster features corresponded respectively to 4%, 22%, and 29% of the samples analyzed. Interestingly, we observed that droplet size also has an impact on the capacity of FtsZ bundles to form on their lipid membrane. Indeed, at 2 μM FtsZ, the droplets showing bundles or clusters on the membrane had an average diameter of respectively dbundles = 13.5 ± 1.1 μm (N = 28) and $d_{clusters}$ = 12.8 ± 1.8 (N = 20), while the droplets where FtsZ filaments appeared homogeneously distributed had an average diameter $d_{filaments}$ = 24.2 ± 3.1 (N = 21). Thus, the condensation of FtsZ filaments appeared to be more robust in the fraction of droplets with smaller diameters. Additionally, at the lowest FtsZ concentration (2 μM), bundles were still able to form even at mild crowding conditions (31.3 mg ml^{-1} Ficoll 70), with 10% of the droplets exhibiting filamentous protein structures on the membrane, indicating the robustness of the process.

We also employed our system to test whether the concentration of ZipA would also promote the association of FtsZ filaments into bundles. To do so, we encapsulated 2 μM of FtsZ alongside 2 μM of ZipA inside the droplets, thus effectively increasing the molar ratio between the two proteins from 1:2 (as explored so far) to 1:1. To understand whether this variation affected the density of ZipA on the membrane, we compared the number of DGS-NTA lipids available on the droplet surface to the number of ZipA molecules encapsulated in the droplet volume. From the density of DGS:DOPC lipids, we estimate that, in droplets with diameter up to 20 μm (which compose the majority of the sample), there were enough DGS-NTA lipids on the membrane to accommodate all ZipA proteins encapsulated, indicating that the enhanced ZipA concentration effectively doubled the anchor surface density on the droplet membrane. The results indicated that such increased concentration seems to positively affects the formation of FtsZ bundles (Fig. 3.4c), as the fraction of droplets where long filamentous bundles or clusters were clearly visible on the membrane increased to 73% and 17% respectively (N = 99), with only less than 1 out of 10 droplets showing the absence of any visible protein structure.

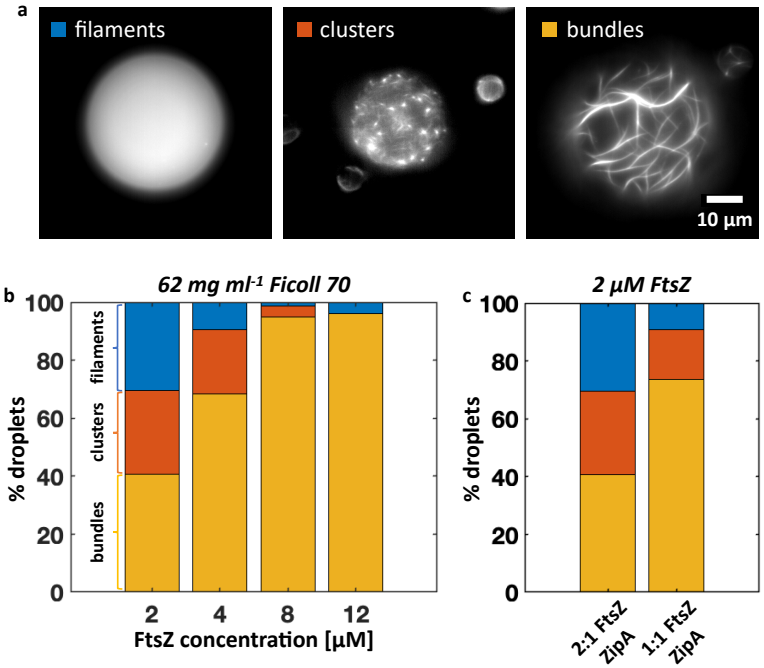

Figure 3.4: **Effect of protein concentration on the condensation of FtsZ filaments into bundles.** (a) Fluorescence microscopy images of different FtsZ filament condensation states on the bottom surface of droplets: in absence of bundle formation, FtsZ filaments appeared homogenously distributed on the droplet surface (left). Alternatively, at low protein concentration, FtsZ filaments were clustered in short structures (center), while they grew into long filamentous bundles at higher concentrations (right). (b) Histogram illustrating the fractions of droplets displaying different aggregation states of FtsZ filaments on the membrane for different protein concentration. As FtsZ and ZipA were systematically lowered (with a fixed molar ratio of 2:1 between the two proteins), the fraction of droplets showing filamentous bundles (yellow) decreased, giving space to droplets where only small FtsZ clusters (red) or no visible structures (blue) were present on the membrane. (c) Histogram showing the effect of the FtsZ:ZipA molar ratio on FtsZ bundling at a low concentration (2 µM). By increasing the molar ratio between ZipA and FtsZ from 1:2 to 1:1, the fraction of droplets (N = 99) where FtsZ condensed into bundles on the membrane increased significantly, indicating the capability of the membrane anchor protein to promote lateral interaction between FtsZ filaments.

Finally, to examine to what extent the heavy crowding present in the cell is responsible for the association of FtsZ filaments into higher-order structures, we systematically varied the concentration of Ficoll 70 in the aqueous phase to change the crowding conditions in the droplets. Because we observed that bundles were fully formed when FtsZ was encapsulated at 12 µM, we employed such a high concentration in all the experiments to identify the effect of crowding on filament condensation. After 1 hour from the production, we counted the number of droplets that did have filamentous bundles visible on the surface. The results showed that the association of FtsZ filaments into bundles on the droplet surface was strongly influenced by the presence of macromolecular crowders: as mentioned, the fraction of droplets exhibiting filamentous structures

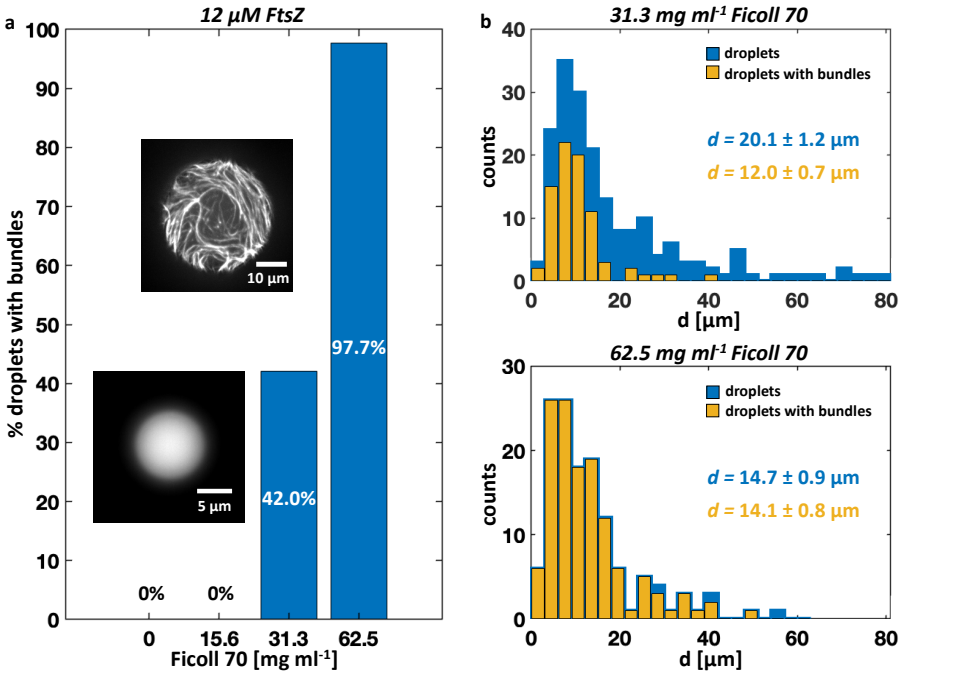

Figure 3.5: **Effect of macromolecular crowding on the condensation of FtsZ filaments into bundles.** (a) Histogram showing the fraction of droplets displaying filamentous FtsZ structures on the membrane. Droplets with bundles on the surface could clearly be distinguished from those where unaggregated filaments appeared homogeneously distributed in the lumen (see insets, droplet bottom surface). When 62.5 mg ml^{-1} (N = 133), 31.3 mg ml^{-1} (N = 188), 15.6 mg ml^{-1} (N = 45), or 0 mg ml^{-1} (N = 24) Ficoll 70 was encapsulated inside the droplets, respectively 98%, 42%, 0% and 0% of the droplets displayed bundles, indicating a strong influence of crowding conditions on the interaction between FtsZ filaments. (b) Histograms of the diameter of the droplet fraction displaying filamentous FtsZ bundles on the membrane (yellow) against the entire droplet populations analyzed (blue) for two different crowding conditions. From comparing the average size of the droplets in the two histograms, it appears that larger droplet size negatively affects FtsZ bundling.

was 98% in presence of 62.5 mg ml^{-1} Ficoll 70 (N = 133), which dropped down to 42% for a reduced concentration of 31.3 mg ml^{-1} (N = 188), while below this concentration, bundles did not form at all (Fig. 3.5a). Furthermore, similarly to what observed at low protein concentration, we identified a significant correlation between the presence of bundles and the size of the droplets. As can be seen from the histograms in Figure 5b, the fraction of droplets having bundles (yellow) compared to the whole droplet population (blue) appeared to have a smaller average size at lower crowding conditions (31.3 mg ml^{-1} Ficoll 70). Specifically, on a droplet population with an average diameter d = 20.1 ± 1.2 µm, the fraction of droplets showing bundles on the surface measured a much lower average size of d = 12.0 ± 0.7 µm. By contrast, in higher crowding conditions, the droplets where bundles formed on the surface had a medium size (d = 14.7 ± 0.9 µm), comparable to the average size of the whole population analyzed (d = 14.1 ± 0.8 µm).

3.3. DISCUSSION

FtsZ filament association into bundles is a key aspect for the assembly and functioning of the Z-ring, the protein machinery responsible for division in most of bacteria. In this work, we recreated an in vitro minimal system that mimics real cell conditions, to explore the dynamics of FtsZ bundles formation on the lipid surface inside microns-size droplets. Specifically, we aimed to clarify the role of the anchor protein ZipA in the bundle formation process, together with the effects that protein concentration, crowding conditions, and confinement size have on the filament condensation.

By imaging the droplet membrane with fluorescence confocal microscopy, we observed that the formation of FtsZ filaments into bundles proceeds in two steps: a first nucleation step, where filaments condense into small clusters, followed by a second phase in which such structures further grow into long filamentous bundles. The protein clusters did not appear to diffuse on the membrane, but to grow and elongate into the fibrous network that, once formed, appeared stable over hours. This indicates that the first structures that adhered to the surface served as a scaffold for further FtsZ filaments to associate with them, so that the network grew into a final stable configuration. The long-lasting stability of the network formed on the lipid membrane greatly exceeded the time required for the FtsZ to hydrolyze all the GTP provided at the moment of the encapsulation, consistent with what was previously reported, where GTP hydrolysis and monomer turnover occurs slower along FtsZ filaments when condensed into bundles in bulk.[22] However, differently from bulk experiments,[22, 23] bundle formation did not occur immediately after addition of GTP, but with a time delay, as observed both on supported lipid bilayers,[29] as well as in closed microns-size volumes.[26]

Interestingly, we observed that the overall protein concentration influenced the elongation of the clusters into bundles, but did not critically impact the first nucleation step: even at 2 μM FtsZ, close to the critical concentration required for FtsZ to polymerize,[36] 70% of droplets exhibited filament condensation on the membrane. On the other hand, a reduction of crowding conditions seemed to heavily impact the condensation of filaments into bundles, with a critical concentration of Ficoll 70 (between 16 and 32 mg ml^{-1}) below which FtsZ filaments appeared homogeneously distributed in the droplet. Notably, inert crowder molecules such as Ficoll 70 might have a stronger effect compared to other biological molecules.[27]

To bind FtsZ filaments to the membrane, we employed the *E. coli* anchor protein ZipA, which appeared, from the analysis of fluorescence signal, to strongly colocalize with the FtsZ filamentous structures. The different behavior of FtsZ bundles previously observed in presence of ZipA or FtsA was hypothesized to depend on the specific capacity of the anchors to preferentially bind, respectively, to short FtsZ oligomers or to longer FtsZ filaments.29 In a scenario where ZipA monomers provide anchoring to FtsZ short filaments, ZipA is expected to abundantly partition within the FtsZ bundles. Our results seem to support this model, as the ratio between FtsZ and ZipA measured along the filamentous bundles equaled a value of 2:1, resembling the physiological one.[29]

Similarly to what reported for different proteins associated to the Z-ring,[37–39] it has been suggested that also ZipA and FtsA play a role in regulating the interactions between FtsZ filaments.[31, 40] In this paper, we focused on ZipA, as its capability to promote FtsZ filament bundling is still under debate. A recent report argued against the formation of

FtsZ bundles in presence of ZipA, as electron microscopy imaging revealed a large spacing between the FtsZ filaments.[41] However, at a high ZipA surface density, FtsZ filaments were observed to switch from a swirl configuration, which favors treadmilling, to a straight parallel alignment. This looks consistent with the long rod-like appearance of ZipA-bond FtsZ bundles observed in this work in spherical droplets, as well as with what previously shown on flat supported lipid bilayers.[29] We suggest that the inhibition of cell division induced by ZipA overexpression in vivo[34] could result from the excessively enhanced interactions between FtsZ filaments, which could force the filaments in a configuration that disrupts the proper treadmilling dynamics necessary for initiating cell division. Indeed, consistently with what previously reported in bulk,[30, 31] our data seem to favor a scenario where ZipA induces FtsZ filaments to bundle, since a higher ZipA concentration led to a higher fraction of droplets with filamentous bundles adhered to the surface. This behavior was confirmed also in control experiments, since in absence of ZipA a higher fraction of droplets presented a homogenous FtsZ filament distribution compared to those lacking DGS-NTA lipids. Given that the ZipA concentration (1-2 μM) is negligible compared to the amount of crowding agent employed in the experiments (0.89 mM), the enhanced bundling appears to be a consequence of the direct interaction between ZipA and FtsZ rather than a crowding effect.

Our data also showed that the confinement geometry plays a relevant role on the assembly properties of protein filaments. FtsZ bundles appeared more stable against variation of crowding and protein concentration in droplets with a smaller size, where a higher surface-to-volume ratio seemed to favor filament assembly. Assuming that FtsZ freely diffuses in the droplet volume, the probability for the protein to interact with the membrane would increase in droplets with higher surface-to-volume ratio, effectively enhancing the local protein concentration and thus explaining the more favorable bundle formation in smaller containers. This is consistent with the fact that such an effect becomes noticeable at lower crowding conditions, as the excluded volume created by the Ficoll 70 molecules effectively increases the surface-to-volume ratio of the droplets. While the influence of the confinement size on the capacity of FtsZ filaments to condensate was not reported before, previous reports mentioned an effect on the arrangement of the bundles on the membrane.[42, 43] Similar to different protein systems involved in cell division (e.g. the prokaryotic Min system[44, 45] and the eukaryotic tubulin),[43] it would be interesting to achieve better control over the formation and spatial configuration of FtsZ bundles in lipid-bound containers by a fine tuning of the confinement geometry.

To conclude, the lateral interactions between FtsZ filaments, which underlies the proper functioning of the Z-ring in bacteria, have been subject to several speculations, including the possibility that they could play a role in the generation of a constrictive force at the division site.[46, 47] Here, we explored the relevant conditions to reproduce in vitro the condensation of FtsZ filaments into bundles on the membrane of cell-mimicking microns-size containers, a necessary step towards the bottom-up assembly of a functional minimal divisome.

3.4. METHODS

DEVICE PRODUCTION

The devices used to collect and visualize the samples were composed by a thick square (~2 x 2 cm^2) piece of polydimethylsiloxane (PDMS) with holes, sealed on the bottom by a PDMS-covered glass coverslip. First, PDMS and curing agent (MAVOM) were mixed in a ratio 1:10 for about five minutes, vacuumed for about 10 minutes to remove air bubbles, and then poured on two plain 4" silicon wafers. On one wafer, coverslips were firmly pressed down into the PDMS to create a thin PDMS layer between the wafer and the coverslips. On the second wafer, aluminum foil was employed to stem the PDMS, which formed a flat slab ~5 mm thick. Both wafers were baked at 80 °C for 4 hours, then the coverslips and the PDMS slab were peeled off. By means of a cutter, the PDMS slab was divided into square pieces (~2 x 2 cm^2), on which 4 mm holes were made using a puncher, and then cleaned in isopropanol. Both the PDMS squares and the coverslips were then activated via Oxygen plasma treatment (Plasmatic System, Inc.), bond together and baked further at 80 °C overnight to restore hydrophobicity.

WATER-IN-OIL DROPLETS

To prepare the oil solution, lipids purchased in chloroform (Avanti Polar Lipids, Inc.) were mixed in a glass vial and dried in vacuum for at least one hour, then resuspended in mineral oil (Sigma Aldrich) and sonicated for 30 minutes at room temperature. The final oil solution contained 1,2-dioleoyl-sn-glycero-3-phosphocholine (DOPC) and 1,2-dioleoyl-sn-glycero-3-[(N-(5-amino-1-carboxypentyl)iminodiacetic acid)succinyl] (nickel salt) (DGS-NTA) lipids on a 50:1 molar ratio, at a final concentration of 25 mg ml^{-1}. The aqueous solution contained FtsZ, ZipA, and Ficoll PM 70 (Ficoll70) at various concentrations (see experimental section for details), 2 mM GTP, 180 mM KCl, 25 mM Tris-HCl (pH 7.4), 5 mM $MgCl_2$, 15% v/v glycerol. All chemicals were purchased by Sigma Aldrich. Proteins were isolated and fluorescently labelled as previously described.[48] Droplets were obtained by vortexing for few seconds 2 μl of aqueous solution into 80 μl of oil solution, so that the induced shear stress ruptured the droplets into smaller ones. The final product was then pipetted in the PDMS well for visualization.

IMAGE ACQUISITION AND PROCESSING

Image acquisition was performed using an Olympus IX-81 inverted microscope in combination with epifluorescence illumination and specific filter sets. Samples were visualized with an Olympus 60× PlanApo (NA 1.45, oil) objective and images recorded using a Zyla 4.2 PLUS CMOS camera (Andor Technology). The microscope was operated through Micromanager software (version 1.4.14). Confocal microscopy imaging was achieved using an inverted Olympus IX81 in combination with an Andor Revolution illumination system and a Yokogawa CSU X1 detection system. Samples were visualized with a 60× UPlanFLN (NA 1.25, oil) objective and images were recorded with an EM-CCD Andor iXon X3 DU897 camera. Images were analyzed, background appropriately subtracted and contrast adjusted using Fiji (ImageJ). Protein fluorescent profiles in Figure 3.2 were obtained by custom MATLAB programs.

3.5. SUPPLEMENTARY INFORMATION

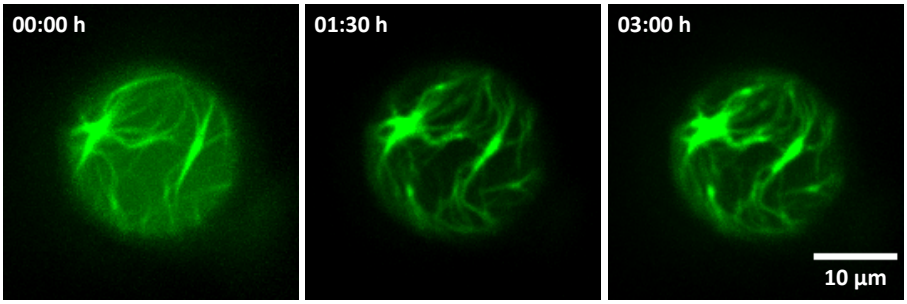

Figure 3.6: **Time evolution of FtsZ bundles in droplets.** After formation, the long filamentous bundles did not appear to undergo major spatial rearrangements, but to retain instead a fixed conformation. Over time, the fluorescence background in the droplet decreased, while the bundles looked to thicken and to get stable, reasonably a sign that more filaments are adhering to the already formed network. Images were reconstituted by confocal Z-stack of the bottom surface of the droplet.

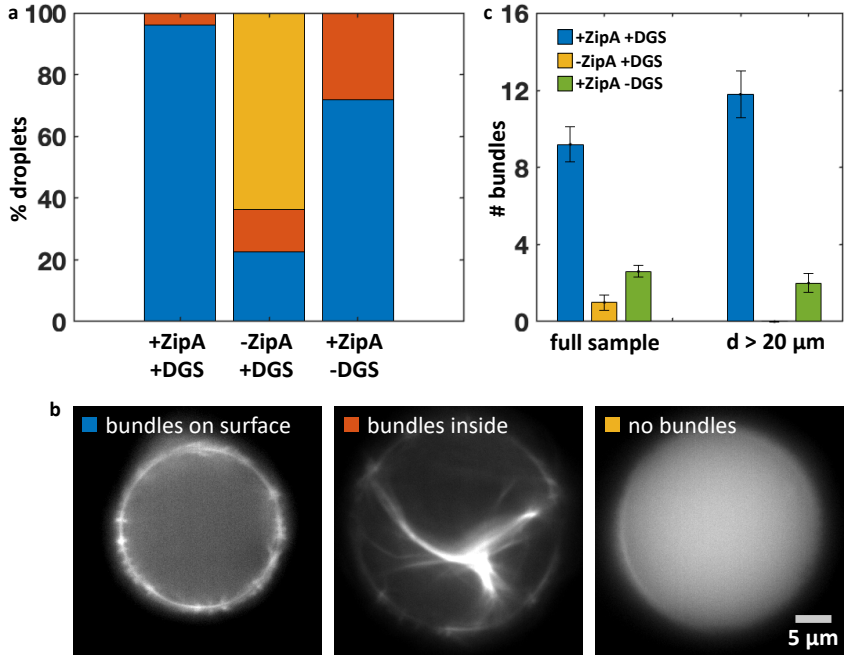

Figure 3.7: **Analysis of FtsZ bundle formation in the absence of the proper anchoring system.** a) Histogram representing the fraction of droplets having bundles on the surface (blue), bundles in the volume (red), or no visible bundles (yellow) in the presence and absence of ZipA or DGS-NTA lipids. Compared to the droplets where the whole anchoring system is present (N = 26), the fraction of droplets having bundles on the surface in absence of ZipA (N = 22) or DGS-NTA lipids (N = 25) decreased from 96% down to, respectively, 23% and 72%. Moreover, in the absence of membrane anchor protein, 64% of the droplets showed no bundles at all. To avoid possible effects induced by the droplet size, the three droplet populations were analyzed for comparable average diameters. b) Fluorescence images of FtsZ protein at the droplet equatorial cross section illustrate the visible difference between the three categories listed above. c) Histogram showing the number of bundles n visible on the bottom surface of droplets for the three different experimental conditions. Droplets where bundles were visible on the inside were excluded from the analysis. The counting was performed by drawing two orthogonal diameter lines spanning the surface of the droplet, and averaging the number n of bundles crossing them. In contrast to the dense bundle network visible on the surface in presence of both ZipA and DGS-NTA lipids (for which we observed $n = 9.2 \pm 0.9$), only a few bundles were visible on the membrane in absence of ZipA or DGS-NTA lipids (respectively, $n = 1.0 \pm 0.4$ and $n = 2.6 \pm 0.3$). In the fraction of droplets with bigger size ($d > 20$ µm), where also the membrane surface analyzed is larger, the number of bundles was, as expected, observed to be increased in the presence of both ZipA and DGS-NTA lipids ($n = 11.8 \pm 1.2$), while it slightly decreased in absence of DGS-NTA lipids ($n = 2.0 \pm 0.5$), and no bundles were visible in absence of ZipA. The latter results indicate that, while in the complete system the bundle network was properly formed on the surface, in the absence of membrane anchors bundles were probably formed within the droplet volume and, given their long size, subsequently appeared localized at the surface, simply because of space constraints.

REFERENCES

[1] D. W. Adams and J. Errington, *Bacterial cell division: Assembly, maintenance and disassembly of the Z ring,* Nature Reviews Microbiology **7**, 642 (2009).

[2] D. P. Haeusser and W. Margolin, *Splitsville: Structural and functional insights into the dynamic bacterial Z ring,* Nature Reviews Microbiology **14**, 305 (2016).

[3] A. Mukherjee and J. Lutkenhaus, *Guanine nucleotide-dependent assembly of FtsZ into filaments,* Journal of Bacteriology **176**, 2754 (1994).

[4] E. Bi and J. Lutkenhaus, *FtsZ ring structure associated with division in Escherichia coli,* Nature **354**, 161 (1991).

[5] A. W. Bisson-Filho, Y. P. Hsu, G. R. Squyres, E. Kuru, F. Wu, C. Jukes, Y. Sun, C. Dekker, S. Holden, M. S. VanNieuwenhze, Y. V. Brun, and E. C. Garner, *Treadmilling by FtsZ filaments drives peptidoglycan synthesis and bacterial cell division,* Science **355**, 739 (2017).

[6] X. Yang, Z. Lyu, A. Miguel, R. Mcquillen, and K. C. Huang, *GTPase activity – coupled treadmilling of the bacterial tubulin FtsZ organizes septal cell wall synthesis,* Science **747**, 744 (2017).

[7] J. Xiao and E. D. Goley, *Redefining the roles of the FtsZ-ring in bacterial cytokinesis,* Current Opinion in Microbiology **34**, 90 (2016).

[8] J. Mingorance, G. Rivas, M. Vélez, P. Gómez-Puertas, and M. Vicente, *Strong FtsZ is with the force: Mechanisms to constrict bacteria,* Trends in Microbiology **18**, 348 (2010).

[9] S. Rueda, M. Vicente, and J. Mingorance, *Concentration and assembly of the division ring proteins FtsZ, FtsA, and ZipA during the Escherichia coli cell cycle,* Journal of Bacteriology **185**, 3344 (2003).

[10] T. den Blaauwen, L. W. Hamoen, and P. A. Levin, *The divisome at 25: the road ahead,* Current Opinion in Microbiology **36**, 85 (2017).

[11] W. Margolin, *Themes and variations in prokaryotic cell division,* FEMS microbiology reviews **24**, 531 (2000).

[12] S. Pichoff and J. Lutkenhaus, *Unique and overlapping roles for ZipA and FtsA in septal ring assembly in Escherichia coli,* EMBO Journal **21**, 685 (2002).

[13] G. Fu, T. Huang, J. Buss, C. Coltharp, Z. Hensel, and J. Xiao, *In Vivo structure of the E. coli FtsZ-ring revealed by photoactivated localization microscopy (PALM),* PLoS ONE **5**, 1 (2010).

[14] V. W. Rowlett and W. Margolin, *3D-SIM Super-resolution of FtsZ and its membrane tethers in Escherichia coli cells,* Biophysical Journal **107**, L17 (2014).

[15] F. Guan, J. Yu, J. Yu, Y. Liu, Y. Li, X.-H. Feng, K. C. Huang, Z. Chang, and S. Ye, *Lateral interactions between protofilaments of the bacterial tubulin homolog FtsZ are essential for cell division,* eLife **7**, 1 (2018).

[16] S. D. Redick, J. Stricker, G. Briscoe, P. Erickson, and H. P. Erickson, *Mutants of FtsZ Targeting the Protofilament Interface : Effects on Cell Division and GTPase Activity Mutants of FtsZ Targeting the Protofilament Interface : Effects on Cell Division and GTPase Activity,* Society **187**, 2727 (2005).

[17] P. J. Buske and P. A. Levin, *A flexible C-terminal linker is required for proper FtsZ assembly in vitro and cytokinetic ring formation in vivo,* Molecular Microbiology **89**, 249 (2013).

[18] K. Sundararajan, A. Vecchiarelli, K. Mizuuchi, and E. D. Goley, *Species- and C-terminal linker-dependent variations in the dynamic behavior of FtsZ on membranes in vitro,* Molecular Microbiology **110**, 47 (2018).

[19] P. J. Buske and P. A. Levin, *Extreme C terminus of bacterial cytoskeletal protein FtsZ plays fundamental role in assembly independent of modulatory proteins,* Journal of Biological Chemistry **287**, 10945 (2012).

[20] H. P. Erickson, D. E. Anderson, and M. Osawa, *FtsZ in Bacterial Cytokinesis: Cytoskeleton and Force Generator All in One,* Microbiology and Molecular Biology Reviews **74**, 504 (2010).

[21] D. Bramhill and C. M. Thompson, *GTP-dependent polymerization of Escherichia coli FtsZ protein to form tubules,* Proceedings of the National Academy of Sciences of the United States of America **91**, 5813 (1994).

[22] J. M. González, M. Jiménez, M. Vélez, J. Mingorance, J. M. Andreu, M. Vicente, and G. Rivas, *Essential cell division protein FtsZ assembles into one monomer-thick ribbons under conditions resembling the crowded intracellular environment,* Journal of Biological Chemistry **278**, 37664 (2003).

[23] M. A. Oliva, S. Huecas, J. M. Palacios, J. Martín-Benito, J. M. Valpuesta, and J. M. Andreu, *Assembly of archaeal cell division protein FtsZ and a GTPase-inactive mutant into double-stranded filaments,* Journal of Biological Chemistry **278**, 33562 (2003).

[24] J. Löwe and L. A. Amos, *Tubulin-like protofilaments in Ca2+-induced FtsZ sheets,* EMBO Journal **18**, 2364 (1999).

[25] Alice B. Fulton, *How Crowded Is the Cytoplasm?* Cell **30**, 345 (1982).

[26] S. Mellouli, B. Monterroso, H. R. Vutukuri, E. te Brinke, V. Chokkalingam, G. Rivas, and W. T. S. Huck, *Self-organization of the bacterial cell-division protein FtsZ in confined environments,* Soft Matter **9**, 10493 (2013).

[27] J. Groen, D. Foschepoth, E. Te Brinke, A. J. Boersma, H. Imamura, G. Rivas, H. A. Heus, and W. T. Huck, *Associative interactions in crowded solutions of biopolymers counteract depletion effects,* Journal of the American Chemical Society **137**, 13041 (2015).

[28] D. A. Ramirez-Diaz, D. A. García-Soriano, A. Raso, J. Mücksch, M. Feingold, G. Rivas, and P. Schwille, *Treadmilling analysis reveals new insights into dynamic FtsZ ring architecture,* PLoS Biology **16**, 1 (2018).

[29] M. Loose and T. J. Mitchison, *The bacterial cell division proteins ftsA and ftsZ self-organize into dynamic cytoskeletal patterns,* Nature Cell Biology **16**, 38 (2014).

[30] A. Kuchibhatla, A. Bhattacharya, and D. Panda, *ZipA binds to FtsZ with high affinity and enhances the stability of FtsZ protofilaments,* PLoS ONE **6**, 4 (2011).

[31] C. A. Hale, A. C. Rhee, P. A. J. D. Boer, and A. M. Y. C. Rhee, *ZipA-Induced Bundling of FtsZ Polymers Mediated by an Interaction between C-Terminal Domains ZipA-Induced Bundling of FtsZ Polymers Mediated by an Interaction between C-Terminal Domains,* Society **182**, 5153 (2000).

[32] V. M. Hernández-Rocamora, C. García-Montañés, G. Rivas, and O. Llorca, *Reconstitution of the Escherichia coli cell division ZipA-FtsZ complexes in nanodiscs as revealed by electron microscopy,* Journal of Structural Biology **180**, 531 (2012).

[33] V. M. Hernández-Rocamora, B. Reija, C. García, P. Natale, C. Alfonso, A. P. Minton, S. Zorrilla, G. Rivas, and M. Vicente, *Dynamic interaction of the Escherichia coli cell division ZipA and FtsZ proteins evidenced in nanodiscs,* Journal of Biological Chemistry **287**, 30097 (2012).

[34] E. J. Cabré, A. Sánchez-Gorostiaga, P. Carrara, N. Ropero, M. Casanova, P. Palacios, P. Stano, M. Jiménez, G. Rivas, and M. Vicente, *Bacterial division proteins FtsZ and ZipA induce vesicle shrinkage and cell membrane invagination,* Journal of Biological Chemistry **288**, 26625 (2013).

[35] N. O. Vischer, J. Verheul, M. Postma, B. van den Berg van Saparoea, E. Galli, P. Natale, K. Gerdes, J. Luirink, W. Vollmer, M. Vicente, and T. den Blaauwen, *Cell age dependent concentration of Escherichia coli divisome proteins analyzed with ImageJ and ObjectJ,* Frontiers in Microbiology **6**, 1 (2015).

[36] A. Mukherjee and J. Lutkenhaus, *Dynamic assembly of FtsZ regulated by GTP hydrolysis,* EMBO Journal **17**, 462 (1998).

[37] E. Small, R. Marrington, A. Rodger, D. J. Scott, K. Sloan, D. Roper, T. R. Dafforn, and S. G. Addinall, *FtsZ Polymer-bundling by the Escherichia coli ZapA Orthologue, YgfE, Involves a Conformational Change in Bound GTP,* Journal of Molecular Biology **369**, 210 (2007).

[38] E. Galli and K. Gerdes, *FtsZ-ZapA-ZapB interactome of Escherichia coli,* Journal of Bacteriology **194**, 292 (2012).

[39] J. K. Singh, R. D. Makde, V. Kumar, and D. Panda, *A membrane protein, EzrA, regulates assembly dynamics of FtsZ by interacting with the C-terminal tail of FtSZ,* Biochemistry **46**, 11013 (2007).

[40] M. Krupka, V. W. Rowlett, D. Morado, H. Vitrac, K. Schoenemann, J. Liu, and W. Margolin, *Escherichia coli FtsA forms lipid-bound minirings that antagonize lateral interactions between FtsZ protofilaments,* Nature Communications **8**, 1 (2017).

[41] M. Krupka, M. Sobrinos-Sanguino, M. Jiménez, G. Rivas, and W. Margolin, *Escherichia coli ZipA Organizes FtsZ Polymers into Dynamic Ring-Like Protofilament Structures,* mBio **9**, 1 (2018).

[42] F. Fanalista, A. Birnie, R. Maan, F. Burla, K. Charles, G. Pawlik, S. Deshpande, G. H. Koenderink, M. Dogterom, and C. Dekker, *Shape and Size Control of Artificial Cells for Bottom-Up Biology,* ACS Nano **13**, 5439 (2019).

[43] K. Zieske, G. Chwastek, and P. Schwille, *Protein Patterns and Oscillations on Lipid Monolayers and in Microdroplets,* Angewandte Chemie - International Edition **55**, 13455 (2016).

[44] Y. Caspi and C. Dekker, *Mapping out Min protein patterns in fully confined fluidic chambers,* eLife **5**, e19271 (2016).

[45] K. Zieske and P. Schwille, *Reconstitution of pole-to-pole oscillations of min proteins in microengineered polydimethylsiloxane compartments,* Angewandte Chemie - International Edition **52**, 459 (2013).

[46] L. G. Monahan, A. Robinson, and E. J. Harry, *Lateral FtsZ association and the assembly of the cytokinetic Z ring in bacteria,* Molecular Microbiology **74**, 1004 (2009).

[47] G. Lan, B. R. Daniels, T. M. Dobrowsky, D. Wirtz, and S. X. Sun, *Condensation of FtsZ filaments can drive bacterial cell division,* Proceedings of the National Academy of Sciences **106**, 121 (2008).

[48] F. Fanalista, S. Deshpande, A. Lau, G. Pawlik, and C. Dekker, *FtsZ-Induced Shape Transformation of Coacervates,* Advanced Biosystems **1800136**, 1 (2018).

4

FTSZ FILAMENT CONDENSATION DRIVES LIPOSOME DEFORMATION

Cell division is achieved by active protein machineries. In prokaryotes, this involves a contractile ring called the Z-ring, a complex structure composed by many proteins. The central element of the Z-ring is the tubulin-homologue FtsZ, a protein that employs guanosine triphosphate (GTP) to assemble the filaments constituting the main scaffold of the ring. Whether and how FtsZ filaments facilitates the constrictive force required at the division site is still under debate. In this work, we show that FtsZ filaments encapsulated in liposomes are capable to deform the lipid membrane as they condensate into multi-strand bundles. To investigate whether such deformations are, as suggested in previous works, induced by a variation of filament curvature consequent to the protein GTPase activity, we analyze single FtsZ filaments using atomic force microscopy (AFM). Our data show that filament curvature is independent by its specific nucleotide state, indicating that the FtsZ-induced constrictive action is likely induced by condensation of filaments into bundles rather than by filament bending.

The work presented in this chapter has not yet been published. Contributions to the work were made by F. Fanalista, J. K. Ryu, and C. Dekker.

4.1. INTRODUCTION

Cell division is a fundamental biological process that ensures the proliferation of a mother cell via its fission into two daughter ones. In most prokaryotic organisms, the central element of cell division is the Z-ring, a complex ring-like structure that constricts the cell mid-plane down to division.[1, 2] This structure is composed by more than 20 known proteins, and remains yet to be understood in full detail.[3, 4] What is known, is that FtsZ, a prokaryotic homologue of tubulin, constitutes the main organizing component of the Z-ring.[5] FtsZ employs guanosine triphosphate (GTP) to polymerize into 100-200 nm long single strand dynamic filaments in a cooperative manner, where subunit turnover by GTP hydrolysis induces treadmilling dynamics.[6–9] At the early stage of the cell cycle, FtsZ filaments, together with membrane anchor proteins ZipA and FtsA, are recruited at the cell-mid plane, forming the skeleton of the ring,[10, 11] which serves to recruit a suite of additional proteins at later stages.[12] Despite its clear role as an essential scaffold for the proper functioning of the divisome, it is yet unclear and still debated whether FtsZ filaments also generate force to perform cell division – an idea prompted by the observation of membrane deformations in *in vitro* reconstitution of purified FtsZ inside soft lipid containers.[13–15]

A popular model that was proposed for FtsZ force generation suggested that, under GTP hydrolysis, a conformational change of the protein would lead to a different binding angle between the monomers. The resulting overall increase of the filament curvature would then generate a force that can deform the membrane.[16, 17] However, there is also quite some skepticism in the field concerning the capability of such a hinge-like mechanism to exert enough force to deform a biological membrane, especially when taking into account the rigid cell wall and the turgor pressure that acts on the cell membrane.[18, 19] Recent results showed that FtsZ filaments undergo treadmilling dynamics,[20] which *in vivo* drive the peptidoglycan synthesis machinery responsible for the cell wall synthesis.[21, 22] These data indicate a role of FtsZ treadmilling filaments to carry the PG synthesis machinery around the division site, which remodels and constricts the septum. Also, despite FtsZ is present at the division site since early stage, cytokinesis does not initiate before the late recruitment of FtsN, an essential protein which is thought to connect the Z-ring to the cell-wall-synthesis enzymes via interaction with FtsA.[23–25] Another possible scenario is that the lateral interactions which drive the condensation of FtsZ filaments into multistrand bundles could generate a constrictive force at the division site.[26, 27] Several proteins composing the divisome machinery appear to be involved in regulating the bundling process,[28–31] and external parameters such as divalent cations and macromolecular crowders have been observed to play a role in the *in vitro* condensation of filaments into higher ordered structures.[32–34] It has however remained unclear why the lateral interactions between FtsZ filaments in the early proto-ring do not induce membrane invagination. Recent TEM measurements showed that FtsA assembles into dodecameric mini-rings on supported lipid bilayers, which lock FtsZ filaments in a spatial arrangement where lateral associations are prevented.[35] This work speculated that one of the late proteins recruited to the ring, possibly FtsN, could induce the conformational opening of FtsA mini-rings, allowing FtsZ filaments to bundle. The condensation of FtsZ filaments could then from one side reduce FtsA self-interaction, allowing the anchor protein to interact with FtsN, but pos-

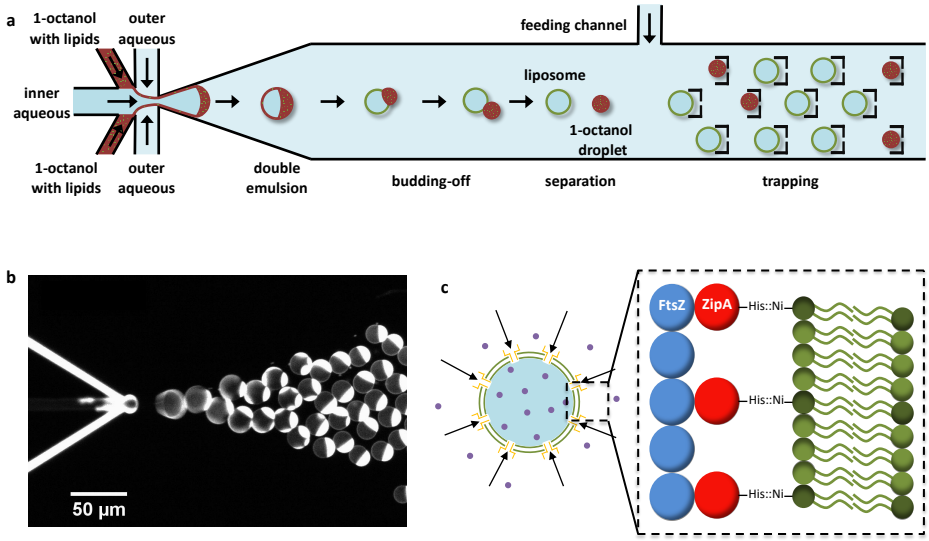

Figure 4.1: **Microfluidic platform employed to reconstitute a minimal Z-ring inside liposomes.** (a) A microfluidic OLA junction to produce liposomes was designed in combination with microfluidic traps and a side feeding channel. In such a way, it was possible to immobilize the liposomes after detachment of octanol pocket, and subsequently provide them with alpha-hemolysin protein and GTP. (b) Fluorescence image of the microfluidics junction representing the double emulsions production process. Signal comes from Rhod-PE lipids dissolved in the octanol solution. (c) Through insertion of membrane pore protein alpha-hemolysin, GTP molecules (purple) were able to diffuse to within the liposomes and trigger FtsZ polymerization (blue). A soluble version of ZipA (red) with a his-tag allowed FtsZ to dock on the membrane by binding to the nickel group of DGS-NTA lipids (dark green) mixed with DOPC (light green).

sibly could also generate a contractive force at the division site.

Here, we aim to study the possible mechanism of force generation by FtsZ. First, we reconstituted a minimal divisome machinery, i.e., FtsZ and a soluble version of its membrane anchor protein ZipA, inside liposomes, to show how membrane deformation is correlated with FtsZ bundle formation on the lipid membrane. Furthermore, we used atomic force microscopy (AFM) to image single FtsZ filaments formed in the presence of different nucleotides: GTP, guanosine diphosphate (GDP), and non-hydrolysable GTP (GMPPCP). The average curvature of FtsZ filaments assembled with GDP or GMPPCP did not show a significant difference, ruling out the possibility that the nucleotide-filament state impacts the filament conformation. Altogether, our results disfavor a model where FtsZ filaments use curvature to generate a force under GTP hydrolysis, and instead the data indicate the importance of FtsZ filament lateral interactions as a potential source for force generation.

4.2. RESULTS

To examine the potential capability of FtsZ filaments to exert a force, we reconstituted a minimal version of the divisome machinery inside liposomes. Specifically, we encapsulated FtsZ together with a soluble version of the membrane anchor protein ZipA inside unilamellar liposomes, by means of a microfluidic platform previously developed in our lab (Fig. 4.1a).[36] The technique (octanol-assisted liposome assembly, OLA) is based on a microfluidic junction, where an inner aqueous solution containing the proteins merges with an octanol stream containing lipids to form a thin film. An outer aqueous stream pinches off the membrane, creating a closed double emulsion formed by lipids and octanol solvent (Fig. 4.1b). Thanks to its physical properties, the excess octanol spontaneously separates from the double emulsion, resulting in an octanol pocket and a unilamellar liposome. To promote the protein solubility in water and reduce aggregation, the hydrophobic transmembrane domain of ZipA was replaced by a his-tag. This binds to a nickel tag on the headgroup of DGS-NTA lipids that are mixed together (at a 10% molar ratio) with DOPC, thus providing the FtsZ filaments a means to dock to the membrane (Fig. 4.1c). To prevent FtsZ polymerization before encapsulation, GTP was administer only to the outer aqueous solution surrounding the liposomes. After production, liposomes moved through the main channel to reach a chamber filled with microfluidic traps, there they were immobilized. Membrane protein alpha-hemolysin was then flushed into the chamber via an additional "feeding" channel, so that pores were formed on the liposome membrane and GTP from the outer aqueous could diffuse inside.

As a result, after a few minutes, the FtsZ inside the liposomes, which at first was distributed homogeneously inside the vesicle lumen, began to show bright local structures on the membrane. These structures indicated the condensation of single FtsZ filaments, which by themselves were too small to be resolved with our fluorescence microscopy setup,[37] into multi-strand visible bundles. In Figure 4.2 it is possible to observe a cluster of three liposomes (connected because of a sub-optimal liposome production), where the formation of FtsZ bundles on the membrane induced a shape transformation. Similarly to what previously reported,[14] liposomes appeared to shrink, losing their original spherical shape and displaying irregular deformations, more accentuated in correspondence of FtsZ bundles. Since liposomes shape was stable before the appearance of FtsZ structures, we argue that the liposome deformation is consequent to the condensation of FtsZ filaments into bundles on the lipid membrane. Figure 4.2 illustrates what qualitatively observed for several different liposome clusters in the microfluidic channel: some liposomes seemed to collapse (yellow arrow), while others displayed severe deformations, especially where the protein signal appeared more prominent (red arrow). During this process, the stress induced on the membrane by the protein bundles may have damaged the integrity of the lipid bilayer, resulting in membrane breaks. The inner aqueous solution then flowed through such openings (and through alpha-hemolysin pores) outside the liposomes, facilitating the shrinking process. The same phenomenon was observed in a similar experiment, where alpha-hemolysin was provided to the outer aqueous solution already at the junction where liposomes were produced (Fig. 4.6). It is good to mention that we did not observe liposome division in any of the experiments performed.

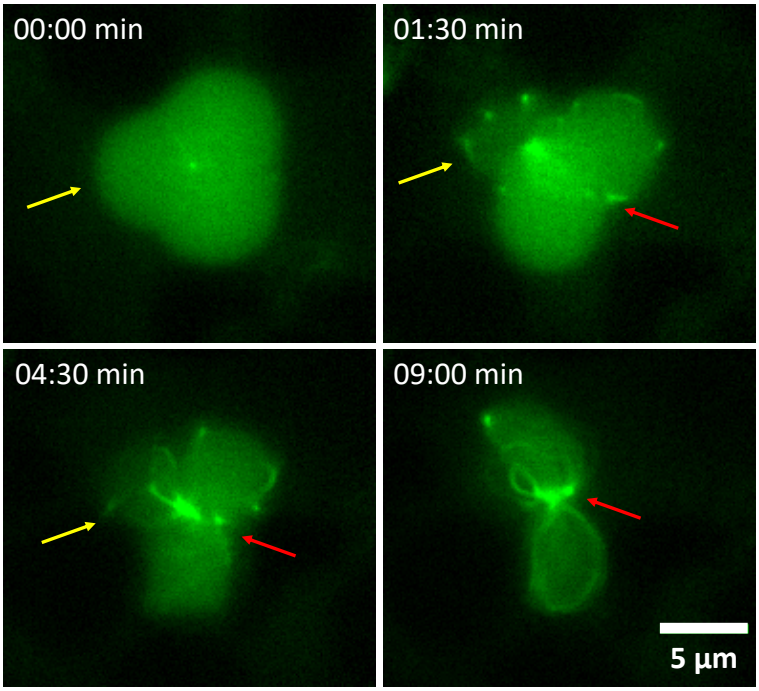

Figure 4.2: **FtsZ filament bundling induces liposome deformation.** Fluorescent signal comes from FtsZ, which initially is distributed homogeneously inside the three liposomes depicted. Given a sub-optimal production, the liposomes were attached together in a cluster. As alpha-hemolysin pore protein was provided to the system, GTP in the outer aqueous solution diffused to within the liposomes and induced FtsZ polymerization. As FtsZ bundles formed on the membrane, the liposomes undergo a shape transformation. The yellow arrow indicates a liposome which, compared to its original spherical shape (top-left), at first exhibits heavy membrane deformations (top-right), and in few minutes shrinks (bottom-left) until it is not visible anymore (bottom-right). Red arrow indicates the neck between two liposomes, which constricted as the FtsZ bundles colocalized. FtsZ was fluorescently labelled with Alexa 488.

Interestingly however, in liposomes with small dimensions ($d < 5$ µm), closer to bacteria sizes, FtsZ bundles did not induce vesicles shrinkage, but arranged instead in a fully formed ring encircling the entire vesicle (Fig. 4.3), in stark contrast with what observed in bigger liposomes. We were unable to resolve the dynamics underlying the formation of FtsZ rings. Once assembled, the rings did not appear to perform any constriction to the liposomes, in contradiction with what could be expected in case mechanical force was resulting from GTP hydrolysis, which should occur constantly in the FtsZ filaments.

The deformations, induced by the FtsZ protein structures on the membrane, hypothetically may have resulted from FtsZ filaments bending into a higher curvature conformation as GTP was hydrolyzed. To test this hypothesis, we analyzed the curvature of single filaments using dry AFM imaging techniques. Specifically, to investigate whether the nucleotide state of the filaments can influence their conformation, we incubated FtsZ for 10 minutes, either with GTP, GDP, or with the non-hydrolysable GTP-analog GMPPCP. Af-

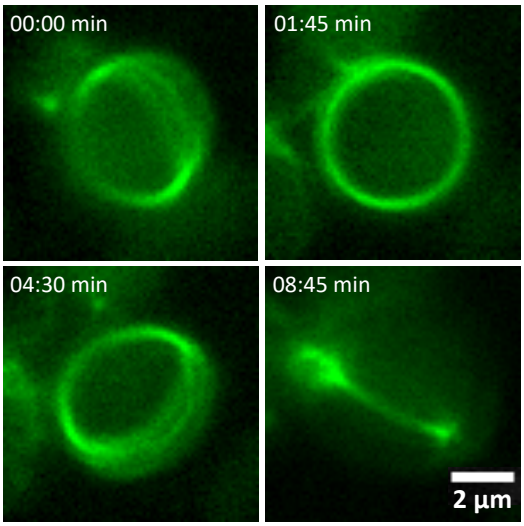

Figure 4.3: **Arrangement of FtsZ filamentous bundles on the liposome surface for small liposome sizes.** Differently from what observed in bigger liposomes, FtsZ filaments condensed in one single ring, which spans the whole liposome circumference. As the liposome rotates over time, the ring appears from the front like a continuous structure (top-right), while multiple fibers are visible from the side (top-left and bottom-left). During the observation time, the ring did not appear to constrict the membrane or to induce any visible modification to the liposome shape. In the same experiment, a single FtsZ ring was consistently observed in different liposomes having a small diameter (d = 3.8 ± 0.2 µm, N = 10). Fluorescent FtsZ signal comes from Alexa488 fluorescent dye.

ter proper dilution, the solution was deposited to mica, excess protein washed out, and the sample was quickly dried by a nitrogen flow. In presence of GTP and GMPPCP, it was possible to resolve short single FtsZ filaments of various lengths and curvatures adhered to the mica surface (Fig. 4.4). In presence of GDP, the deposition time on the plate had to be accurately tuned, since the filaments were more unstable and prone to disassemble (Fig. 4.7), but the GDP-FtsZ filaments that were observed appeared to have no clear differences compared to the ones assembled with GTP or GMPPCP. Only in absence of any nucleotide, FtsZ remained in monomeric form, and no organized assembled structures were visible.

To better investigate a possible contribution of the nucleotide hydrolysis over the filament conformation, we analyzed the geometry of single FtsZ filaments (Fig. 4.5a) formed in presence of GDP (N = 473) and GMPPCP (N = 638), that reflect two opposite states (hydrolyzed and not hydrolyzed nucleotide), altogether with filaments formed in presence of GTP (N = 47). Specifically, we measured the radius of curvature of each single filament, and plotted the results in the histograms in Figure 4.5b. The average radius r appeared comparable in presence of GDP or GMPPCP (r_{GDP} = 266 ± 9 nm, r_{GMPPCP} = 275 ± 7 nm; errors are s.e.m.). The FtsZ filaments formed in presence of GTP had, on average, a slightly higher curvature (r_{GTP} = 319 ± 35 nm), but the statistical sample obtained for this condition was quite limited. More importantly, the data obtained from

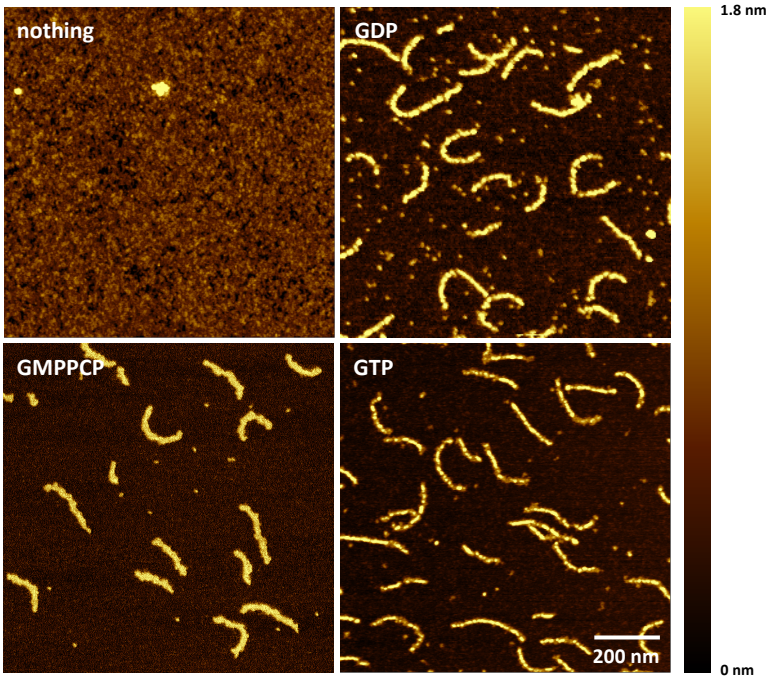

Figure 4.4: **Dry AFM imaging of single FtsZ filaments formed by the addition of different nucleotides.** Coherently with the notion that FtsZ requires a guanosine-nucleotide for polymerization, in absence of nucleotides FtsZ remains in monomeric form, and no filaments were observable on the mica plate (top-left). Upon addition of GDP, FtsZ forms filaments of various lengths and curvature (top-right), which, qualitatively, do not show any visible difference compared to the filaments formed upon addition of GMPPCP (bottom-left) or GTP (bottom-right). Compared to the other experiments, around the GDP-formed filaments is visible a larger amount of unpolymerized FtsZ, consistent with the fact that the GDP forms weak bonds between FtsZ monomers. Scale bar applies to all panels.

filaments assembled with GDP and GMPPCP were similar, both showing an asymmetric distribution with a peak near 130 nm, suggesting that FtsZ filaments do not undergo a significant conformational change in consequence of nucleotide hydrolysis. Also, the curvature appeared to be independent of the length of the filaments (Fig. 4.5c), as confirmed by the very small correlation coefficient measured between the two quantities in all the three experimental conditions explored (c_{GDP} = -0.05, c_{GMPPCP} = +0.02, c_{GTP} = +0.05). In particular, it appears that, while the length of FtsZ filaments formed in presence of GMPPCP was more sharply distributed around a value of about 100 nm, filaments formed in presence of GDP displayed a broader range of lengths, mostly between 100 and 300 nm. Overall, the analysis pointed out that the conformation of single FtsZ filaments appeared to be independent by the specific nucleotide employed in the polymerization process.

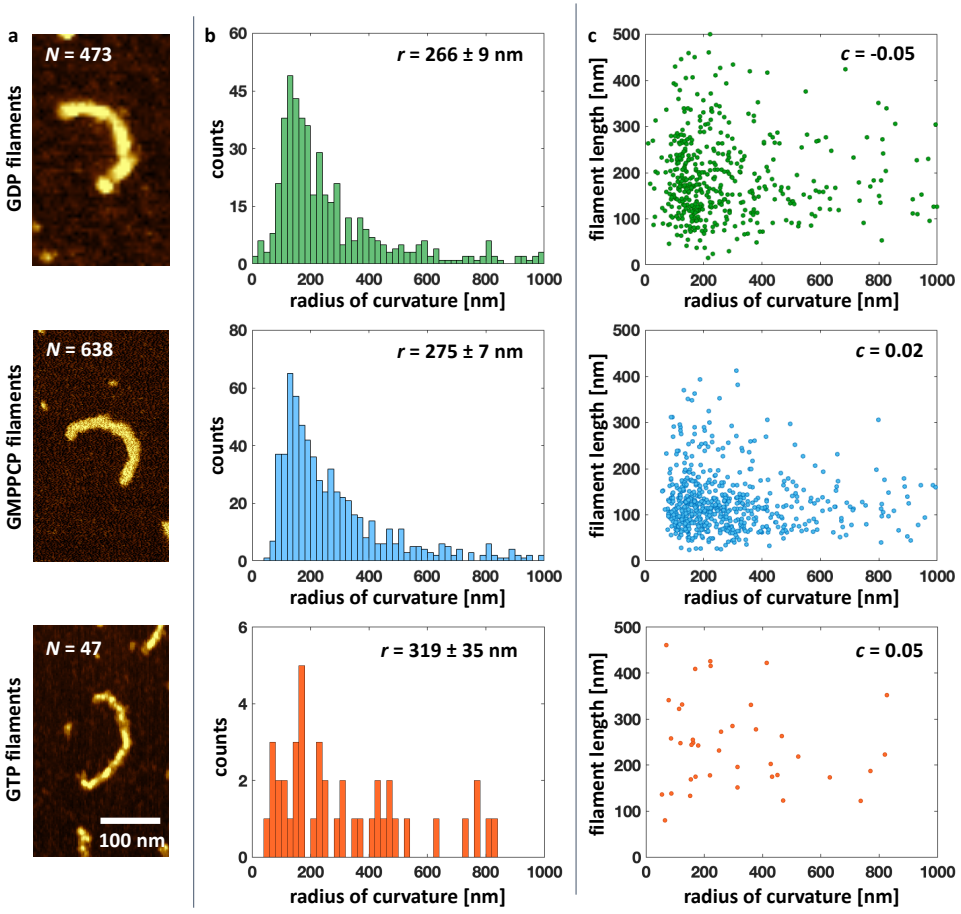

Figure 4.5: **Analysis of single FtsZ filaments formed in presence of GDP, GMPPCP or GTP.** (a) Dry AFM imaging of single FtsZ filaments formed under addition of different nucleotides. (b) Histogram of the radius of curvature measured on single FtsZ filaments. The curvature distribution of FtsZ filaments formed upon addition of GDP (top), compared to the ones formed upon addition of GMPPCP (middle) or GTP (bottom), does not present visible differences. The average radius of curvature also denote that filaments formed in presence of hydrolyzed (GDP) or not hydrolyzed (GMPPCP) nucleotides possess a comparable curvature. (c) Distribution of single FtsZ filament lengths versus their radius of curvature. The scatter plots, as well as the correlation coefficients c, indicate that the filament length does not depend from the curvature, independently from the specific nucleotide employed to induce FtsZ polymerization.

4.3. DISCUSSION

Given the fundamental role of FtsZ in the proper assembling and functioning of the Z-ring in bacteria, many groups in the last 15 years aimed to understand whether this protein is also directly involved in the contractile force exerted by the divisome ring.[38–40] Most of the speculations on this topic were induced by results obtained from *in vitro* reconstitutions of FtsZ filaments on soft lipid membranes. Since curved FtsZ filaments have been shown to directionally bend a lipid membrane,[16] and electron-microscopy imaging showed different FtsZ filament conformation depending on their nucleotide state,[41] the hypothesis that FtsZ filament could exert a force by changing curvature under GTP hydrolysis became appealing. However, convincing evidence that FtsZ rings reconstituted *in vitro* can dynamically constrict a lipid membrane is still missing.

In this work, we showed that FtsZ filaments that were assembled using different nucleotides, do not present significant conformational differences. In particular, we measured that the curvature of filaments does not depend on the specific nucleotide employed, as filaments formed in presence of GDP and the non-hydrolysable GTP-analog GMPPCP were essentially the same. Given the similarity of the single filaments, a possible source for the contractile force exerted by FtsZ on the lipid membrane may be searched in the lateral attractive interactions between filaments that lead to bundle formation. In support of this hypothesis, in this work we have shown how liposome membrane deformations correlate with the formation of FtsZ bundles on the lipid membrane. In this scenario, GTP hydrolysis could play an important role not to trigger a curvature change, but to ensure the dynamic nature of the system: GTP hydrolysis, followed by monomer turnover, would allow the rearrangement of filaments, granting the mobility necessary to further condense the bundle network.

The scenario where FtsZ filament condensation into bundles could contribute *in vivo* to a contractile force is coherent with recent findings showing how FtsA prevents bundle formation.[42] Later recruitment of additional components could potentially unlock this state, allowing FtsZ filament bundling and membrane invagination. However, it is unlikely that the force driving cell division is entirely provided by FtsZ filaments: given the high turgor pressure and the rigid cell wall present at the membrane, it is reasonable to assume that the cell wall synthesis plays a consistent role in the constriction process.[19] Furthermore, FtsZ *in vivo* leaves the septum before division is finalized,[43] and it has also been recently proven that FtsZ treadmilling is not required for cytokinesis to proceed once septation already progressed.[44]

In conclusion, although *in vitro* efforts are useful to understand how divisome components work, the emerging set of data on FtsZ suggest to reconsider the possibility of employing a minimal machinery based merely on FtsZ to divide a liposome, as additional components may be required to induce scission and division.

4.4. METHODS

LIPOSOME PRODUCTION

Liposomes were produced using octanol-assisted liposome assembly (OLA) microfluidic technique. Microfluidic devices were produced accordingly to the protocol described.[36] At the junction, three streams are crossing: an inner aqueous solution,

containing 12 μM FtsZ and 6 μM ZipA in buffer solution (25 mM Tris pH 7.4, 180 mM KCl, 5 mM $MgCl^2$, 15% glycerol); an outer aqueous solution, containing same buffer as inner aqueous with additional 2mM GTP and 5% poloxamer 188 surfactant necessary for the liposome production; a lipid solution, where 0.2% lipids were dissolved in 1-octanol. After production, a second outer aqueous solution containing 3 μM alpha-hemolysin was flushed into the channel to form pores on the membrane and allow GTP to diffuse inside the liposomes and trigger FtsZ polymerization. Lipids were purchased in chloroform from Avanti Polar Lipids, Inc. All chemicals by Sigma Aldrich. Proteins were purified and fluorescently labelled according to the protocol previously described.[45]

FLUORESCENCE MICROSCOPY

Images were acquired using an Olympus IX-81 inverted microscope combined with epi-fluorescence illumination and specific filter sets. Samples were observed with an Olympus 60× PlanApo (NA 1.45, oil) objective and images recorded using a Zyla 4.2 PLUS CMOS camera (Andor Technology). The microscope was controlled through Micromanager software (version 1.4.14). Image background was appropriately subtracted and contrast adjusted using Fiji (ImageJ).

AFM IMAGING

5 μM of FtsZ in buffer (20 mM Tris pH 8, 150 mM KCl, 5 mM $MgCl^2$, 15% glycerol) were mixed, depending on the specific experiment, with 2 mM of different nucleotides (GTP, GMPPCP or GDP). After 10 minutes of incubation, solution was diluted between 10 and 50 times to obtain a filament density suitable for proper visualization, then deposited on mica for few seconds, rinsed with MilliQ water, and finally gently dried using a nitrogen gun. Imaging was performed in peakforce tapping mode, with a ScanAsyst-Air-HR silicon tip on nitride lever. All image analysis was done using custom MATLAB programs.

4.5. SUPPLEMENTARY INFORMATION

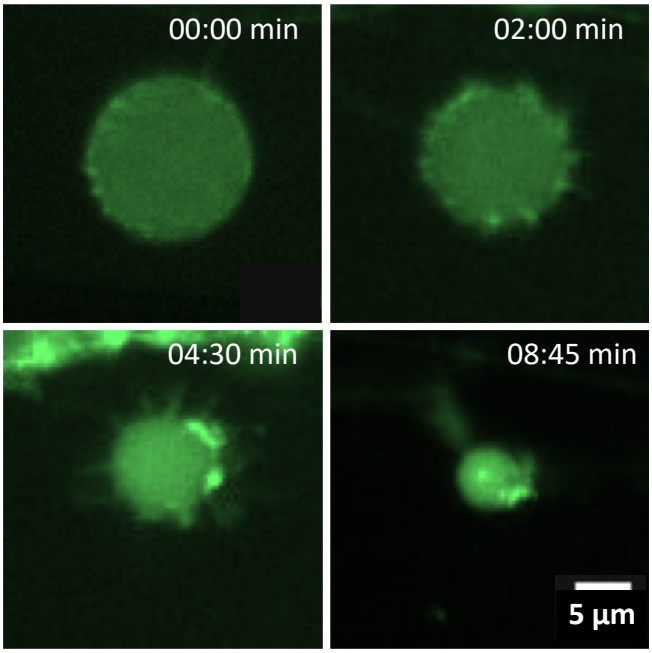

Figure 4.6: **FtsZ-induced shrinkage of liposomes.** In this experiment, membrane pore protein alpha-hemolysin is provided to the outer aqueous solution at the moment of liposome production. As soon as the liposomes are formed, GTP is then able to flow to within the liposomes, and trigger FtsZ polymerization. FtsZ bundles were already visible as brighter spots at the membrane when image acquisition started (top-left). Consequentially, liposome surface presented an irregular profile (top-right), including some protrusions more visible after 4'30" (bottom-left). After few more minutes, the whole liposome collapsed into a small chunk (bottom-right). FtsZ signal comes from Alexa488 fluorescent dye.

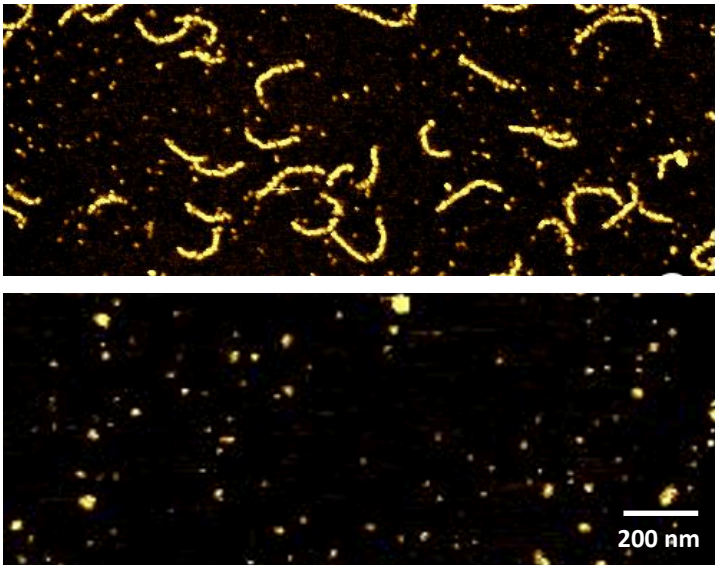

Figure 4.7: **Dry AFM imaging of FtsZ filaments formed upon addition of GDP.** Proper visualization of GDP-built filaments was found to depend on the amount of dilution and on the incubation time of the solution on the mica before drying. A sample prepared by 20 times dilution and 1 second deposition on mica displays FtsZ filaments (top), which are not visible in a sample prepared by 50 times dilution and 10 seconds deposition (bottom).

REFERENCES

[1] D. P. Haeusser and W. Margolin, *Splitsville: Structural and functional insights into the dynamic bacterial Z ring,* Nature Reviews Microbiology **14**, 305 (2016).

[2] S. Du and J. Lutkenhaus, *At the Heart of Bacterial Cytokinesis: The Z Ring,* (2019).

[3] D. W. Adams and J. Errington, *Bacterial cell division: Assembly, maintenance and disassembly of the Z ring,* Nature Reviews Microbiology **7**, 642 (2009).

[4] J. Lutkenhaus, S. Pichoff, and S. Du, *Bacterial Cytokinesis: From Z Ring to Divisome,* Cytoskeleton **790**, 778 (2012).

[5] E. Bi and J. Lutkenhaus, *FtsZ ring structure associated with division in Escherichia coli,* Nature **354**, 161 (1991).

[6] P. de Boer, R. Crossley, and L. Rothfield, *The essential bacterial cell-division protein FtsZ is a GTPase,* Nature **359**, 254 (1992).

[7] A. Mukherjee and J. Lutkenhaus, *Guanine nucleotide-dependent assembly of FtsZ into filaments,* Journal of Bacteriology **176**, 2754 (1994).

[8] H. P. Erickson, *Modeling the physics of FtsZ assembly and force generation,* Proceedings of the National Academy of Sciences **106**, 9238 (2009).

[9] A. Mukherjee and J. Lutkenhaus, *Analysis of FtsZ Assembly by Light Scattering and Determination of the Role of Divalent Metal Cations Analysis of FtsZ Assembly by Light Scattering and Determination of the Role of Divalent Metal Cations,* Journal of Bacteriology **181**, 823 (1999).

[10] S. Rueda, M. Vicente, and J. Mingorance, *Concentration and assembly of the division ring proteins FtsZ, FtsA, and ZipA during the Escherichia coli cell cycle,* Journal of Bacteriology **185**, 3344 (2003).

[11] M. E. Aarsman, A. Piette, C. Fraipont, T. M. Vinkenvleugel, M. Nguyen-Distèche, and T. Den Blaauwen, *Maturation of the Escherichia coli divisome occurs in two steps,* Molecular Microbiology **55**, 1631 (2005).

[12] T. den Blaauwen, L. W. Hamoen, and P. A. Levin, *The divisome at 25: the road ahead,* Current Opinion in Microbiology **36**, 85 (2017).

[13] P. Szwedziak, Q. Wang, T. A. M. Bharat, M. Tsim, and J. Löwe, *Architecture of the ring formed by the tubulin homologue FtsZ in bacterial cell division,* eLife **3**, e04601 (2014).

[14] E. J. Cabré, A. Sánchez-Gorostiaga, P. Carrara, N. Ropero, M. Casanova, P. Palacios, P. Stano, M. Jiménez, G. Rivas, and M. Vicente, *Bacterial division proteins FtsZ and ZipA induce vesicle shrinkage and cell membrane invagination,* Journal of Biological Chemistry **288**, 26625 (2013).

[15] M. Osawa, D. E. Anderson, and H. P. Erickson, *Reconstitution of Contractile FtsZ Rings in Liposomes,* Science **320**, 792 LP (2008).

[16] M. Osawa, D. E. Anderson, and H. P. Erickson, *Curved FtsZ protofilaments generate bending forces on liposome membranes,* EMBO Journal **28**, 3476 (2009).

[17] Y. Li, J. Hsin, L. Zhao, Y. Cheng, W. Shang, K. C. Huang, H.-W. Wang, and S. Ye, *FtsZ Protofilaments Use a Hinge-Opening Mechanism for Constrictive Force Generation,* Science **341**, 392 LP (2013).

[18] M. Osawa and H. P. Erickson, *Turgor pressure and possible constriction mechanisms in bacterial division,* Frontiers in Microbiology **9**, 1 (2018).

[19] J. Xiao and E. D. Goley, *Redefining the roles of the FtsZ-ring in bacterial cytokinesis,* Current Opinion in Microbiology **34**, 90 (2016).

[20] M. Loose and T. J. Mitchison, *The bacterial cell division proteins ftsA and ftsZ self-organize into dynamic cytoskeletal patterns,* Nature Cell Biology **16**, 38 (2014).

[21] A. W. Bisson-Filho, Y. P. Hsu, G. R. Squyres, E. Kuru, F. Wu, C. Jukes, Y. Sun, C. Dekker, S. Holden, M. S. VanNieuwenhze, Y. V. Brun, and E. C. Garner, *Treadmilling by FtsZ filaments drives peptidoglycan synthesis and bacterial cell division,* Science **355**, 739 (2017).

[22] X. Yang, Z. Lyu, A. Miguel, R. Mcquillen, and K. C. Huang, *GTPase activity – coupled treadmilling of the bacterial tubulin FtsZ organizes septal cell wall synthesis,* Science **747**, 744 (2017).

[23] D. S. Weiss, *Last but not least: New insights into how FtsN triggers constriction during Escherichiacoli cell division,* Molecular Microbiology **95**, 903 (2015).

[24] B. Liu, L. Persons, L. Lee, and P. A. J. D. Boer, *Roles for both FtsA and the FtsBLQ subcomplex in FtsN-stimulated cell constriction in Escherichia coli,* Molecular Microbiology **95**, 945 (2015).

[25] J. Lutkenhaus, *FtsN—trigger for septation,* Journal of bacteriology **191**, 7381 (2009).

[26] G. Lan, B. R. Daniels, T. M. Dobrowsky, D. Wirtz, and S. X. Sun, *Condensation of FtsZ filaments can drive bacterial cell division,* Proceedings of the National Academy of Sciences **106**, 121 (2008).

[27] F. Guan, J. Yu, J. Yu, Y. Liu, Y. Li, X.-H. Feng, K. C. Huang, Z. Chang, and S. Ye, *Lateral interactions between protofilaments of the bacterial tubulin homolog FtsZ are essential for cell division,* eLife **7**, 1 (2018).

[28] K. H. Huang, J. Durand-Heredia, and A. Janakiraman, *FtsZ ring stability: Of bundles, tubules, crosslinks, and curves,* Journal of Bacteriology **195**, 1859 (2013).

[29] A. Dajkovic, G. Lan, S. X. Sun, D. Wirtz, and J. Lutkenhaus, *MinC Spatially Controls Bacterial Cytokinesis by Antagonizing the Scaffolding Function of FtsZ,* Current Biology **18**, 235 (2008).

[30] H. H. Low, M. C. Moncrieffe, and J. Löwe, *The crystal structure of ZapA and its modulation of FtsZ polymerisation,* Journal of Molecular Biology **341**, 839 (2004).

[31] C. A. Hale, A. C. Rhee, P. A. J. D. Boer, and A. M. Y. C. Rhee, *ZipA-Induced Bundling of FtsZ Polymers Mediated by an Interaction between C-Terminal Domains ZipA-Induced Bundling of FtsZ Polymers Mediated by an Interaction between C-Terminal Domains,* Society **182**, 5153 (2000).

[32] J. Groen, D. Foschepoth, E. Te Brinke, A. J. Boersma, H. Imamura, G. Rivas, H. A. Heus, and W. T. Huck, *Associative interactions in crowded solutions of biopolymers counteract depletion effects,* Journal of the American Chemical Society **137**, 13041 (2015).

[33] J. Löwe and L. A. Amos, *Tubulin-like protofilaments in Ca2+-induced FtsZ sheets,* EMBO Journal **18**, 2364 (1999).

[34] J. M. González, M. Jiménez, M. Vélez, J. Mingorance, J. M. Andreu, M. Vicente, and G. Rivas, *Essential cell division protein FtsZ assembles into one monomer-thick ribbons under conditions resembling the crowded intracellular environment,* Journal of Biological Chemistry **278**, 37664 (2003).

[35] M. Krupka, V. W. Rowlett, D. Morado, H. Vitrac, K. Schoenemann, J. Liu, and W. Margolin, *Escherichia coli FtsA forms lipid-bound minirings that antagonize lateral interactions between FtsZ protofilaments,* Nature Communications **8**, 1 (2017).

[36] S. Deshpande, Y. Caspi, A. E. Meijering, and C. Dekker, *Octanol-assisted liposome assembly on chip,* Nature Communications **7**, 1 (2016).

[37] J. O. E. Lutkenhaus and A. Mukherjee, *Analysis of FtsZ assembly by light scattering and determination of the role of divalent metal cations.* Journal of bacteriology **181**, 823 (1999).

[38] J. Mingorance, G. Rivas, M. Vélez, P. Gómez-Puertas, and M. Vicente, *Strong FtsZ is with the force: Mechanisms to constrict bacteria,* Trends in Microbiology **18**, 348 (2010).

[39] H. P. Erickson, D. E. Anderson, and M. Osawa, *FtsZ in Bacterial Cytokinesis: Cytoskeleton and Force Generator All in One,* Microbiology and Molecular Biology Reviews **74**, 504 (2010).

[40] C. Coltharp and J. Xiao, *Beyond force generation: Why is a dynamic ring of FtsZ polymers essential for bacterial cytokinesis?* BioEssays **39**, 1 (2017).

[41] C. Lu, M. Reedy, and H. P. Erickson, *Straight and curved conformations of FtsZ are regulated by GTP hydrolysis,* Journal of Bacteriology **182**, 164 (2000).

[42] M. Krupka, M. Sobrinos-Sanguino, M. Jiménez, G. Rivas, and W. Margolin, *Escherichia coli ZipA Organizes FtsZ Polymers into Dynamic Ring-Like Protofilament Structures,* mBio **9**, 1 (2018).

[43] B. Söderström, K. Skoog, H. Blom, D. S. Weiss, G. von Heijne, and D. O. Daley, *Disassembly of the divisome in Escherichia coli: Evidence that FtsZ dissociates before compartmentalization,* Molecular Microbiology **92**, 1 (2014).

[44] J. M. Monteiro, A. R. Pereira, N. T. Reichmann, B. M. Saraiva, P. B. Fernandes, H. Veiga, A. C. Tavares, M. Santos, M. T. Ferreira, V. Macário, M. S. VanNieuwenhze, S. R. Filipe, and M. G. Pinho, *Peptidoglycan synthesis drives an FtsZ-treadmilling-independent step of cytokinesis,* Nature **554**, 528 (2018).

[45] F. Fanalista, A. Birnie, R. Maan, F. Burla, K. Charles, G. Pawlik, S. Deshpande, G. H. Koenderink, M. Dogterom, and C. Dekker, *Shape and Size Control of Artificial Cells for Bottom-Up Biology,* ACS Nano **13**, 5439 (2019).

5

FtsZ-induced Shape Transformation of Coacervates

Recently, both the cellular and synthetic biology communities have expressed a strong interest in coacervates, membraneless liquid droplets composed of densely packed multivalent molecules that form as a result of spontaneous phase separation. Here, we study how FtsZ, a protein that plays a key role in the bacterial division process, remodels coacervates made of polylysine (pLL) and guanosine triphosphate (GTP). We show that FtsZ strongly partitions at the surface of the coacervates and induces their disassembly due to the hydrolysis of GTP by FtsZ. Surprisingly, the coacervates are found to promote lateral interactions between FtsZ filaments, inducing the formation of an emanating network of FtsZ bundles that interconnect neighboring coacervates. Under mechanical stress, coacervates are shown to fracture, resulting in profound invaginations along their circumference. Our results bring out the potential of coacervates for their use as membrane-free scaffolds for building synthetic cells as well as are possibly relevant for coacervation in prokaryotic cells.

This chapter has been published: F. Fanalista, S. Deshpande, A. Lau, G. Pawlik, and C. Dekker, *FtsZ-Induced Shape Transformation of Coacervates*, Advanced Biosystems, 1800136, 1 (2018).

5.1. INTRODUCTION

The compartmentalization of biomolecules and regulation of their biological activities are vital aspects of living systems. In order to obtain spatiotemporal control over the numerous chemical reactions occurring within the cell, eukaryotic cells employ internal compartmentalization in the form of membrane-bound organelles. However, it is becoming clear that intracellular organization is not just limited to lipid-encompassed compartments, but is complemented by a variety of membraneless organelles such as germ granules, stress granules, the nucleolus, and many others.[1] These structures are now being categorized as 'biological condensates', which arise from a physical process of liquid-liquid phase separation, commonly known as coacervation.[2] Coacervation is generally mediated by electrostatic interactions between multivalent molecules, such as polypeptides and nucleotides,[3] where for a certain range of concentrations of such charged molecular species, the decrease in the overall entropy is overcome by the favorable mutual electrostatic attractions, leading to the spontaneous phase separation into a large-volume dilute phase and a small-volume concentrated phase.[4] Importantly, the chemical potentials of the molecular species remain the same in both the phases, thus allowing equilibrium. Owing to the absence of a physical boundary at the interface, such condensates allow for a continuous influx and efflux of individual molecules. Coacervates provide a crowded microenvironment to perform reactions at enhanced rates, they sequester specific molecules promoting their interactions, and they also act as organizing centers.[2] These characteristics of biological condensates make them versatile players in cells. Due to their unique properties, coacervates also provide ample opportunities outside the *in vivo* context of live cells, for example as potential architectural scaffolds for assembling an artificial minimal cell, as an alternative to traditional membranous structures such as liposomes.[5, 6] Given their emerging importance in living cells as well as for *in vitro* bottom-up biology, various aspects of coacervates are currently being studied extensively, for example how external parameters (pH and ionic strength), as well as the properties of the coacervate components (molecular length and charge content), affect the formation and dissolution of polypeptide-based coacervates.[7] Also, the manipulation of coacervates has been explored using enzymatic reactions that enhance/decrease the multivalent nature of specific components.[8, 9] Interestingly, various cytoskeletal proteins such as actin and microtubules were shown to partition into coacervates, resulting in an enhanced activity and even significant changes of the coacervate morphology.[10, 11]

While the majority of these studies involved proteins belonging to eukaryotic systems, the same principles may apply to prokaryotic biomolecules such as FtsZ, a central protein essential for the process of cell division in most bacteria.[12] As a prokaryotic homologue of tubulin,[13] FtsZ polymerizes into filaments that assemble into a ring structure at the cell mid-plane. This structure serves as a scaffold to recruit and coordinate further proteins constituting the so-called Z-ring,[14] which directs the constriction and division of the cell into two daughters. Guanosine triphosphate (GTP) plays a fundamental role in the assembly[15] and dynamics of FtsZ filaments. Two FtsZ monomers can stably bind by incorporating a GTP molecule at their interface, and repetition of such dimerization leads to the assembly of ~100 nm long filaments.[16] The

GTP is hydrolyzed into GDP (guanosine diphosphate) with a rate that strongly depends on the buffer conditions.[17] As the GTP gets hydrolyzed by FtsZ, the bond between two FtsZ monomers gets weaker and prone to unbinding. The process of continuous GTP hydrolysis and repletion leads to the turnover of monomers and filament treadmilling dynamics, as has been shown *in vitro*[18] as well as *in vivo*. The recent discovery of the treadmilling dynamics *in vivo* indicated that FtsZ is the main architectural driver for the synthesis of new cell wall.[19] *In vitro* reconstitutions of FtsZ filaments inside liposomes has shown how the protein on itself is capable to deform the lipid membrane,[20, 21] suggesting the possibility to employ the protein to re-create a minimal artificial divisome. A popular model for force generation by FtsZ is based on the higher curvature of GDP-bound FtsZ filaments compared to GTP ones,[22] suggesting GTP hydrolysis as the energy source for bending force. *In vitro* reconstitution of FtsZ inside liposomes has also shown that FtsZ bundles can deform the soft membrane with dynamics that depend on the GTP hydrolysis rate.[23] In comparison, the possibility of FtsZ to interact with membraneless coacervates is largely unexplored. A recent *in vitro* work has shown that FtsZ forms coacervates with SlmA,[24] a protein involved in the inhibition of the septal ring assembly in the vicinity of chromosomes. However, it remains to be seen whether FtsZ has the ability to dynamically interact with membraneless condensates, possibly leading to morphological changes to them, as is the case with membrane-bound containers.

In this paper, we use a microfluidic set up to study the dynamics of a three-component system: FtsZ, the key protein involved in bacterial division; polylysine (pLL) which is a positively charged multivalent peptide; and GTP as a negatively charged multivalent nucleoside triphosphate. While pLL and GTP self-assemble to form coacervates, FtsZ is a GTPase and thus has the potential to impact the stability of these coacervates. We show that FtsZ filaments partition strongly at the interface of pLL-GTP coacervates where they can induce a variety of morphological changes. Under continuous flow of a buffer without GTP, we observe an isotropic shrinkage of coacervates, which can be attributed to the hydrolysis of GTP molecules by FtsZ. Indeed, externally providing GTP to compensate for its loss from the condensate prevents any structural changes to the coacervates. Furthermore, we observe that FtsZ filaments assemble into thick bundles at the coacervate interface. Such bundling is remarkable, as it is observed *in vitro* only in the presence of crowding agents[25] or additional accessory proteins that *in vivo* form crosslinks between the FtsZ filaments.[26, 27] Interestingly, these bundles do not remain confined to the interface, but grow and emanate from the coacervates, ultimately joining each other to form a dense network of bundles. Lastly, compressing the FtsZ-coated coacervates causes them to fracture, leading to distinct flower shapes with pronounced indentations.

By selecting a key bacterial divisome protein and using the energy source for its polymerization as one of the components of the coacervate, we thus are able to observe interesting morphological changes of the coacervate itself. In the context of assembling a minimal divisome, the basic requirements of a minimal scaffold for an artificial cell include the need to induce localization of the proteins, to preserve and enhance their functionality, to allow energy exchange, and to undergo morphological changes. The

remarkable partitioning of FtsZ on the surface of coacervates in the absence of a lipid membrane, the enhanced assembling into bundles without additional promoters, and the ability of FtsZ to induce morphological changes to the coacervates, are encouraging indicators that coacervates may indeed constitute a membrane-free alternative scaffold for minimal artificial cells. The observed phenomena may also have biological relevance for the localization and bundling of FtsZ filaments *in vivo*, suggesting that coacervation may also be a relevant feature in prokaryotic cells.

5.2. Results

FtsZ partitions at the interface of GTP/pLL coacervates

Coacervation of pLL and GTP took place readily and could be seen by the immediate increase in the turbidity of the solution. To maximize the size of the coacervates and minimize the free charges in the diluted phase to a negligible amount, we mixed pLL and GTP in a stochiometric ratio so as to balance their negative and positive charges (see Materials and Methods). The obtained coacervates were flushed into a PDMS-based microchamber, where they sedimented and adhered to the bottom of the chamber. This adherence helped the coacervates maintain their position despite a flow, allowing stable imaging over long times during experimentation. Coacervates that were still floating in the microchamber merged with the adhered ones, forming bigger coacervates, resulting in polydispersely sized samples (Fig. 5.5). This process of coalescences was allowed to continue until a sizeable fraction of coacervates reached a diameter d ≥ 5 μm, a size convenient for visualization (Fig. 5.1a). As expected, the fluorescent signal from pLL was homogeneously distributed in the coacervates (Fig. 5.1b).

To examine how FtsZ interacted with the pLL/GTP coacervates, a solution containing FtsZ and GTP was flushed in the microchamber. We observed immediate, pronounced localization of FtsZ at the interface of the coacervates, in the form of a bright fluorescent ring at the equatorial plane (Fig. 5.1c). To analyze the preferential localization of FtsZ at the interface between the two liquid phases, we compared the fluorescent signal in the interior and at the interface of the coacervates with that measured in the surrounding dilute phase. When the coacervates and the FtsZ solution were simply mixed in equal amounts, we obtained an internal partition coefficient P_i = 0.6 ± 0.1 (mean ± standard deviation) and a surface partition coefficient P_s = 2.3 ± 0.3 (n = 30). On the other hand, when we constantly flushed FtsZ solution through the chamber, we observed an increase in the magnitude of the surface partition coefficient. After one hour of constant flushing, we measured P_i = 0.7 ± 0.2 and P_s = 4.5 ± 1.2 (n_s = 24), indicating that the fraction of proteins partitioned on the surface of the coacervates increased as more proteins were provided via the surrounding solution. The internal partition coefficient, on the other hand, remained unchanged.

The reason for the preferential localization of FtsZ on the surface of the coacervates is likely the electrostatic interactions between the FtsZ protein filaments and the coacervates. To understand the process, we measured the zeta potential relative to the surface of GTP/pLL coacervates. In the absence of FtsZ, we obtained a value Z = 12.7 ± 2.3 mV (n_{runs} = 6) indicating that the interface was positively charged, likely due to an excess of pLL molecules on the surface of coacervates. Since FtsZ is overall negatively charged at

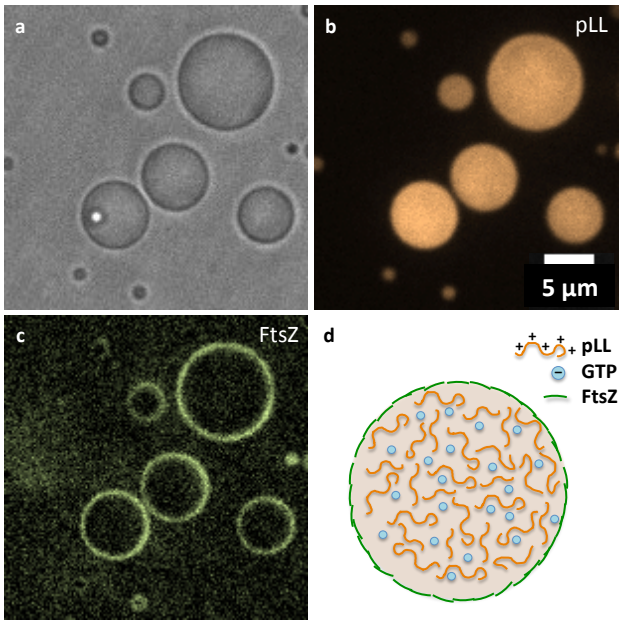

Figure 5.1: **FtsZ localizes at the interface of self-assembled pLL/GTP coacervates.** a) Bright-field image showing a polydisperse population of coacervates in a PDMS-based microchamber. These membraneless droplets are spontaneously formed as a result of electrostatic interactions between positively charged pLL and negatively charged GTP molecules. b) Fluorescence image showing that such phase-separated droplets indeed have an increased concentration of pLL inside them. pLL is labeled with cy5 for visualization. c) Fluorescence image showing that FtsZ strongly partitions at the interface of the coacervates. Protein was labelled with Alexa Fluor 488 for visualization. d) Schematic representation of pLL/GTP condensates with localization of FtsZ filaments at the interface.

pH 7.4 (given its isoelectric point of 4.9)[28], it will be driven to the surface through electrostatic attraction. Indeed, when we measured the Z potential on FtsZ-coated coacervates, we obtained Z = -5.8 ± 0.6 mV (n_{runs} = 12), consistent with the fact that the negatively charged FtsZ molecules were covering the coacervates.

GTP HYDROLYSIS BY FTSZ INDUCES DISASSEMBLY OF COACERVATES

Realizing the strong tendency of FtsZ to concentrate on the surface of the coacervates, we wondered whether the GTPase activity of FtsZ could induce morphological changes to the liquid droplets. As stability of coacervates critically relies on the balanced interaction between opposite charges, hydrolysis of GTP into GDP and a phosphate group, which reduces the number of negative charges per molecule, would be expected to destabilize the liquid droplets. Indeed, we observed that GTP hydrolysis by FtsZ significantly affects the coacervates. This is illustrated in Fig. 5.2a, where we flushed the coacervates with a solution containing FtsZ and GTP, followed by a buffer solution to

remove the excess of proteins and nucleotides from the microchamber: after the first five minutes, the FtsZ fluorescent signal started to become more homogenous over the coacervates. This was probably due to a continuous reduction of the coacervate volume, with the top surface now coming into the initial equatorial focal plane. After 20 minutes, the reduction of the volume became much more pronounced, as the coacervates dramatically shrunk to less than half of their original diameter. The FtsZ shell around the coacervates concomitantly decreased in diameter, following the shrinking outer contour of the coacervates. Ultimately, the coacervates underwent a drastic reduction in their volume, to the point that only very small agglomerates were left. The overall collapse of the coacervates structure can be attributed to the hydrolysis of GTP by FtsZ. As the nucleotides get hydrolyzed, the phosphate groups are prone to leave the coacervates, creating a deficiency of negative charges. As a result, excess pLL gets released in the surrounding solution together with GDP, as schematically shown in Fig. 5.2c. This explains the continuous shrinkage of the coacervates. The resulting remnants might be made up of some pLL and FtsZ residuals adhering together, or they could be pLL/GDP coacervates still covered by a layer of FtsZ. In the latter case, the smaller coacervate size can be given by the fact that GDP, having less charges than GTP, leads to a less efficient coacervation. To explore this possibility, we formed coacervates by mixing GDP and pLL in the same stoichiometric ratio as the one used for GTP/PLL coacervates (Fig. 5.6). In these conditions, we indeed observed negligible amount of coacervation; only a few very small droplets were visible.

To verify that the observed shrinkage is indeed a consequence of the GTPase activity of FtsZ, we investigated whether the coacervates were able to replace any hydrolyzed GTP by the uptake of fresh GTP molecules from the surrounding environment and thus prevent their disassembly. Indeed, in conditions where we flushed a solution containing GTP through the chamber, the coacervates remained stable and their size remained unchanged over time (Fig. 5.2b). It appears that in this case, the efflux of GDP generated by hydrolysis of GTP in the coacervates was compensated by an influx of fresh GTP, as schematically shown in Fig. 5.2d. This maintained the charge balance and hence the structural stability. Finally, when we repeated the experiment illustrated in Fig. 5.2a in absence of FtsZ, the coacervates did not show any appreciable change in size, further confirming that the observed shrinkage is indeed a consequence of the FtsZ activity (Fig. 5.7). Thus, we conclude that pLL/GTP coacervates not only serve as energy reservoir by providing GTP to the adhered FtsZ, but they can also replenish the energy-rich molecules from the surrounding environment.

LOCALIZATION ON THE COACERVATE SURFACE PROMOTES BUNDLING OF FTSZ FILAMENTS

Together with the capability of FtsZ to dissolve GTP/pLL coacervates, we observed that the coacervates promoted the aggregation of FtsZ filaments into a dense interconnected network of bundles, which we were able to visualize using confocal microscopy (Fig. 5.3a). We flushed a solution containing FtsZ and GTP in a microchamber containing GTP/pLL coacervates for about two hours, instead of twenty minutes as with previous experiments, in order to increase the FtsZ concentration on the coacervate surface and promote bundle formation. In order to visualize the possible microstructures, we removed the excess of proteins from the microchamber by gently flushing a protein-free buffer solution, until the fluorescent background was greatly reduced. Interestingly, we

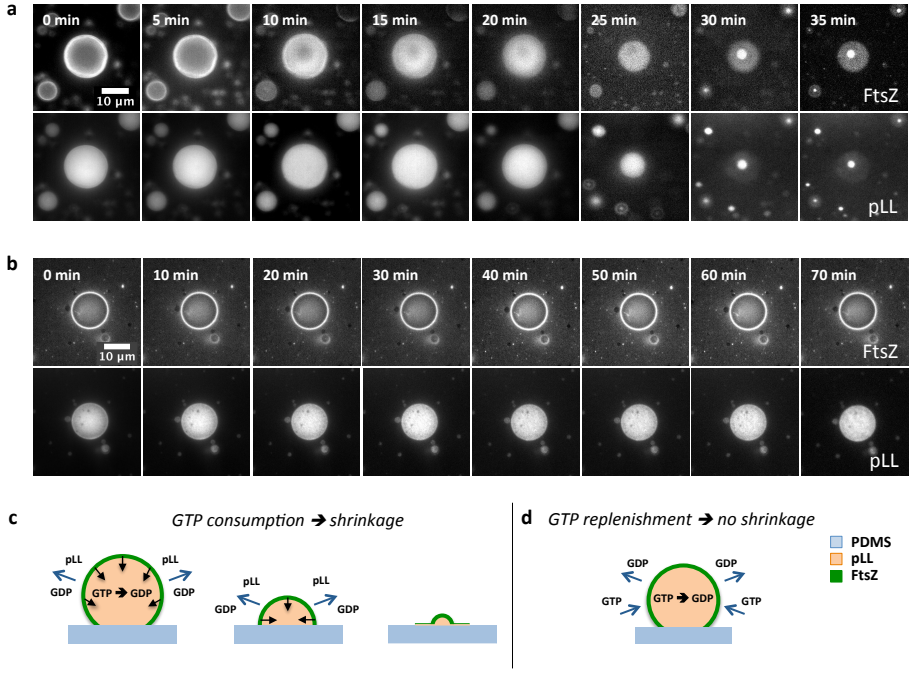

Figure 5.2: **GTP hydrolysis by FtsZ filaments promotes rapid disassembly of coacervates, leading to isotropic shrinkage.** a) Once FtsZ-coated coacervates were washed free of any excess protein and GTP in the surrounding environment, the coacervates became unstable and underwent a drastic shrinkage. The end state showed small bright aggregates, presumably composed of FtsZ and pLL remnants. A faint halo observed around the remnants is probably a mark left from the original contact area between the coacervate and the microchamber. b) Coacervate instability (in the form of shrinkage) is not observed, if GTP is externally provided to replenish the GTP hydrolyzed by FtsZ. The coacervates maintained their shape and size over a prolonged period of time. c) Schematic interpretation of the disassembly process: as FtsZ hydrolyses trivalent GTP molecules into divalent GDP molecules, the balance between positive and negative charges within the coacervates is altered. As this process continues, the electrostatic interactions are weakened and as a result, pLL and GDP molecules are released from the coacervates into the surrounding solution, and the coacervates shrink. d) Schematic interpretation to explain the observed stability of coacervates when GTP is externally provided. The GTP turnover inside the coacervates is balanced by the influx of GTP. As a result, the coacervates are able to replace the newly formed GDP with GTP to preserve the charge balance and thus their integrity.

observed a network of filamentous structures protruding from the coacervates into the surrounding environment, giving the coacervates aster-like appearance. We measured the distribution of FtsZ in different planes along the z-axis (Fig. 5.3b). At the top surface of the coacervates, FtsZ filaments had clearly reorganized in filamentous bundles. At the equatorial plane, localization of FtsZ filaments on the surface was evident, as well as the bundles emerging out of the surface. Interestingly, in absence of a physical membrane and membrane-anchoring proteins such as ZipA and FtsA, FtsZ bundles did not remain confined at the interface, but grew out into the surrounding environment. At the bottom plane, the contact surface between the PDMS and the coacervate was free

of proteins and appeared as dark disk, and it was surrounded by an interconnected network of FtsZ bundles emanating from neighboring coacervates. If the gentle buffer flow was continued, the coacervates underwent the same shrinkage process as previously described (Fig. 5.2a). However, a dense network of thick bundles surrounding the small shrunken agglomerates remained present towards the sides of the microchamber, where the flow was relatively weak and thus did not disrupt the network of bundles. Interestingly, the long filamentous structures constituting this network were composed of both FtsZ and pLL (Fig. 5.8). As the FtsZ bundles protruded out of the coacervates, the pLL molecules thus appeared to interact and co-localize with them. To better assess the driving forces underlying the enhanced bundling of FtsZ, we also examined the interaction between pLL and FtsZ in the absence of GTP, see Figure 5.9. It is evident that, even in absence of coacervation, pLL and FtsZ interacted to form fiber-like structures. Although these filamentous assemblies looked different from the FtsZ bundles obtained in presence of coacervates (Fig. 5.3 and Fig. 5.8), it seems reasonable to attribute the enhanced bundling properties of FtsZ to the presence of positive charges carried by pLL on the coacervate surface that act to promote the lateral association of negatively charged FtsZ filaments into bundles.

COACERVATES CRACK AND DEVELOP INVAGINATIONS UNDER MECHANICAL STRESS

Finally, we investigated whether the localization of FtsZ at the interface of the coacervates influences their mechanical properties. To check how the coacervates would react under mechanical stress, we squeezed ~20 μL solution containing FtsZ and pLL/GTP coacervates between two coverslips. To our surprise, the bigger coacervates seemed to 'crack open' and showed deep invaginations, giving them a flower-like appearance. The number of invaginations tended to increase with the coacervate size and their location was fairly evenly placed along the circumference. These flowers sometimes displayed prominent triangular petals, seemingly on the verge of separation from each other (Fig. 5.4a). The coacervates thus appeared to behave more like gel/glass-like objects than like liquid droplets, as upon pressing the sides of the droplets, where the stress tensor was highest, the interface got ripped apart to form a flower-like shape. To check whether this effect was indeed caused by the mechanical stress applied on the coacervates, we employed a wedge device (Fig. 5.4b), where the distance h between the two coverslips was varied from tens of micrometers to less than a micrometer. By having the two coverslips fluorescently labeled, it was possible to measure h for each field-of-view and compare it with the diameter d of the coacervates. By comparing h and d, we could infer whether each coacervate was vertically confined ($h/d < 1$) or not ($h/d > 1$). Plotting a frequency histogram of 'flowers' and regular spheres against h/d (Fig. 5.4c) showed that the flower shape was exclusively obtained for $h/d < 1$, showing that, indeed, the flowers were induced by the mechanical stress applied on the coacervates. Several control experiments were performed to check whether this effect was indeed given by the presence of FtsZ and its activity on the surface of the coacervates. Compressing pure coacervates in absence of FtsZ did not lead to any deformations, and the coacervates behaved like liquid droplets (Fig. 5.10a). Repeating the mechanical test on ATP/pLL coacervates mixed with FtsZ solution also resulted in liquid droplets without any deformations (Fig. 5.10b). However, when we mixed GTP/pLL coacervates with just the buffer that FtsZ was dissolved in, we again observed flower-like deformations, although to a lesser extent and

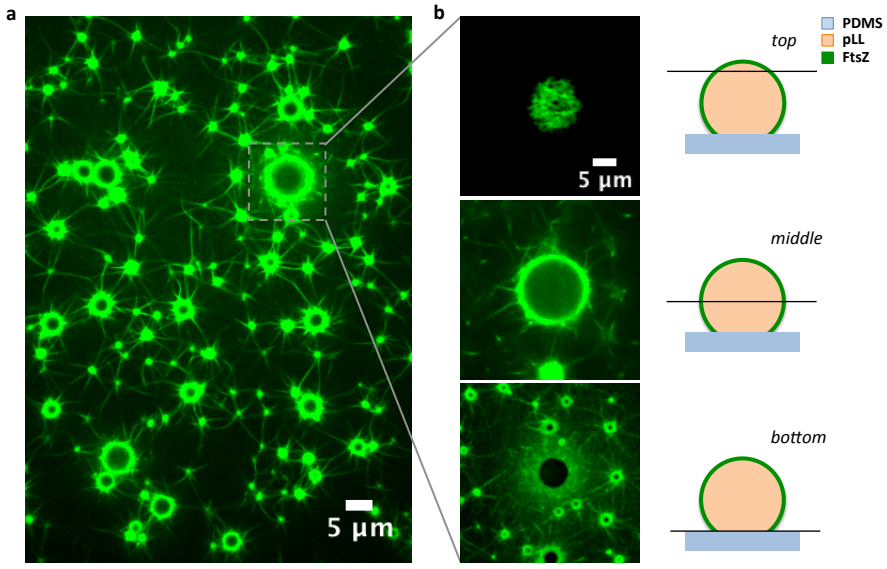

Figure 5.3: **Localization at the coacervate surface promotes bundling of FtsZ filaments and subsequent protrusion of the bundles to form an interconnected network across multiple coacervates.** a) Fluorescence image showing bundles of FtsZ filaments emanating from coacervates, giving them aster-like appearance. Bundles protruding from adjacent coacervates merged with each other to form a single, interconnected, hybrid network. b) A zoom-in on a single coacervate showing three slices at different planes. The confocal scan at the top surface of the coacervate showed a dense mesh of bundles (top image). A scan across the equator showed bundles emerging out of the droplet (middle image). A scan across the bottom surface showed numerous bundles at the interface forming a dense mesh (bottom image) and dark circular regions that correspond to the area where the coacervate adhered to the surface, preventing FtsZ from gaining access.

less symmetric than those seen in presence of FtsZ (Fig. 5.10c). Possibly, the presence of FtsZ filaments and their interaction with pLL created a relatively rigid layer around the coacervate, producing deeper and more regular fractures under mechanical stress. Even more surprisingly, when we performed the previous experiment with ATP/pLL coacervates, we did not observe these fractures. This led us to conclude that the 'flower formation' is dependent on the specific nucleotide (GTP against ATP) used to form the coacervates. When glycerol was removed from the buffer to check the effect of viscosity, the flower shape remained absent (Fig. 5.10e), and also when all the individual components of the buffer were mixed separately with GTP/pLL coacervates (Fig. 5.10f-i). Thus, the severe shape deformations of FtsZ-coated coacervates under mechanical stress that we observe may not be solely induced by FtsZ, but instead, they are more likely enhanced by its presence at the interface. On the dependence of the specific nucleotide, we note that it is plausible that, given the different molecular structure of their bases, GTP molecules

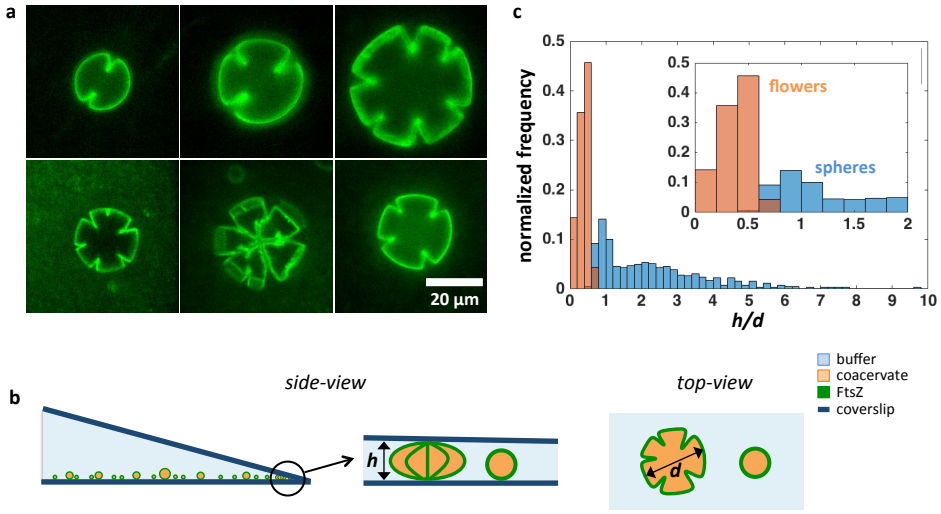

Figure 5.4: **FtsZ-coated coacervates display extensive invaginations when deformed under mechanical pressure.** a) Fluorescence images showing several examples of FtsZ-coated deformed coacervates, exhibiting pronounced defects in the form of multiple invaginations. We address these shapes as 'flowers'. In some cases (bottom center), invaginations divide the flower into separate petals. b) A schematic showing the wedge device with a variable height that was employed to verify whether coacervates transformed into flowers only when pressed. A deformed and a non-deformed coacervate is also sketched, showing a cracked and a smooth interface respectively. c) A frequency histogram (N=540) that shows that coacervates adopt a flower shape only when mechanically pressed, *i.e.*, when the height h of the microchamber is lower than the diameter d of the coacervate.

form more extensive hydrogen bonding with polylysine polymers as compared to ATP molecules, creating more compact, and hence less deformable, coacervates. Also, the presence of cations, such as K^+, has been reported to enhance the formation of hydrogen bonds between the guanine bases.[29] Furthermore, π-π stacking of the aromatic surfaces can lead to the creation of supramolecular assemblies inside the coacervates,[30] potentially transforming the droplets from a liquid phase into a denser gel phase.

5.3. Discussion

In this work, we explored how FtsZ, a highly conserved protein responsible for cell division in bacteria, dynamically interacts with liquid droplets (coacervates) made up of polylysine and GTP. By performing microfluidic on-chip experiments, we showed that FtsZ partitions at the coacervate interface where it is able to induce structural changes and reshape the coacervates. At the same time, the liquid droplets also have a clear impact on the self-assembly of FtsZ filaments. It has been previously reported how coacervates made of polymers and nucleotides have the capability to absorb a variety of different molecules, from fluorescent dyes to proteins.[31] However, in our case we found that FtsZ does not localize in the interior of the coacervates, but strongly parti-

tions on their surface despite the lack of a lipid membrane and membrane-anchoring proteins. This is likely driven by interactions with positively charged pLL at the surface of the coacervates. A similar membranization-like process was previously reported when a synthetic triblock copolymer molecule was employed to construct a shell around liquid droplets.[32]

Due its GTPase nature, FtsZ further utilizes the high concentration of GTP within the droplets as an energy reservoir, which destabilizes the coacervates and induces their disassembly. When GTP is externally provided, the shrinkage process is completely inhibited as the hydrolyzed GTP is continuously replenished.

Another key feature of FtsZ filaments that we have observed is their lateral organization into bundles in absence of any external agent. In bacteria, FtsZ filaments laterally associate into bundles that further constitute the ring structure responsible for the division. *In vitro*, this self-assembly process can occur in confined environments in the presence of additional macromolecules such as Ficoll or polyethylene glycol, that recreate the necessary crowding conditions.[25] Other *in vitro* works have shown aggregation of FtsZ filaments into bundles by interaction with specific proteins that play the role of crosslinks between the filaments *in vivo*, such as the membrane anchor ZipA[27] or the bundling agent ZapA.[33] Finally, FtsZ has been reported to form dynamic bundles when tethered to a lipid membrane via one of its natural anchor proteins,[18] or when modified to bind a lipid membrane without the need of additional proteins.[34]

We showed that the lateral association between FtsZ filaments is enhanced when partitioned on the surface of the coacervates, presumably due to interactions with the positively charged pLL molecules. Consequent bundling of FtsZ filaments constitutes a mode of spatial organization that, interestingly, does not involve auxiliary crowders or proteins that are normally required for FtsZ to bundle *in vitro* and *in vivo*. The bundling of FtsZ on the surface induced a morphological change, where the liquid droplets acted as nodes with FtsZ bundles protruding out in the surrounding environment, creating a dense network. Our results bear some resemblance to a previous report, where the pH-triggered assembly of nanofibers drove spontaneous shape transformation of spherical coacervates into aster-like fibrous structures.[35] Also, shape deformation of coacervates induced by polymerization of tubulin cytoskeletal proteins was recently observed, where the growth of microtubules inside coacervates led the coacervates to assume a rod-like shape.[10]

Finally, we observed that FtsZ-coated coacervates, when subjected to mechanical pressure, showed unexpected solid-like behavior, which manifested itself in the form of deep invaginations, giving them a flower-like appearance. Although this effect is more pronounced with protein-coated droplets, we observed similar deformations under specific conditions without any proteins, and the observed intriguing phenomenon can be attributed to the presence of a specific nucleotide in specific buffer conditions.

Overall, we explored the use of coacervates as both potential scaffolds as well as energy reservoirs for NTPase proteins such as FtsZ. We showed how GTP/pLL coacervates provide and exchange nucleotides with the surrounding environment and the

proteins. The self-assembly of FtsZ filaments, which were partitioned on the surface of the coacervates, was greatly enhanced and the formed protein bundles reshaped the liquid droplets. Such a dynamic system might prove to be an important tool in synthetic biology, especially towards the creation of a minimal cell. The strong affinity of FtsZ for coacervates may also be of relevance in bacteria where, along with other factors, the localization and bundling of FtsZ filaments at the mid-cell could be facilitated by coacervation.

5.4. METHODS

MICROFABRICATION AND SOFT LITHOGRAPHY

Microchamber designs were produced in a cleanroom with the following procedure: a 4-inch silicon wafer was cleaned in fuming nitric acid (100% HNO3) for 10 minutes using a sonication bath, and further rinsed with water. The wafer was then spin-coated with hexamethyldisilazane (HMDS) and subsequently with NEB22a (Sumitomo Chemical) negative resist. Both layers were spun at 1000 rpm for 1 minute and baked at 200 °C for 2 minutes and 110 °C for 3 minutes respectively. The HMDS layer is necessary to ensure proper adhesion of NEB22a onto the silicon surface. Electron-beam lithography (EBPG-5000+, Raith GmbH) was used to write the designs on the coated wafer (dose: 16 μC cm^{-2}, acceleration voltage: 100 kV, aperture: 400 μm). A post-bake was performed at 105 °C for 3 minutes. The structures were developed in MF322 (Dow Chemical Company) for 30 seconds, followed by rinsing in diluted MF322 (10 times in deionized water) for 15 seconds, and finally rinsing in deionized water for 15 seconds. Structures were then dry-etched using Bosch deep reactive-ion etching, with an inductive coupled plasma (ICP) reactive-ion etcher (Adixen AMS 100 I-speeder). The procedure consisted of alternating SF6 etching steps with C4F8 passivation steps. At the end of the process, the wafer was exposed to Oxygen plasma for 10 minutes to remove the excess of resist from the wafer. To facilitate subsequent peeling-off of polydimethylsiloxane (PDMS) from the wafer, the hydrophobicity of the surface was enhanced by silanizing it with (tridecafluoro-1,1,2,2-tetrahydrooctyl) trichlorosilane (ABCR GmbH & Co.) overnight in a vacuum desiccator. Curing agent and PDMS (Mavom) were mixed in a mass ratio 1:10, degassed in vacuum, and the mixture was poured on a plain silanized wafer and on the wafer containing the required patterns. The plain wafer was used to prepare glass coverslips with a thin PDMS coating. For that, coverslips were firmly pressed down on the wafer, so that a thin PDMS layer was formed beneath them. Both wafers were baked at 80 °C for 4 hours. Coverslips and the PDMS block containing the designs were removed from the wafers, and single microchambers were separated with a cutter and cleaned using isopropanol. Both chips and coverslips were activated using Oxygen plasma (Plasmatic System, Inc.) for about 10 seconds, then immediately bonded and baked for other 20 minutes at 80 °C. The solutions were introduced into the microchambers using pressure pumps (Fluigent) via appropriately connected tubing (Tygon Microbore Tubing, inner diameter) and home-built metal connectors. The flow was finely tuned using a MAESFLO software (Fluigent).

WEDGE DEVICE PREPARATION

A piece of double-face Scotch tape was put at one end of a coverslip, along with 40 μl of sample. A second coverslip was then put on top, with one end in contact with the

bottom coverslip and the other end on the tape, to create the desired tilted angle. Finally, the sides of the resulting wedge geometry were sealed with epoxy (Devcon). Before preparing the device, the coverslips were surface covered with fluorescent labels in order to precisely measure the height throughout the device. For labeling the surfaces, a drop of a solution containing cy5-labeled MinE protein (1 μM) was squeezed between two PDMS-covered coverslips. After incubating for 30 minutes, the coverslips were extensively washed with MilliQ water to remove the excess of proteins from the surface.

COACERVATES PREPARATION

Unlabeled polylysine (15-30 kDa) was purchased from Sigma Aldrich. Polylysine (25 kDa), labeled with cy5 fluorescent dye, was purchased from Nanocs. The powders were dissolved in MilliQ water at a concentration of 50 mg/mL and 1mg/mL, respectively. Labeled and unlabeled polylysine were mixed together in a molar ratio of 1:100. Guanosine triphosphate sodium salt hydrate was purchased from Sigma Aldrich and dissolved in MilliQ water to a final stock concentration of 100 mM. Just before the experiment, GTP and pLL were diluted separately to 25 mM and 0.44 mM respectively. Finally, 20 μl of solution containing 25 mM GTP was mixed with 20 μl solution containing 0.44 mM pLL by pipetting up and down extensively. Guanosine diphosphate sodium salt was purchased from Sigma Aldrich. Preparation of stock solutions and coacervates with GDP followed the same procedure as described for GTP.

SOLUTION COMPOSITIONS

The composition of the aqueous solution containing FtsZ was as follows: 12 μM FtsZ, 180 mM KCl, 25 mM Tris-HCl (pH 7.4), 5 mM $MgCl_2$, 15% v/v glycerol. When required, 25 mM GTP was added to the solution. The aqueous solution used to remove excess of proteins and nucleotides from the microchamber had the following composition: 150 mM KCl, 25 mM Tris HCl (pH 7.4), 5 mM $MgCl_2$. Again, if the experiment required it, 25 mM GTP was added. FtsZ purification and labeling (with Alexa Fluor 488) were performed in the lab following the protocol described elsewhere.[28] Protein plasmids were a kind gift from Germán Rivas (Centro de Investigaciones Biológica-CSIC, Madrid). Labeled and unlabeled FtsZ were mixed in a ratio 1:8, flash-frozen in liquid nitrogen and stored at -80 °C.

IMAGE ACQUISITION AND PROCESSING

Sample imaging was performed using an Olympus IX-81 inverted microscope with epifluorescence illumination and specific filter sets. Images were acquired using 20x UPlanSApo (NA 0.75) and 60x PlanApo (NA 1.45, oil) objectives, and recorded with a Zyla 4.2 PLUS CMOS camera (Andor Technology) and a micromanager software (version 1.4.14). Confocal imaging was performed using an inverted Olympus IX81 combined with Andor Revolution illumination system. Confocal images were acquired using a Yokogawa CSU X1 detection system, a 60x UPlanFLN (NA 1.25) objective, and an EM-CCD Andor iXon X3 DU897 camera. Images were analyzed and background appropriately subtracted using Fiji (ImageJ).

ZETA POTENTIAL MEASUREMENTS

For zeta potential measurements (Zetasizer Nano, Malvern Instruments), pLL/GTP coacervates were prepared by mixing 20 μL of 0.44 mM (15-30 kDa) pLL and 20 μL of 25 mM GTP, and vortexing for 10 seconds. 10 μL of the resulting solution was immediately taken and diluted in 760 μL of MQ water and equilibrated for 2 hours before inserting it into a flow cell. For measurements involving FtsZ-coated coacervates, 20 μL of unlabeled FtsZ solution in buffer was added to the coacervates and mixed by pipetting up and down. The rest of the procedure was as described above.

STATISTICAL ANALYSIS

The size distribution of the coacervates (Fig. 5.5) was obtained by manually measuring the diameter of individual coacervates (n = 331). The diameter of flower-shaped coacervates was determined similarly (Fig. 5.4c). These diameter values were acquired for 540 coacervates, of which 70 showed clear fracturing. The local height of the wedge-shaped device was measured by taking a stack of images (step = 1 μm) along the z-axis of the device and by further measuring the distance between the two fluorescent peaks, corresponding to the two labeled coverslips. To calculate the partition coefficients, a fluorescent intensity profile for each coacervate (n = 24) was obtained along the equatorial plane. The fluorescence at the surface was determined as the peak of the intensity profile, while the intensity inside and outside the coacervates was determined as the lowest values in their respective regions. The error bars in all of the analyses correspond to a single standard deviation. All image processing was done using Fiji (ImageJ) and the graphs were plotted using MATLAB 2015 (Mathworks).

5.5. SUPPLEMENTARY INFORMATION

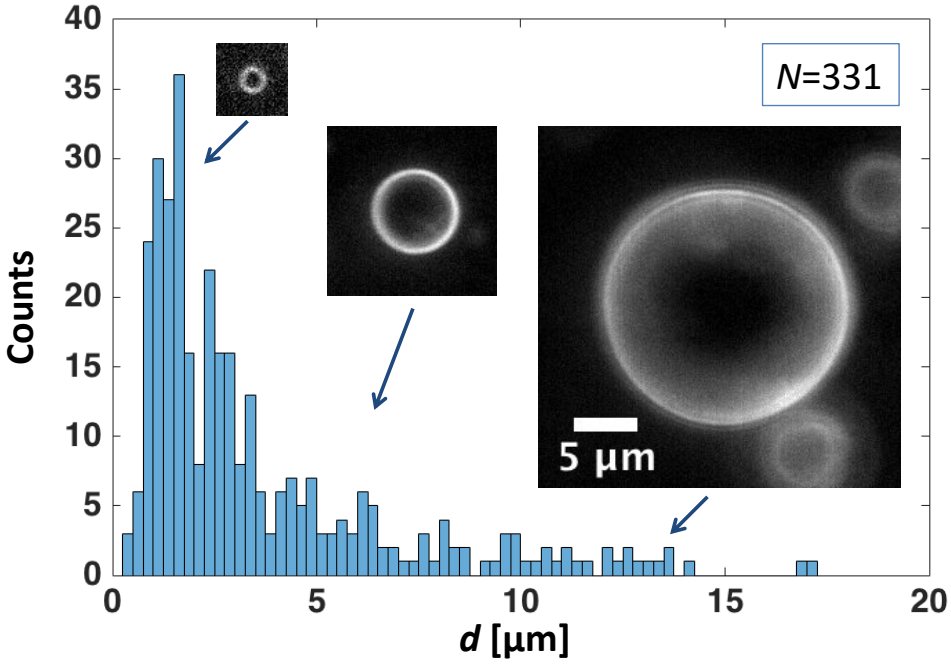

Figure 5.5: **Size distribution of coacervates.** Frequency histogram showing a polydisperse size distribution of pLL/GTP coacervates (N = 331). As can be seen, majority of the population lies between 1-5 µm.

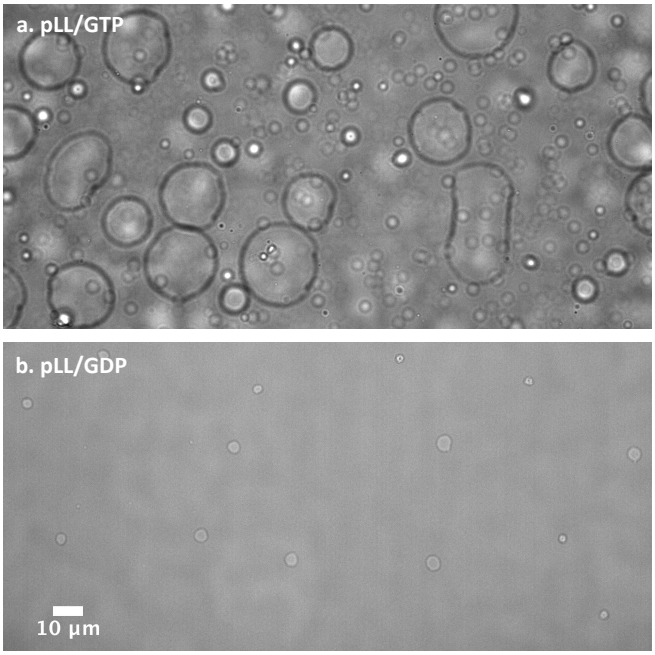

Figure 5.6: **Coacervation efficiency is strongly influenced by the extent of multivalency of the nucleotide.** a) GTP and pLL readily formed numerous coacervates when mixed together. b) GDP and pLL, on the other hand, formed only a few and much smaller coacervates. The lower efficiency of the coacervation process can be attributed to the lower amount of negative charges carried by GDP molecules.

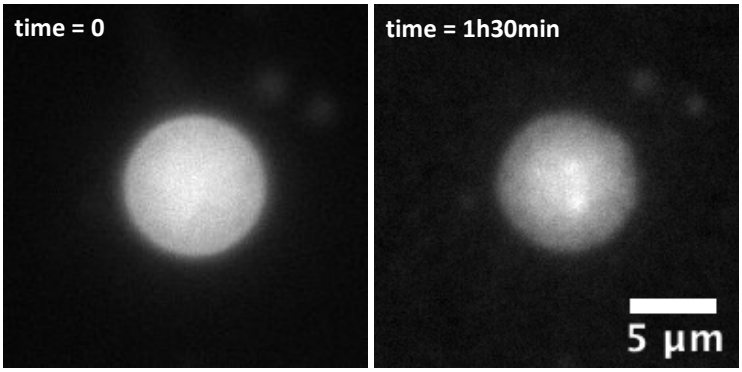

Figure 5.7: **In absence of FtsZ, coacervates remain stable, even when flushed with a buffered solution.** When the microchamber containing the coacervates was gently flushed with a buffered solution to get rid of the excess proteins and nucleotides, the coacervates remained stable and did not change their volume.

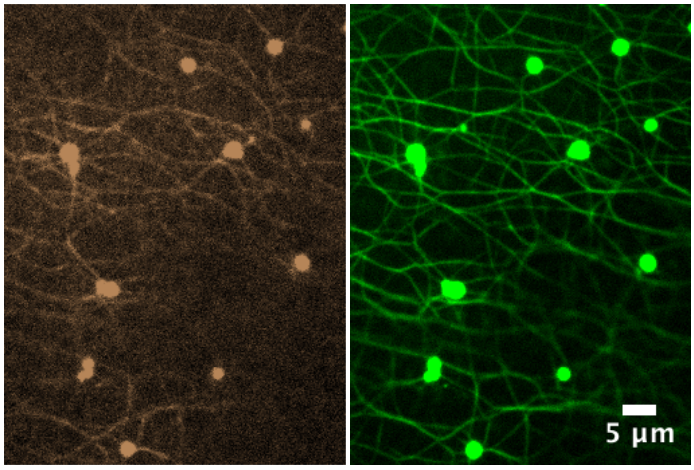

Figure 5.8: **pLL colocalizes with the network of emanating FtsZ bundles.** Incubating the coacervates with FtsZ solution for two hours and subsequently removing the proteins and the nucleotides from the surrounding solution led to the formation of thick bundles and shrinkage of coacervates. Interestingly, the fluorescent signal from cy5-labelled pLL, colocalized with the signal from FtsZ bundles, indicating that pLL molecules interacted with, and adhered to FtsZ bundles.

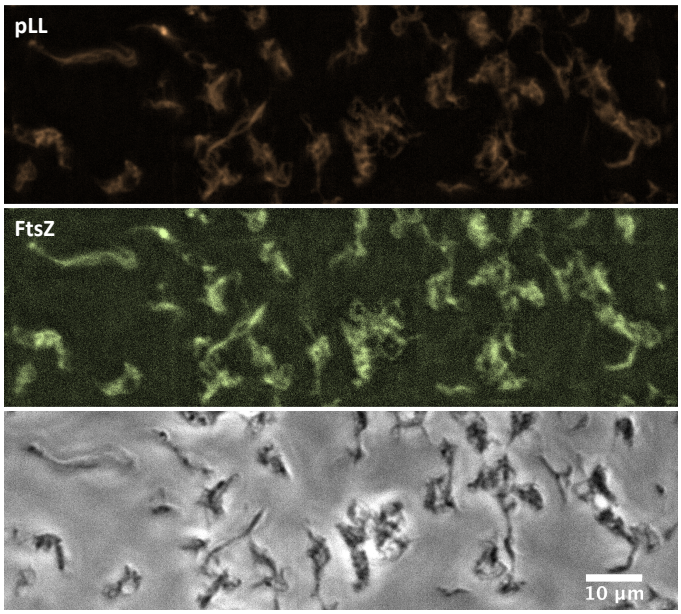

Figure 5.9: **pLL and FtsZ interact with each other to form fiber-like structures.** When mixed together, pLL (440 µM) and FtsZ (205 µM, buffer described in Materials and Methods) aggregate to form filamentous structures. Co-localization is evident from overlapping of fluorescent signal of cy5-labelled pLL and Alexa488-labelled FtsZ.

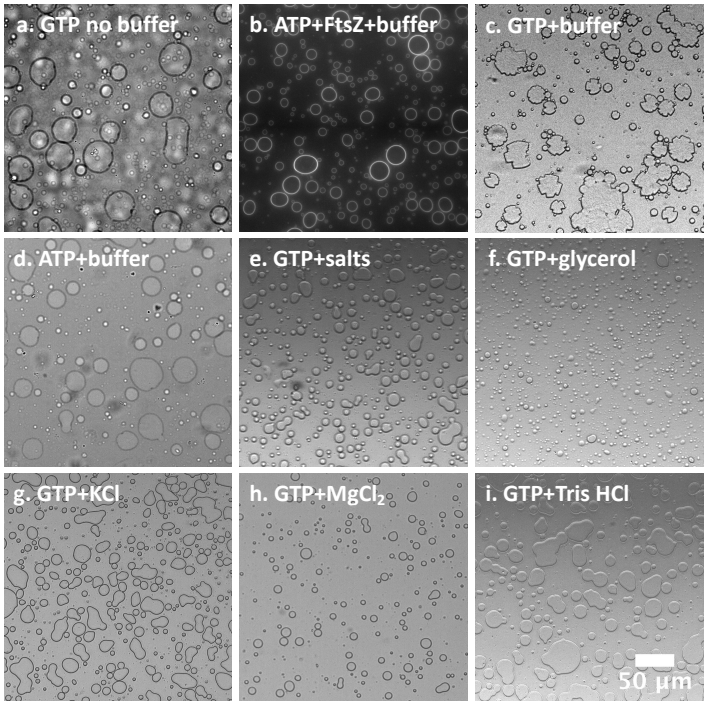

Figure 5.10: **The morphology adopted by the coacervates under mechanical stress depends on the nucleotides base and on the buffer conditions.** a) GTP/pLL coacervates did not show any invagination under mechanical stress in absence of buffer and FtsZ. b) ATP/pLL coacervates covered with FtsZ did not deform into a flower-like shape. c) GTP/pLL coacervates in presence of buffer showed flower-like shapes, while ATP/pLL coacervates in the same conditions did not (d). Without FtsZ, flower-like coacervates were not present in absence of glycerol (e), or when mixed only with individual buffer components, specifically 15% v/v glycerol (f), 150 mM KCl (g), 5 mM $MgCl_2$ (h), 25 mM Tris HCl (i).

REFERENCES

[1] S. F. Banani, H. O. Lee, A. A. Hyman, and M. K. Rosen, *Biomolecular condensates: organizers of cellular biochemistry,* Nature Reviews Molecular Cell Biology **18**, 285 (2017).

[2] Y. Shin and C. P. Brangwynne, *Liquid phase condensation in cell physiology and disease,* Science **357** (2017), 10.1126/science.aaf4382.

[3] S. Koga, D. S. Williams, A. W. Perriman, and S. Mann, *Peptide-nucleotide microdroplets as a step towards a membrane-free protocell model,* Nature Chemistry **3**, 720 (2011).

[4] A. A. Hyman, C. A. Weber, and F. Jülicher, *Liquid-Liquid Phase Separation in Biology,* Annual Review of Cell and Developmental Biology **30**, 39 (2014).

[5] W. K. Spoelstra, S. Deshpande, and C. Dekker, *Tailoring the appearance: what will synthetic cells look like?* Current Opinion in Biotechnology **51**, 47 (2018).

[6] M. Li, X. Huang, T. Y. Tang, and S. Mann, *Synthetic cellularity based on non-lipid micro-compartments and protocell models,* (2014).

[7] D. Priftis and M. Tirrell, *Phase behaviour and complex coacervation of aqueous polypeptide solutions,* Soft Matter **8**, 9396 (2012).

[8] W. M. Aumiller and C. D. Keating, *Phosphorylation-mediated RNA/peptide complex coacervation as a model for intracellular liquid organelles,* Nature Chemistry **8**, 129 (2015).

[9] K. K. Nakashima, J. F. Baaij, and E. Spruijt, *Reversible generation of coacervate droplets in an enzymatic network,* Soft Matter (2017), 10.1039/C7SM01897E.

[10] A. Hernández-Vega, M. Braun, L. Scharrel, M. Jahnel, S. Wegmann, B. T. Hyman, S. Alberti, S. Diez, and A. A. Hyman, *Local Nucleation of Microtubule Bundles through Tubulin Concentration into a Condensed Tau Phase,* Cell Reports **20**, 2304 (2017).

[11] P. M. McCall, S. Srivastava, S. L. Perry, D. R. Kovar, M. L. Gardel, and M. V. Tirrell, *Partitioning and Enhanced Self-Assembly of Actin in Polypeptide Coacervates,* Biophysical Journal **114**, 1636 (2018).

[12] K. Dai and J. Lutkenhaus, *ftsZ is an essential cell division gene in Escherichia coli,* J Bacteriol **173**, 3500 (1991).

[13] H. P. Erickson, *FtsZ, a prokaryotic homolog of tubulin?* Cell **80**, 367 (1995).

[14] T. den Blaauwen, L. W. Hamoen, and P. A. Levin, *The divisome at 25: the road ahead,* Current Opinion in Microbiology **36**, 85 (2017).

[15] A. Mukherjee and J. Lutkenhaus, *Dynamic assembly of FtsZ regulated by GTP hydrolysis,* EMBO Journal **17**, 462 (1998).

[16] Y. Chen and H. P. Erickson, *Rapid in vitro assembly dynamics and subunit turnover of FtsZ demonstrated by fluorescence resonance energy transfer,* Journal of Biological Chemistry **280**, 22549 (2005).

[17] A. Mukherjee and J. Lutkenhaus, *Analysis of FtsZ Assembly by Light Scattering and Determination of the Role of Divalent Metal Cations Analysis of FtsZ Assembly by Light Scattering and Determination of the Role of Divalent Metal Cations,* Journal of Bacteriology **181**, 823 (1999).

[18] M. Loose and T. J. Mitchison, *The bacterial cell division proteins ftsA and ftsZ self-organize into dynamic cytoskeletal patterns,* Nature Cell Biology **16**, 38 (2014).

[19] A. W. Bisson-Filho, Y. P. Hsu, G. R. Squyres, E. Kuru, F. Wu, C. Jukes, Y. Sun, C. Dekker, S. Holden, M. S. VanNieuwenhze, Y. V. Brun, and E. C. Garner, *Treadmilling by FtsZ filaments drives peptidoglycan synthesis and bacterial cell division,* Science **355**, 739 (2017).

[20] P. Szwedziak, Q. Wang, T. A. M. Bharat, M. Tsim, and J. Löwe, *Architecture of the ring formed by the tubulin homologue FtsZ in bacterial cell division,* eLife **3**, e04601 (2014).

[21] M. Osawa and H. P. Erickson, *Liposome division by a simple bacterial division machinery.* Proceedings of the National Academy of Sciences of the United States of America **110**, 11000 (2013).

[22] C. Lu, M. Reedy, and H. P. Erickson, *Straight and curved conformations of FtsZ are regulated by GTP hydrolysis,* Journal of Bacteriology **182**, 164 (2000).

[23] E. J. Cabré, A. Sánchez-Gorostiaga, P. Carrara, N. Ropero, M. Casanova, P. Palacios, P. Stano, M. Jiménez, G. Rivas, and M. Vicente, *Bacterial division proteins FtsZ and ZipA induce vesicle shrinkage and cell membrane invagination,* Journal of Biological Chemistry **288**, 26625 (2013).

[24] B. Monterroso, S. Zorrilla, M. Sobrinos-Sanguino, M. A. Robles-Ramos, M. López-Álvarez, C. D. Keating, and G. Rivas, *Bacterial division FtsZ forms liquid condensates with nucleoid-associated Z-ring inhibitor SlmA,* bioRxiv (2018).

[25] J. Groen, D. Foschepoth, E. Te Brinke, A. J. Boersma, H. Imamura, G. Rivas, H. A. Heus, and W. T. Huck, *Associative interactions in crowded solutions of biopolymers counteract depletion effects,* Journal of the American Chemical Society **137**, 13041 (2015).

[26] F. J. Gueiros-Filho and R. Losick, *A widely conserved bacterial cell division protein that promotes assembly of the tubulin-like protein FtsZ,* Genes and Development **16**, 2544 (2002).

[27] C. A. Hale, A. C. Rhee, P. A. J. D. Boer, and A. M. Y. C. Rhee, *ZipA-Induced Bundling of FtsZ Polymers Mediated by an Interaction between C-Terminal Domains ZipA-Induced Bundling of FtsZ Polymers Mediated by an Interaction between C-Terminal Domains,* Society **182**, 5153 (2000).

[28] Q.-M. Yi and J. Lutkenhaus, *The nucleotide sequence of the essential cell-division genefts2 of Escherichia coli,* Gene **36**, 241 (1985).

[29] J. T. Davis and G. P. Spada, *Supramolecular architectures generated by self-assembly of guanosine derivatives,* Chem. Soc. Rev. **36**, 296 (2007).

[30] S. Lena, S. Masiero, S. Pieraccini, and G. P. Spada, *Guanosine hydrogen-bonded scaffolds: A new way to control the bottom-up realisation of well-defined nanoarchitectures,* Chemistry - A European Journal **15**, 7792 (2009).

[31] D. S. Williams, S. Koga, C. R. C. Hak, A. Majrekar, A. J. Patil, A. W. Perriman, and S. Mann, *Polymer/nucleotide droplets as bio-inspired functional microcompartments,* Soft Matter **8**, 6004 (2012).

[32] A. F. Mason, B. C. Buddingh, D. S. Williams, and J. C. Van Hest, *Hierarchical Self-Assembly of a Copolymer-Stabilized Coacervate Protocell,* Journal of the American Chemical Society **139**, 17309 (2017).

[33] H. H. Low, M. C. Moncrieffe, and J. Löwe, *The crystal structure of ZapA and its modulation of FtsZ polymerisation,* Journal of Molecular Biology **341**, 839 (2004).

[34] M. Osawa, D. E. Anderson, and H. P. Erickson, *Reconstitution of Contractile FtsZ Rings in Liposomes,* Science **320**, 792 LP (2008).

[35] R. Krishna Kumar, R. L. Harniman, A. J. Patil, and S. Mann, *Self-transformation and structural reconfiguration in coacervate-based protocells,* Chem. Sci. **7**, 5879 (2016).

6

CONCLUDING REMARKS

"Wisdom comes to us when it can no longer do any good."

Gabriel García Márquez

The improvement of experimental techniques that the biological sciences have witnessed in the recent years has led to a more frequent employment of in vitro essays for the reconstitution, study, and characterization of biological systems. Such experiments conducted in a bottom-up approach proved to be useful to isolate single components from the multitude of interactions occurring in the reaction under analysis. Division is one of the most fascinating processes occurring in the cell that can be tackled with such approach.[1, 2] The divisome is indeed a complex machinery, composed of many proteins that all together, via multiple interactions not yet entirely understood, lead to a progressive cell invagination and division into two daughters. Specifically, in bacteria such machinery is called the Z-ring, a multi-protein complex that contracts at the cell mid-plane and performs the division.[3–5] The question: "how does this machinery work?" was first approached with hierarchical in vivo top-down experiments on the proteins constituting the ring.

6.1. FTSZ APPROACHING ITS 30S

Early on, FtsZ was identified as a fundamental component of the machinery, as it constitutes an essential core of the ring.[6, 7] Whether this protein was, on its own, responsible for cytokinesis became one of the major questions in the field of cell division. Confronted by the huge complexity of the process, the idea that one single component could both lead the assembly and perform the main function of the whole ring was an appealing one, though perhaps naive.[8, 9] This model led to the idea to assemble a minimal cell, reconstituted in a bottom-up way from isolated cellular components, with FtsZ as the lead player: reconstitution of FtsZ filaments into soft lipid containers, such as liposomes, might allow to observe membrane deformation and, possibly, division. In the last 20 years, different labs around the world have put significant energy and efforts in attempting to establish such a reconstitution of the division process, with limited success however. While first several encouraging examples of membrane deformations performed by FtsZ filaments were reported,[10–13] subsequent efforts were more challenging. Currently, we still lack a clear liposome division performed by a minimal FtsZ-based ring. It is now safe to say that there is a growing skepticism in the field of cell division towards the idea that FtsZ alone can be the force generator in bacteria.[14] Together with the fact that certain in vitro results concerning FtsZ capacity to divide a liposome appeared rather questionable,[15] more recent results obtained in vivo do not seem to agree with a minimalistic conception of the divisome. The recent findings that FtsZ treadmilling drives the machinery responsible for peptidoglycan synthesis around the division site indicate a major role of cell wall synthesis in the progressive constriction, implying that many more components are vital for synthetic cell division rather than FtsZ alone.[16–18]

6.2. WHAT'S NEXT?

It is not entirely clear how the field of synthetic cell division will now proceed, given these new insights about FtsZ. While the notion that FtsZ is not the main responsible for cell division in bacteria is increasingly acknowledged, it is reasonable to state, based on the evidences obtained so far, that the protein can deform lipid membranes to a certain

extent, so that pursuing synthetic cell division via FtsZ could potentially turn out to be feasible in the future. In general, if the goal is to engineer a minimal cell based on biological components, one can conceive to employ proteins to perform specific functions, disregarding whether these are physiologically relevant. An example of such approach is offered by two recent fascinating works on Min protein oscillations reconstituted in liposomes, which induced substantial membrane remodeling: while in vivo Min proteins are not even essential for cell division, such results may suggest a route towards synthetic cell division that is different than the one defined by mother nature.[19, 20] A fracture now seems to emerge between the assembly of a minimal cell as a route towards a better understanding of the real system, and the minimal cell as the ultimate goal of biological engineering. In the case of cell division, for example, whether FtsZ or Min proteins will eventually lead to liposome division should not be interpreted as an indication of their role in bacteria, but as remarkable engineering achievements. It is important to keep this distinction in mind, so to avoid that even interesting results are phrased such to become misleading in their biological relevance.

While the future of FtsZ as a tool to divide a liposome is somewhat foggy, several aspects concerning its functionality in cells will still be largely studied. If the work presented in this thesis will be continued, it will, for example, be interesting to better explore the nature of the lateral interactions between FtsZ filaments. Given the preliminary results obtained in Chapter 4, it would be necessary to develop a more efficient liposome production system, to systematically observe and understand the mechanism behind the membrane deformations observed. In this context, it will be important to understand which role GTP-hydrolysis plays in membrane constriction. While our work has been performed solely by employing ZipA as a membrane anchor, it is important to understand the difference between ZipA and FtsA in regulating the FtsZ filament assembly and dynamics, with a particular attention on the interplay between lateral interactions and treadmilling. Also, it is important to better define the notion of "bundles", i.e. how the filaments organize in higher-ordered structures, and how different arrangements unlock specific dynamics. Recent works from Margolin and co-workers offer a good example of such an approach.[21, 22] Finally, more than pushing FtsZ to divide a liposome, a bottom-up approach could be useful to better clarify how other proteins constituting the ring (e.g. FtsN) interact and regulate the FtsZ-FtsA treadmilling structures, with the final goal to elucidate the mechanism that triggers cytokinesis in bacteria.[23, 24] In this context, the recent work from Martin Loose and co-workers definitely deserves special attention.[25, 26]

REFERENCES

[1] P. Schwille, *Division in synthetic cells,* .

[2] Y. Caspi and C. Dekker, *Divided we stand: splitting synthetic cells for their proliferation,* Systems and Synthetic Biology **8**, 249 (2014).

[3] D. P. Haeusser and W. Margolin, *Splitsville: Structural and functional insights into the dynamic bacterial Z ring,* Nature Reviews Microbiology **14**, 305 (2016).

[4] T. den Blaauwen, L. W. Hamoen, and P. A. Levin, *The divisome at 25: the road ahead,* Current Opinion in Microbiology **36**, 85 (2017).

[5] D. W. Adams and J. Errington, *Bacterial cell division: Assembly, maintenance and disassembly of the Z ring,* Nature Reviews Microbiology **7**, 642 (2009).

[6] E. Bi and J. Lutkenhaus, *FtsZ ring structure associated with division in Escherichia coli,* Nature **354**, 161 (1991).

[7] K. Dai and J. Lutkenhaus, *ftsZ is an essential cell division gene in Escherichia coli,* J Bacteriol **173**, 3500 (1991).

[8] J. Mingorance, G. Rivas, M. Vélez, P. Gómez-Puertas, and M. Vicente, *Strong FtsZ is with the force: Mechanisms to constrict bacteria,* Trends in Microbiology **18**, 348 (2010).

[9] H. P. Erickson, D. E. Anderson, and M. Osawa, *FtsZ in Bacterial Cytokinesis: Cytoskeleton and Force Generator All in One,* Microbiology and Molecular Biology Reviews **74**, 504 (2010).

[10] E. J. Cabré, A. Sánchez-Gorostiaga, P. Carrara, N. Ropero, M. Casanova, P. Palacios, P. Stano, M. Jiménez, G. Rivas, and M. Vicente, *Bacterial division proteins FtsZ and ZipA induce vesicle shrinkage and cell membrane invagination,* Journal of Biological Chemistry **288**, 26625 (2013).

[11] M. Osawa, D. E. Anderson, and H. P. Erickson, *Reconstitution of Contractile FtsZ Rings in Liposomes,* Science **320**, 792 LP (2008).

[12] M. Osawa, D. E. Anderson, and H. P. Erickson, *Curved FtsZ protofilaments generate bending forces on liposome membranes,* EMBO Journal **28**, 3476 (2009).

[13] P. Szwedziak, Q. Wang, T. A. M. Bharat, M. Tsim, and J. Löwe, *Architecture of the ring formed by the tubulin homologue FtsZ in bacterial cell division,* eLife **3**, e04601 (2014).

[14] J. Xiao and E. D. Goley, *Redefining the roles of the FtsZ-ring in bacterial cytokinesis,* Current Opinion in Microbiology **34**, 90 (2016).

[15] M. Osawa and H. P. Erickson, *Liposome division by a simple bacterial division machinery.* Proceedings of the National Academy of Sciences of the United States of America **110**, 11000 (2013).

[16] A. W. Bisson-Filho, Y. P. Hsu, G. R. Squyres, E. Kuru, F. Wu, C. Jukes, Y. Sun, C. Dekker, S. Holden, M. S. VanNieuwenhze, Y. V. Brun, and E. C. Garner, *Treadmilling by FtsZ filaments drives peptidoglycan synthesis and bacterial cell division,* Science **355**, 739 (2017).

[17] X. Yang, Z. Lyu, A. Miguel, R. Mcquillen, and K. C. Huang, *GTPase activity – coupled treadmilling of the bacterial tubulin FtsZ organizes septal cell wall synthesis,* Science **747**, 744 (2017).

[18] J. M. Monteiro, A. R. Pereira, N. T. Reichmann, B. M. Saraiva, P. B. Fernandes, H. Veiga, A. C. Tavares, M. Santos, M. T. Ferreira, V. Macário, M. S. VanNieuwenhze, S. R. Filipe, and M. G. Pinho, *Peptidoglycan synthesis drives an FtsZ-treadmilling-independent step of cytokinesis,* Nature **554**, 528 (2018).

[19] T. Litschel, B. Ramm, R. Maas, M. Heymann, and P. Schwille, *Beating Vesicles: Encapsulated Protein Oscillations Cause Dynamic Membrane Deformations,* Angewandte Chemie - International Edition **57**, 16286 (2018).

[20] E. Godino, J. N. López, D. Foschepoth, C. Cleij, A. Doerr, C. F. Castellà, and C. Danelon, *De novo synthesized Min proteins drive oscillatory liposome deformation and regulate FtsA-FtsZ cytoskeletal patterns,* Nature Communications **10** (2019), 10.1038/s41467-019-12932-w.

[21] M. Krupka, V. W. Rowlett, D. Morado, H. Vitrac, K. Schoenemann, J. Liu, and W. Margolin, *Escherichia coli FtsA forms lipid-bound minirings that antagonize lateral interactions between FtsZ protofilaments,* Nature Communications **8**, 1 (2017).

[22] M. Krupka, M. Sobrinos-Sanguino, M. Jiménez, G. Rivas, and W. Margolin, *Escherichia coli ZipA Organizes FtsZ Polymers into Dynamic Ring-Like Protofilament Structures,* mBio **9**, 1 (2018).

[23] J. Lutkenhaus, *FtsN—trigger for septation,* Journal of bacteriology **191**, 7381 (2009).

[24] D. S. Weiss, *Last but not least: New insights into how FtsN triggers constriction during Escherichiacoli cell division,* Molecular Microbiology **95**, 903 (2015).

[25] N. Baranova, P. Radler, V. M. Hernández-Rocamora, C. Alfonso, M. López-Pelegrín, G. Rivas, W. Vollmer, and M. Loose, *Ftsz assembles the bacterial cell division machinery by a diffusion-and-capture mechanism,* bioRxiv (2018), 10.1101/485656, https://www.biorxiv.org/content/early/2018/12/03/485656.full.pdf .

[26] P. Caldas, M. López-Pelegrín, D. J. Pearce, N. B. Budanur, J. Brugués, and M. Loose, *Cooperative ordering of treadmilling filaments in cytoskeletal networks of FtsZ and its crosslinker ZapA,* Nature Communications **10** (2019), 10.1038/s41467-019-13702-4.

SUMMARY

Cell replication is a fascinating biological process that ensures the proliferation of a species via division of a mother cell into two daughter ones. This process in bacteria is performed by a complex protein machinery named the Z-ring, which assembles at the cell mid-plane and promotes progressive membrane constriction down to division. A central element of this machinery is FtsZ, a protein that polymerizes into filaments that constitute the main scaffold of the ring. Even though this protein was found to be essential, many aspects concerning the Z-ring assembly, the role of FtsZ-associated proteins, and the contribution of FtsZ to the constricting force in the division process are not yet clearly determined. To address these questions, in this thesis we aimed to reconstitute a minimal divisome *in vitro*, in order to isolate single components from the complex cellular environment, and study their functionality in a bottom-up way. Following this approach, we aimed to better understand the dynamics and the parameters involved in FtsZ filament association into bundles, and to verify whether such structures are capable to generate a force on the lipid membrane.

In **Chapter 1**, we introduce the concept of a minimal cell, explaining why a bottom-up assembly of cellular components can be helpful to recreate and understand fundamental life-sustaining processes, such as division, metabolic pathways, and genome expression. We spotted two essential components required for a minimal divisome: a container, and a protein machinery. We then introduced the main containers employed in bottom-up reconstitutions, such as liposomes, droplets and coacervates, and we gave a concise review of the literature involving the assembly, localization, and functioning of the Z-ring in bacteria.

Intrigued by the large variety of shape and sizes that nature conferred to cells, and the impact that such geometrical parameters have over different cellular features, **Chapter 2** presents a simple and effective microfluidic platform that we developed to finely tune the shape and the size of a large variety of containers. Specifically, we designed an innovative type of microfluidic traps where droplets, liposomes and double emulsions can be stably inserted to adopt rod-like shapes with a large range of aspect ratios. We showed that microfluidics features (such as side channels and multi-height devices) can be used to induce an osmotic stress and tune the size of double emulsions and droplets. As a proof of concept, we studied how bundle-forming proteins encapsulated in droplets varied their arrangement depending on the droplet geometry. Specifically, we showed that tubulin and collagen bundles, while randomly oriented in spherical containers, tend to align along the main symmetry axis in rod-shaped droplets.

In **Chapter 3**, we resolved the dynamics of FtsZ bundle formation on the membrane of closed cell-like minimal confinements. In order to do so, we encapsulated FtsZ inside

droplets coated by a lipid monolayer, together with a soluble version of its anchor protein ZipA. We showed that the condensation of filaments into bundles occurs into two steps: a nucleation step, where small clusters form, followed by a second step, where such structures elongate into long filamentous bundles embracing all the droplet surface. By keeping the molar ratio between ZipA and FtsZ fixed to a physiological level, we observed that macromolecular crowding is essential for the condensation process to occur, while protein concentration affects mainly the second elongation step. In smaller droplets, we found that the formation of bundles on the membrane is more robust against variation of protein and crowding concentration, revealing how the filament condensation is sensitive towards the size of the confinement.

In **Chapter 4**, we employed a microfluidics platform to encapsulate FtsZ inside liposomes, to verify whether the protein filaments are capable to deform a soft lipid membrane. While the liposomes contained FtsZ and a soluble version of its membrane anchor protein ZipA, the outer aqueous solution surrounding the liposomes contained GTP. By addition of the transmembrane pore protein alpha-hemolysin, GTP could flow inside the liposomes and trigger FtsZ polymerization. In a few minutes, bright fluorescent FtsZ bundles formed on the liposome membrane, and progressively induced shrinkage. In small liposomes (diameter < 5 μm), FtsZ filaments arranged in one single ring-like structure, while larger liposomes did not exhibit any evident constriction on the same time-scale. A long-standing hypothesis suggests that FtsZ filaments undergo a curvature increase upon GTP hydrolysis, which would generate a constriction force at the division septum. For this reason, we measured the curvature and length of single FtsZ filaments with atomic force microscopy, as they formed upon addition of nucleotides in different hydrolyzed states. Filaments assembled with GDP, GTP, or the non-hydrolysable analog GMPPCP did not show any obvious different conformations, suggesting that GTP hydrolysis does not induce the curvature change that was proposed. Overall, our data suggested that the observed membrane deformations could be the consequence of the condensation of filaments into bundles, rather than conformational changes of single filaments.

Finally, in **Chapter 5**, we explored whether alternative forms of containers could be employed as platforms for assembling a synthetic cell. To this purpose, we studied the interaction between FtsZ and coacervates, membraneless droplets generated by the spontaneous liquid-liquid phase separation of oppositely charged molecules in water. Specifically, we formed coacervates upon mixing negatively charged GTP and positively charged polylysine (pLL), and observed that FtsZ strongly partitions on their surface. When GTP was depleted from the surrounding environment, coacervates underwent evident shrinkage, while they remained stable in absence of FtsZ, or when GTP was replenished. This suggests that FtsZ, being a GTPase, is capable to consume the GTP forming the coacervates, thus inducing a charge imbalance and a consequent structural instability of the droplets. Furthermore, FtsZ filaments on the membrane were observed to form thick bundles, protruding from the surface of the coacervates and deforming them into aster-like shapes.

To conclude, in this thesis we worked towards the bottom-up assembly of a minimal FtsZ-based divisome. The data presented showed that FtsZ bundles have the potential to induce liposome deformation. The condensation of FtsZ filaments into bundles not only consistently relies on the crowding and protein concentrations, but also on the geometry of the confinement. To this purpose, we developed a microfluidic technique to obtain artificial containers with physiologically relevant geometries. To obtain a membrane constriction at a selected site, it would be interesting to combine these results, and achieve control over the formation and localization of FtsZ bundles via the manipulation of the container shape.

SAMENVATTING

Celdeling is een fascinerend biologisch proces dat de vermenigvuldiging van een organisme waarborgt door de deling van een moedercel in twee dochtercellen. In bacteriën wordt dit delingsproces uitgevoerd door een ingewikkelde machinerie die is gemaakt van eiwitten, die de Z-ring genoemd wordt. Deze ring vormt zich in het midden van de cel en bevordert de insnoering van het celmembraan totdat de cel in tweeën is gesplitst. Een centraal element van deze celdelingsmachine is het eiwit FtsZ dat polymeriseert in kleine vezeltjes die de belangrijkste substructuur vormen van de Z-ring. Hoewel eerder is bepaald dat dit eiwit essentieel is voor celdeling, zijn verschillende aspecten nog onduidelijk, met name over de assemblage van de Z-ring, de rol van andere FtsZ-bindende eiwitten en de bijdrage van FtsZ aan de insnoeringskracht tijdens het delingsproces. Om deze vragen te beantwoorden, hadden we in dit proefschrift als doel om een gesimplificeerde reconstructie van de celdelingsmachine *in vitro* samen te stellen. Dit hebben we gedaan om de individuele componenten te isoleren van de complexe omgeving van de cel, en om hun werking te bestuderen in een bottom-up benadering. Met deze aanpak hoopten we meer inzicht te krijgen in de dynamica en de verschillende parameters die belangrijk zijn voor de condensatie van FtsZ-vezels in dikkere FtsZ-bundels, en om erachter te komen of zulke structuren in staat zijn een kracht uit te oefenen op een lipidenmembraan.

In **Hoofdstuk 1** introduceren we het concept van een minimale cel. We leggen uit waarom de assemblage van componenten in een bottom-up benadering nuttig is om basale levensprocessen, zoals celdeling, metabolisme en genexpressie, na te bootsen en te begrijpen. Er zijn twee essentiële componenten nodig voor een minimale versie van de celdelingsmachine: een celomhulsel en een eiwitmachine. We geven aan wat de verschillende typen celomhulsels zijn in dit onderzoeksveld, namelijk liposomen, druppels en coacervaten. In een bondig literatuuroverzicht wordt duidelijk gemaakt wat de huidige stand van zaken is met betrekking tot de assemblage, de positionering en werking van de Z-ring in bacteriën.

Geïntrigeerd door de grote verscheidenheid aan vormen en groottes van cellen, en de invloed die zulke geometrische parameters hebben op cellulaire processen, presenteren we in **Hoofdstuk 2** een simpele en effectieve methode om de vorm en grootte van een reeks celomhulsels te manipuleren. We hebben hiervoor een innovatief type microfluidische val ontworpen waarin we druppels, liposomen en dubbele emulsies kunnen opsluiten in cilinder- en discusachtige vormen, over een breed bereik van hoogte-breedteverhoudingen. We laten zien dat microfluidische zijkanalen en multi-hoogte chips gebruikt kunnen worden om een osmotisch drukverschil aan te leggen en de grootte van druppels en dubbele emulsies te veranderen. Ter illustratie van het nut van deze methode, hebben we enkele bundelvormende eiwitten in druppels opgesloten en

aangetoond dat de organisatie van de resulterende bundels afhangt van de geometrie van de druppels. Bij zowel tubuline- als collageenbundels was de bundeloriëntatie willekeurig in bolvormige druppels, maar in de cilindervormige druppels kregen de bundels de neiging zich langs de symmetrieas van de druppel te oriënteren.

In **Hoofdstuk 3**, hebben we de dynamica van FtsZ-bundelformatie bestudeerd op het membraan van een gesloten minimale kunstmatige cel. Hiertoe hebben we FtsZ en een membraanankereiwit ZipA in druppels opgesloten die een enkele lipide laag aan het oppervlak hebben. We laten zien dat de condensatie van FtsZ-vezels in bundels in twee stappen gebeurt: een nucleatiestap, waarin kleine clusters zich vormen, en een tweede stap, waarbij deze clusters zich uitspreiden in lange vezelachtige bundels die het gehele druppeloppervlak omvatten. Door de molaire verhouding tussen ZipA en FtsZ constant te houden op een fysiologisch niveau, observeerden we dat macromoleculaire crowding essentieel is voor het gehele proces, terwijl de eiwitconcentratie hoofdzakelijk de tweede stap van het proces beïnvloedt. In kleinere druppels zagen we dat de bundelformatie op het membraan robuust is tegen variaties in de eiwit- en crowderconcentraties, wat aangeeft dat de vezelcondensatie gevoelig is voor de grootte van het opsluitende kunstmatige celomhulsel.

In **Hoofdstuk 4** hebben we een microfluidisch platform gebruikt om FtsZ in liposomen op te sluiten. Hiermee hoopten we erachter te komen of de eiwitbundels in staat zijn om het zachte lipide membraan te vervormen. De binnenkant van de liposomen bevatte de FtsZ en een oplosbare versie van het membraanankereiwit ZipA, terwijl GTP in de oplossing aan de buitenkant zat. Door het membraanporie-eiwit alfa-hemolysine toe te voegen, kunnen de GTP-moleculen van buiten de liposomen naar binnen diffunderen, en zo de formatie van FtsZ-bundels teweegbrengen. Binnen een paar minuten werden er duidelijke fluorescente FtsZ-bundels gevormd op het membraan van de liposomen, die ervoor zorgden dat de liposomen langzaamaan krompen. In kleine liposomen, met een diameter onder de 5 μm, organiseerden de FtsZ-bundels zich in ring-vormige structuren, terwijl grotere liposomen geen duidelijke ring vertoonden op dezelfde tijdsschaal. Een oude hypothese suggereerde dat FtsZ-vezels een verhoogde kromming vertonen na GTP-hydrolyse, wat vervolgens de insnoeringskracht zou genereren bij het delingsseptum. Om deze reden hebben we de kromming en lengte van enkele FtsZ-vezels gemeten met atomaire krachtmicroscopie, na toevoeging van nucleotiden in verschillende hydrolysetoestanden. FtsZ-vezels die gevormd zijn met GDP, GTP of de niet-hydrolyseerbaare versie GMPPCP vertoonden geen duidelijke verschillen in conformatie, wat lijkt te suggereren dat GTP-hydrolyse niet de krommingsverandering induceert die eerder was voorgesteld. Tezamen genomen, lijken onze resultaten aan te geven dat de geobserveerde membraandeformaties het gevolg zijn van de condensatie van vezels in bundels, en niet van de structuurverandering van enkele vezels.

Tot slot hebben we in **Hoofdstuk 5**, hebben we verkend of andere typen celomhulsels gebruikt kunnen worden als de basis van een kunstmatige cel. Hiervoor hebben we de interactie tussen FtsZ en coacervaten onderzocht, membraanloze druppels die gemaakt worden door een spontaan fasescheidingsproces van moleculen met tegenovergestelde ladingen in water. We hebben in dit geval coacervaten gemaakt met negatief geladen GTP en positief geladen polylysine (pLL), en we observeerden dat FtsZ sterk bond aan het oppervlak van de coacervaten. Als we GTP uit de omgeving weghaalden, krompen

de coacervaten, maar in de afwezigheid van FtsZ bleven ze stabiel, net als wanneer GTP weer werd toegevoegd. Dit suggereert dat FtsZ in staat is om de GTP in de coacervaten te hydroliseren, en op die manier de ladingsbalans in de coacervaten uit evenwicht te halen, wat leidt tot een instabiele structuur van de coacervaten. Verder hebben we laten zien dat FtsZ-vezels op het oppervlak van de coacervaten dikke uitstekende bundels kunnen vormen, resulterend in asterachtige objecten.

In dit proefschrift hebben we gewerkt in een bottom-up benadering aan de assemblage van een minimale celdelingsmachine gebaseerd op het bacteriële eiwit FtsZ. De meetgegevens in dit proefschrift hebben aangetoond dat FtsZ-bundels de mogelijkheid hebben om een vormverandering van liposomen te induceren. De condensatie van FtsZ-vezels naar bundels hangt niet alleen af van crowding- en eiwitconcentraties, maar ook van de geometrie van het celomhulsel. Hiertoe hebben we een microfluidische techniek ontwikkeld om kunstmatige celomhulsels te verkrijgen met fysiologisch relevante vormen en groottes. Om een membraaninsnoering te induceren op een vooraf gedefinieerde locatie, is het noodzakelijk om nauwkeurige controle te krijgen over de assemblage en positionering van de FtsZ bundels, mogelijk doormiddel van de manipulatie van de vorm van het kunstmatige celomhulsel.

ACKNOWLEDGEMENTS

My sister asked me not long ago whether she should do a PhD. I realized I did not have a good answer. Eventually, after few days (or maybe weeks) I told her: “Look, if it was me, I would not do it again, but I do not regret it”. Together with knowledge and experience, friendship is one of the main reasons why eventually these 4.something years were worth it. I am happy to take a moment (actually it took me way more than expected to write this part) to thank the people I met during this period of time, especially those who dedicated part of their time to teach me something, or simply to share some good moments with me. So here we go.

I would first like to thank my supervisor, Cees Dekker. I can see how your mentorship made me a better scientist. From you I have learned to pay great attention to the details, and to communicate our discoveries and ideas in a clear, simple and enthusiastic way. Thanks also for giving me the freedom to explore different directions parallel to my project. If I have to pick a favorite moment, I’d like to remember when we were in Catania, lining in a huge crowd at the airport: you sat down, picked up your guitar and started to play and sing in the middle of the hall. That, and the (too few!) times when we played guitar after a couple of good bottles of wine. Thanks also to the members of the committee for reading my thesis and providing useful comments. In particular, I would like to thank Gijsje for giving me the exciting opportunity to join her lab as a PostDoc, Marileen for wisely captaining this ship called BN, Germàn for the wise advices he gave me in Madrid in the beginning of my PhD, Tanneke for organizing the last EMBO meeting on cell division, Seamus for the nice chats we had at the EMBO meetings, and Christophe for his noble effort of "not playing the game".

When I think about the people I met that meant something to me in these past years, figures from different places and moment of times come to my mind, and it is difficult to make order. I would start from the CD lab, going back in time to when I was a fresh PhD student, just arrived to a place where people appeared like giants to me. The old crew. Good times. Stephanie, I would start with you, as you’ve been the first one I met: my office mate, my sister in arms. Thanks for all the infinite times you’ve been there listening to my complaints, for showing me how much endurance someone can have towards a difficult project, and to always be lovely, no matter what. Kubes, my buddy. When I look back, I only see good memories: us winning the foosball tournament, us playing guitars, us sitting on a bench in Leuven or at the lake sharing stories. Thanks for being such a sensitive and fun friend. Also, thanks for teaching me the noble art of foosball. Greg, my big brother: sometimes I regret that we’ve never been young together, as we did not share as many beers and songs as I would have liked to. Luckily, the success of our experiments together has been inversely proportional to the fun we had. So eventually it was worth it. Thanks for being there in my darkest hours. Yaron, what can I say: if

you did not exist, they should invent you! I love how, during every discussion we have, I learn something new or I gain a broader picture of a specific topic. Thanks for being such a knowledgeable and honest friend to me. Daniel, you're just a great guy: I admire your eagerness for happiness and I love how you try to put your contagious smile on everyone around you. Thanks also for always being willing to help, no matter how busy you were. Jorine, I am still pissed at you for booking the house in L.A. with the banana couch. Really uncomfortable. Adi, I will never forget the night we had together on the banana couch. Sorry for punching you because you were snoring. Sergii: thanks for punching Adi because he was snoring. That was necessary indeed, even if you were piccolo. Laura, thanks for the useful advices you gave me when I had to write the thesis and choose a committee. I will always save the image of you singing "Papi Chulo" in the street. Fabai, I remember that night at the party after our first concert, when you cheered at me with a glass full of wine and a fancy smile. Like to say: hell yeah baby! I hope to see you again soon. Siddharth, thanks for the patience you had at the beginning of my PhD in training me and teaching me microfluidics. I wish you good luck as a group leader. Yoones, you are a funny one, thanks for the fun parties at your place. Calin and Felix: we did not really have the time to get to know each other, but you both gave me the same very valid advice, which I should have followed sooner along my PhD.

After this trip back in time, my thoughts go to the people who are still working in the CD lab. First things first: Tony, you're a real modern gentleman, a brilliant thinker, and a great friend. My sincere gratitude goes to you, not only for your positive input on my work, but also because the time we have spent working together has been the most fun in my whole PhD. I like to think that one day we will collaborate again, and if not, we will always have midweek beers. Wayne, my next desk buddy: you're one of the best scientists I've ever met, but more important, you're a good man. Thank you for all our profound conversations, both for the sober ones about science and the drunk ones about life. Ale, if I had to be Mick, you'd be my Keith. And not only because of the great stories we share involving a hotel room, but mostly for the great music we did together. Thanks for the emotion. Speaking of which: Sandro, given the way you play bass, I find amazing how much I love you. Thanks for the wise words you shared with me when the future appeared scary. Alberto, my foosball pupil: I see a lot of me in you, except that you're probably a better person. Trust me when I say that, one day, you'll make it through this mess. Please, in the meantime, do never change. JK: you are really a fun guy! Thanks for all your drumming skills, and for showing to the world that the Backstreet Boys are still cool. Michel, you're between the toughest women I've ever met, and you'll always have my most sincere admiration. Jacob, I kind of see you like the nice and wise uncle of the lab: thanks for all our self-reflective conversations, and for being the one always reminding me that in a few years, I would have looked back and realized it was good after all. Jaco, I think your natural tendency of being helpful to everybody is extraordinary. Thanks for all the times you've listened to my problems in the lab, trying to come up with smart solutions even if you were not directly involved in the project. Eli, you've been quite of a pleasant surprise: thanks for that time you gave the protein purification one last trial, even if it was already late in the afternoon: you resurrected the project. Thank you also for our post-group-meetings conversations, you've been a sea-light in the storm. Daniel Shi, I think the global energy crisis will be easily solved the

day scientists find out what kind of source powers you. I wish you the best in your future career. Sabina, I am sorry our voices have never matched, but the rehearsal before the concerts (where you dumped me twice) were fun! Paola, thank you for bringing a bit of my roots also here in the cold North. We should make a proper Parmigiana together once. Sonja, I liked the sweet side of you, even if sometimes I wonder whether I really know you... a bit like the mineral oil composition. Eugene, you're one of the few women I know that can drink more beers than me with no evident consequences: well done! Oskar, I have the impression that we could have been good friends, if only we did not cross our paths for such a short time. Maybe in the next life we'll get a better chance. Mitasha, thanks for always being cheerful and smiling, and for helping with my skis in Courchevel. Nils, I hope you appreciate the order and the silence around the office now that I am gone. Thanks for your efforts of making the department more ecofriendly. Bis, you are a sport marvel, I think you should reconsider your career as a professional boulder. Allard, thanks for being the number one fun of the band. Nicola, good luck with your PostDoc and your new job as a father. To those who joined at the time I've left: Milosh, Sabrina, Martin and Pinyao, I wish you good luck with your new adventure!

I would also like to thank all the PIs working at BN, for coming up with creative ideas and challenging projects that make this department an exciting place to do science. I feel honored to have taken part of such stimulating environment. Also, BN would not be such a smooth engine without our irreplaceable team of people working behind the scenes: many thanks to Marije, Joline, Tracey, Emmylou, Dijana, Tahnee, Chantal and Esther for their precious help in realizing all the activities occurring in our department. In particular, a warm thanks to Amanda for providing support to me and all the members of the CD lab, and to Sacha, for his indispensable technical skills in maintaining machines properly working around the building. Also, thanks to Jelle and Dimitri, for their precious contribution from the workshop.

I have met so many fun and great people in BN who actually did leave a sign, that I really hope I am not going to forget anyone. I would start with those people I haven't mentioned yet that formed that "pretentious bunch" that was the Pickwick Club: Mehran, thanks for that afternoon of common despair and exhaustion in the sun, it was one of the several occasions where you made feel I wasn't alone; Johannes, thanks for always joining with enthusiasm, also to the movie nights, even with only one leg; Chris (I hope you do not get offense by being included in the BN section): you're a nerd with a pure and uncontaminated bohemian soul. Thanks for the infinite jam session nights, for desolation row, and for your vibe of freedom. Talking about music, I have had the pleasure to play with different people over the last years. Going back in time, this brings me to you, Helena: singing together in the evenings until the neighbors were coming complaining. Thanks for our friendship, so shining, colorful, loud, and finite like a firework. Misha, sometimes I see you getting spellbound by the song while you play the keys, and those are the moments where I see your blinding light exploding. Thanks for all the music we played in these years, and for adapting your tastes to mines. Sam, BN is definitely less fun and more quiet since you're gone. I miss your loud laughs, your dirty jokes and your cello sound. Louis, it was fun when we discovered that you did not know the song bass line two days before the concert. Rehearsing in the hallway was hilarious! Filip, thanks

for joining the band to give us such a cool rhythm, we could have not made some awesome songs without you. I would also like to thank Margreet, Yiteng, Hirad, Vladimir, Ivo and Maurits for always actively participating to the concerts. In particular, I would like to thank Da: from that night at my place when we sang “Can you feel the love tonight” with quite inebriated spirits, I loved all the times you shared your beautiful voice with all of us.

Independently from music, there are a bunch of people in BN with which I shared good memories who deserve to be mentioned. Mathia, I don’t remember I have ever met anyone with such inextinguishable and immense positive charm. I keep safe in my mind our moments together. May your smile never fade away. Becca, thanks for all the dinners, cooking, drinks, and complaints about life we shared. I am sure that one day, I don’t know when, I will come to visit you and Jochem in New Zealand. Vicky, thanks for teaching me so much in such a short amount of time, and for helping with the furniture in Fortuinstraat. I wish you the very best. Alicia, I am waiting for the day where we can go again to a folk concert together. David, you’re definitely a guy I am happy I have met. Nicole, thanks for your sense of humor and the fun moments together. Ben, thanks for making this department more fit and capable to defend itself. Elisa, thank you for doing science, and for making impossible projects come true. Kim, thanks for sharing useful advices on tedious protein reconstitutions. Renu, I enjoyed a lot our collaboration, thanks for being such a persevering and tenacious scientist. Richard, thanks for all your wise words shared while smoking a cigarette. Sumit, I admire your capability of being fun in a random and irreproducible way. George, thanks for believing in a social department. Christian, thanks for your sparkling and cheerful presence. Also, I would like to acknowledge my students, Thomas and Kevin, for helping me with my project, and my new colleagues, Lennard, Lucia, Gerard, Jeffrey, Cristina and Irene for warmly welcoming me in their lab. Given the awful architecture of our building, there are plenty of people scattered around different corners with which I did not have the pleasure to properly interact. I am not going to make a boring and pointless list of names, but I’d rather just thank you all for any nice, even if minor, gesture you could have had towards me.

Outside BN, I had the great luck to experience the love, friendship and support of the AlFeZeMa & Co., my irreplaceable crew, my Italian family in the Netherlands. Alessandro (Iannaré), I do admire your passion for building stuff, your sincere interest in the simple things, and your tormented love for life. Thanks for taking me away and share a little piece of your countryside life when I needed it the most. Whatever you’ll do in life, I hope you will always see your rumbling feelings as a strength. Zeno (Il Potente), thanks for sharing with me such a hammering, melancholic and vaguely poetic sense of unsatisfaction. Looking back at these years, probably the promised land we imagined to be somewhere was exactly the one we have built together with our stories. And our strive for more was the fire in our engine. Matteo (Ommemmerda), it is very difficult to not love you. Proof of your good heart: up to today, you’re still the one who managed to live with me the longest period of time. Thank you for being a great friend, from the very first day I came to your house and started to complain about life, up till today. Costanza (Cochi), if I don’t have any regret in life, it is because the choices

I made at every crossroads brought me to you. Between all the people, you're the one who deserves the most heartfelt acknowledgement, for all the love, life, happiness and infinite support you gave me along these last years. I would have probably not made it without you.

To complete the great Italian gang, I would like to acknowledge Anna for the great holidays we have spent together, for the fancy dinners, and for keeping Zeno alive. Thanks also to Ellie for all the evenings at her place, Ale Cavalli for his infinite composure and fine sense of humor, Giulia for sharing her mid-PhD experience story with me, and Nicolone for his inextinguishable eagerness for fun. In particular, I would like to thank Giulia G. and Federica for continuing together with me our troublesome journey through science and life here in the Netherlands, from the very first day they picked me up at Schiphol Airport, to our evenings running around Amsterdam, to the cozy afternoons spent talking about life. Like if nothing ever changed. Giulia B. also deserves my acknowledgement for making me feel at home in this Nordic country. When you came to the Netherlands, we went around Delft on one bike, almost falling in the canal: it feels like we were younger than now, but still us. I would also like to thank George and Ivo, my semi-housemates, for always warmly welcome me at their place (especially when I had to leave mine for quarantine reasons), for the good laughs when it was "Friday, Friday!", and their free bouldering lessons.

Going back to Italy, vorrei ringraziare anche i miei amici di sempre: i Cazzoni, le Caroline, Albi, Teino, Zacca ed Ale P. per le volte che mi sono venuti a trovare, ma soprattutto per dimostrare con il loro affetto che il tempo non ha effetto su certe cose. Per ultimi ma non ultimi, vorrei soprattutto ringraziare i membri della mia famiglia, per avermi sempre dato tutto l'amore che si può trovare in questo mondo. Voglio ringraziare i miei zii, Angela, Giancarlo, Sebastiana e Gianni per farmi sempre sentire a casa ogni volta che passo per una visita, a qualsiasi orario del giorno. I miei nonni, Tore, Nina, Ignazio e Vita, per l'inestimabile eredità di affetto, saggezza e tradizioni con cui hanno arricchito la mia infanzia. Le mie sorelle, Margherita e Carolina. Meggie, sebbene tu abbia cinque anni in meno di me, sei già uno scienziato migliore di quanto io sia ora. Non avere paura di inseguire quello che ti piace veramente fare, anche quando è difficile e ti fa sentire inadeguata. Carol, mi fa piacere che almeno qualcuno in famiglia affronti le discussioni senza strillare. Hai il dono di riuscire in qualsiasi impresa ti cimenti: spero che quell'impresa sarà infine la tua grande passione. Mamma, sono sicuro che al mondo esistono montagne meno resistenti di te. Grazie per l'immensa forza emotiva e l'enorme impegno che hai mostrato in questi anni. Se, nonostante tutto, tutto procede come deve andare, è perché nella tempesta hai tenuto ferma la bussola per tutti noi. Papà, quello che di buono ho raccolto nella vita è sempre stato seminato sul terreno smosso dai tuoi instancabili passi. Ovunque tu sia, mi piace pensare che mi sorridi, come quel giorno alla stazione. Il mio treno è partito. Grazie di tutto.

Federico Fanalista, December 2019

CURRICULUM VITÆ

Federico FANALISTA

31-05-1989 Born in Milan, Italy.

EDUCATION

2010–2012 B.Sc Physics
University of Milan, Milan, Italy

2012–2015 M.Sc Physics
University of Milan, Milan, Italy

2015–2019 Ph.D. Bionanoscience
Technische Universiteit Delft, Delft, The Netherlands
Thesis: On-chip reconstitution of an FtsZ-based divisome for synthetic cells.
Promoter: Prof. dr. C. Dekker

LIST OF PUBLICATIONS

4. R. Maan, N. Taberner, K. Vendel, E. van der Sluis, **F. Fanalista**, A. Birnie, C. Dekker, M. Dogterom, *Reconstitution of Pom1 Gradient in Droplets*, in preparation.

3. **F. Fanalista**, J. W. J. Kerssemakers, C. Dekker, *FtsZ bundle formation in cell-mimicking droplets*, submitted.

2. **F. Fanalista**,* A. Birnie,* R. Maan, F. Burla, K. Charles, G. Pawlik, S. Deshpande, G. H. Koenderink, M. Dogterom, C. Dekker, *Shape and Size Control of Artificial Cells for Bottom-Up Biology*, ACS Nano **13**, 5439-5450 (2019).

1. **F. Fanalista**,* S. Deshpande,* A. Lau, G. Pawlik, C. Dekker, *FtsZ-Induced Shape Transformation of Coacervates*, Advanced Biosystems **2** (9), 1800136 (2018).

*equal contribution